

https://dspace.org/

Wetting of the diamond surface

Hansen, John Olaf

2015-01-23
http://hdl.handle.net/10539/16720

Downloaded from a DSpace repository. https://dspace.org/

WETTING OF THE DIAMOND SURFACE

JOHN OLAF HANSEN

A Thesis submitted to the Faculty of Science, University of the Witwatersrand, Johannesburg for the Degree of Doctor of Philosophy

ABSTRACT

The surface conditions which lead to a wide variation in the wettability of diamond surfaces have been investigated using macroscopic surfaces rather than powders, to allow for the crystal anisotropy. A wetting balance method of calculating adhesion tension and hence contact angle has been used for diamonds having major faces near the [111] and [110] lattice planes. Three classes of behaviour have been identified: an extremely hydrophobic state (H) after hydrogenation at > 870 K; a hydrophilic (O) state after oxidation at 670 K; and an intermediate, (I) but net hydrophobic, state after mechanical polishing of the surface. Surface analyses by Rutherford Backscattering of helium ions, X-ray Photoelectron Spectroscopy and Low Energy Electron Diffraction (LEED) have been used to define the role of the oxygen coverage of the surface in the transition H -> O -> H. The H state corresponds to low (< 0,1 monolayer) coverage by oxygen, but no reconstruction of the surface, and hence near total coverage by surface hydrogen atoms of wettability similar to the methyl groups in paraffin wax. The O state is characterized by more than 0,3 monolayer of oxygen, some of which may be bonded to two carbon atoms, and a high wettability, approaching that of an oxide or silica surface. The I state is characterized by a "one third" monolayer coverage by oxygen, in the form of poorly ionizing hydroxyl groups, the balance being hydrogen. The I-state hydrophobicity (by advancing contact angle) is greater than that of bituminous coal (64 degrees), but less than that of cleaved graphite (80 degrees). The stable configuration on the [111] face, that most frequently produced by abrasion, is thought to be a random distribution of hydroxyl groups which avoid nearest neighbour positions. A computer simulation has shown that this will produce between 0,23 and 0,32 monolayer coverage by oxygen, depending upon the frequency of edge sites. At edge sites, bridging attachment of oxygen is possible. The exclusion of nearest neighbours in this model relies upon the repulsive Van der Waal's interaction between non-bonding oxygen atoms when approaching closer than 280 pm. The spacing of carbon atoms in the diamond [111] surface is 252 pm. Because of the randomized position of the hydroxyl groups, there is no surface superlattice, and so there is no appearance of second order spots in the LEED image.

The hydroxyl groups present in this state are alcohol-like in character and poorly ionized at pH in the range 1 to 11. There is no dependence of adhesion tension on ionic strength using a neutral (alkali metal halide) solution.

Ferric ion has a hydrophilizing effect on the diamond surface, thought to be the consequence of attachment to the hydroxyl groups at the surface by a ligand mechanism. Other transition metal ions did not show this effect. The phenomenon of hydration of the surface, i.e. progressively more hydrophilic behaviour on prolonged exposure to liquid water, has been quantified. Imbibition or water penetration at microcracks are thought unlikely, and a water cluster build-up at hydrophilic sites is thought to be the best explanation.

Dynamic studies indicate little dependence of the advancing contact angle on velocity for velocities up to 10^{-4} m/s, and slight dependence of the receding contact angle. Hence advancing angles by this technique are similar to equilibrated contact angles found by optical techniques, but the receding angles are lower than found by other, non-dynamic measurements.

DECLARATION

I declare that this dissertation is my own, unaided work. It is being submitted for the degree of Doctor of Philosophy in the University of the Witwatersrand, Johannesburg. It has not been submitted before for any degree or examination in any other University.

J.O. Hansen

10th day of July, 1987

PREFACE

I have undertaken this study because it flows naturally out of the work which I, and several colleagues at De Beers Diamond Research Laboratory, have done on the adhesion method of diamond recovery from the ore. This industrial process involves the fusion of three factors, the oil rich "grease" phase which makes the adherent bond, the mechanical system of spreading and stripping of the particles, and the unique properties of the mineral surfaces which allow adhesion of some and removal of others. The motivation for a continued interest in this rather medieval technology comes from its cost effectiveness and selectivity for diamonds.

Developments in the engineering systems for the handling of the adherent phase and the distribution of the particles have been completed with success, but the third factor, the behaviour of the diamond surface, remains less predictable and even less controllable. As a general rule, diamonds mined at depth are tractable, while those from a riverine or beach deposit are not.

With a first degree in Chemical Engineering and several years of work in applied electrochemistry, the study of the diamond surface, and particularly the rare property of natural hydrophobicity, attracted me. Because a detailed study would have involved more fundamental work than is usually justified in an industrial laboratory, I was permitted to enroll as a postgraduate student with the Department of Chemistry at the University of the Witwatersrand and to pursue the study of this fascinating crystal, using additional techniques available only at the University.

During the course of this study, papers were delivered at two conferences on aspects of the work :

"Wetting of the diamond surface" to the 1985 Diamond Conference at Reading University in July 1985.

"A capillarographic method for the study of hydrogen- and oxygen terminated diamond surfaces" to the SA Institute of Physics annual conference in Johannesburg in July 1986.

PREFACE

I have undertaken this study because it flows naturally out of the work which I, and several colleagues at De Beers Diamond Research Laboratory, have done on the adhesion method of diamond recovery from the ore. This industrial process involves the fusion of three factors, the oil rich "grease" phase which makes the adherent bond, the mechanical system of spreading and stripping of the particles, and the unique properties of the mineral surfaces which allow adhesion of some and removal of others. The motivation for a continued interest in this rather medieval technology comes from its cost effectiveness and selectivity for diamonds.

Developments in the engineering systems for the handling of the adherent phase and the distribution of the particles have been completed with success, but the third factor, the behaviour of the diamond surface, remains less predictable and even less controllable. As a general rule, diamonds mined at depth are tractable, while those from a riverine or beach deposit are not.

With a first degree in Chemical Engineering and several years of work in applied electrochemistry, the study of the diamond surface, and particularly the rare property of natural hydrophobicity, attracted me. Because a detailed study would have involved more fundamental work than is usually justified in an industrial laboratory, I was permitted to enroll as a postgraduate student with the Department of Chemistry at the University of the Witwatersrand and to pursue the study of this fascinating crystal, using additional techniques available only at the University.

During the course of this study, papers were delivered at two conferences on aspects of the work :

"Wetting of the diamond surface" to the 1985 Diamond Conference at Reading University in July 1985.

"A capillarographic method for the study of hydrogen- and oxygen terminated diamond surfaces" to the SA Institute of Physics annual conference in Johannesburg in July 1986.

LIST OF ABBREVIATIONS

Symbol	Meaning
A	Surface area, m^2
A_i	Hamaker constant for species i
AR	Analytic reagent
a	Laplace capillary constant, m
$\tilde{a}_1, \tilde{a}_2$	Basis vectors for unit cell of crystal surface mesh
Ca	Capillary number, dimensionless
d	Spacing of differing centres on surface mesh, m
C_i	London constant for species i
c.p.s	Counts per second
E	Ion energy, eV
E_s	Strain energy of a bond, kJ/mol
ESCA	Electron Spectroscopy for Chemical Analysis (see XPS)
F	Gibbs free energy, J/mol
G	Gibbs free energy, J
$\mathcal{G}$	Gibbs free energy per unit volume, J/m^3
GP	General purpose reagent
g	Acceleration due to gravity, 9.81 m/s^2
H	Hydrogenated (hydrophobic) surface state
ΔH_{of}	Heat of formation, kJ/mol
h	A small height interval, m
h	Planck's constant, 6.626×10^{-34} Js
I	Intermediate state of wettability
LEED	Low Energy Electron Diffraction
K	Degree of temperature on the Kelvin scale
Kα	Specific transition defining X-ray energy
kJ	Kilojoule
l	length, m
M_i	Mass number of nucleus i
M	Molar concentration, mols/litre
ML	Monolayer of surface adatoms - corresponding 1:1 with carbon atoms in the crystal surface
m	Particle mass, kg
mJ/m^2	Millijoule per square metre, unit of surface energy numerically equal to the cgs unit erg/cm^2
mm	Millimetre ($m \times 10^{-3}$)
mol	Gram mole of a chemical species
N_{av}	Avogadro's number, 6.023×10^{23}
n	Number of mols, dimensionless
n_i	Number of dispersion force centres per unit volume
O	Oxidized (hydrophilic) surface state
P	Pressure, N/m^2
P	Counts in surface layer peak
PTFE	Polytetrafluoroethylene
p	Perimeter, m
pH	Acidity scale, $\log [H^+] \times (-1)$
pm	Picometre ($m \times 10^{-12}$)
RBS	Rutherford Backscattering Spectroscopy
R_1, R_2	Radii of curvature, m
r	Capillary radius, m

rpm	Revolutions per minute
S	Spreading coefficient, mN/m
ΔS	Counts per channel in substrate spectrum
T	Absolute temperature, degrees Kelvin
U	Accelerating voltage, volts
UHP	Ultra high purity
UHV	Ultra high vacuum
$\bar{V}$	Molar volume, m^3/mol
v	Particle velocity, m/s
v/v	Volume basis
XPS	X-ray photoelectron spectroscopy
Z_i	Atomic number of species
z	Height coordinate, m
Δ	Small increment
δ	Infinitessimal increment
γ_{sv}	*Surface free energy of solid:vapour interface* measured in mJ/m^2
γ_{sl}	Surface free energy of the solid:Liquid interface measured in mJ/m^2
γ_{lv}	Surface free energy of the liquid:vapour interface or equivalent surface tension, measured in mJ/m^2 or mN/m
cos	Cosine function
λ	Wavelength, m
ρ	Density, kg/m^3
θ	Contact angle measured through the liquid phase
υ	Frequency of exciting X-ray
η	Viscosity, kg/m s
ϕ	Coefficient to include polar force interactions (eqn. 6)
ϕ	Slope of liquid:vapour interface, degrees
ϕ	Angle of constructive interference in diffraction pattern
[111]	Miller indices for octahedral crystal plane
[110]	Miller indices for dodecahedral crystal plane
[100]	Miller indices for cube crystal plane
1 x 1	Identification of LEED pattern based on unit cell of surface mesh
(1s)	First, spherical electron orbital
(2p)	Second, directional electron orbital
sp^3	Hybridization of one s and three p orbitals to give four orbitals with tetrahedral disposition
π	Numerical constant = 3,14159
π	Film pressure of an adsorbed film, mN/m
π-bond	Bonding by orbitals which are not collinear with the axis joining the two nuclei

Subscript

a	Advancing
b	Binding energy
c	Critical
calc	Calculated
capill	Capillary
d	Due to dispersion forces alone
dia	Diamond
g	Graphite
i	At the interface
inc	Incident at the target
kin	Kinetic
l	Liquid
obs	Observed
r	Receding
s	Solid
th	*Thermodynamic*
scat	Scattered by target
v	Vapour
w	Water
∞	At infinity (in the bulk phase)

CONTENTS

		Page Number
1.	INTRODUCTION	1
1.1	Diamond The diamond crystal Reactivity of diamond Diamond hydrophobicity Reconstruction *Oxygen and Hydrogen* at the diamond surface Adsorption on powders	1
1.2	Wetting Definition The contact angle Geometrical difficulties Thermodynamic validity Alternative techniques Wetting by metals Dynamics of wetting	11
1.3	Surface Forces Surface tension of a pure liquid Interfacial tension London-Van der Waal's forces Dipole-dipole interaction Dipole-induced dipole interaction Hydrogen bonds	18
2.	THEORY OF CAPILLARY FORCES	24
2.1	Capillarity and buoyancy Buoyancy Capillarity	24
2.2	The thermodynamic contact angle Core region Gravitational and curvature energy terms	31
2.3	Kinetic and hysteresis effects Approach to equilibrium	33
3.	MEASUREMENT OF THE CONTACT ANGLE	36
3.1	Optical methods	36
3.2	Capillary pressure	38
3.3	Capillarography - the *Wilhelmy plate* Testplate Shape Liquid level disturbance Liquid interface cleaning	38

		Page Number
4.	CAPILLAROGRAPHIC APPARATUS	45
	4.1 Cell and weighing linkage	45
	4.2 Displacement and force transducers	51
	4.3 Water preparation	52
	4.4 Data capture	53
	4.5 Shaping and orientation of diamonds Crystal Orientation	53
	4.6 Cleaning techniques Polishing and cleaving *Chemical cleaning* Soft polishing Cleaning of the cell Cleaning of tweezers and hanger wires	56
	4.7 Surface reaction Reaction with gases Reaction with aqueous reagents	60
5.	SPECTROSCOPIC TECHNIQUES	64
	5.1 Surface analysis	64
	5.2 Rutherford Backscattering Theory Experimental details Test diamond	64
	5.3 Low Energy Electron Diffraction Theory Experimental details	68
	5.4 X-ray Photoelectron Spectroscopy Theory Depth sensitivity Experimental details	70
6.	RESULTS	77
	6.1 Capillarographs	77
	6.2 Polished diamond surfaces	83
	6.3 Oxidized diamond surfaces Hydrogenation in solution Oxidation by chromic acid	85

		Page Number
6.4	Hydrogenated diamond surfaces	89
6.5	Zisman plot	94
6.6	Optical contact angle measurement	96
7.	SPECTROSCOPIC RESULTS	100
7.1	Sequence of experimentation	100
7.2	Rutherford Backscattering results	100
7.2.1	Oxygen analysis	100
7.2.2	Identification of adsorbed species	104
7.3	Low Energy Electron Diffraction	105
7.4	X-ray Photoelectron Spectroscopy	107
8.	SURFACE MODELS	111
8.1	Molecular model	111
8.2	Fully hydrogenated	111
8.3	Fully oxidized	112
8.4	Intermediate state Uniform one third monolayer coverage Randomized nearest neighbour exclusion	114
8.5	Interpretation of diamond hydrophobicity	119
9.	SOLUTION EFFECTS	120
9.1	Hydration	120
9.2	pH	123
9.3	Temperature	125
9.4	Ionic strength	127
9.5	Aqueous oxidants	127
9.6	Plant water sampled at the Venetia deposit	128
9.7	Specific metal cations	132
9.8	Dynamic effects	135
10.	CONCLUSIONS	137
11.	REFERENCES	140

	Page Number
APPENDIX 1 : Derivation of the thermodynamic contact angle	151
APPENDIX 2 : Flowsheet for computer controlled experiment	157
APPENDIX 3 : Computer control program	159
APPENDIX 4 : Derivation of the LEED equation for spot spacing	165
APPENDIX 5 : Wetting results on clean polished surfaces	168
APPENDIX 6 : Computer simulation of random coverage	169
APPENDIX 7 : Ellipsometric measurements	171
APPENDIX 8 : Wettability of silicon	173

FIGURE		Page Number
42	Effect of ionic strength on adhesion tension	126
43	Capillarograph in Venetia water	129
44	Long exposure to Venetia water	131
45	Effect of calcium ion concentration on adhesion tension	131
46	Effect of aluminium ion concentration on adhesion tension	133
47	Effect of chromic ion concentration on adhesion tension	133
48	Effect of ferric ion concentration on adhesion tension	134
49	Effect of ferric ion with time	134
50	Removal of ferric ion by water and acid rinses	134
A1	Derivation of Young's equation by energy method vertical plate with gravitational potential	156
A8.1	Capillarograph Silicon [111]	175
A8.2	Capillarograph SI [111] OXID	176

FIGURES

FIGURE		Page Number
1	The diamond unit cell	2
2	Two views of the diamond lattice	3
3	Surface views on low index planes	4
4	The mechanical equilibrium of Thos Young	13
5	A droplet hanging from a leaf	27
6	Basis of the capillarographic method	40
7	Numerical solution of the meniscus curve for water	43
8	Capillarographic apparatus - schematic	46
9	Detail of capillarographic cell and lid	47
10	Detail of clip for diamond test plates	48
11	Capillarographic apparatus	49
12	*Capillarographic cell*	50
13	Diamonds used in wetting tests	50
14	X-ray diffractometer (Laue) photograph of polished [111] diamond	55
15	Tube reactor for gas reaction	61
16	Rutherford Backscattering of helium ions	65
17	Low energy electron diffraction apparatus	71
18	XPS apparatus	75
19	Stages in the wetting hysteresis loop	78
20	Capillarograph on [111]	79
21	Capillarographs for three states of the [111] surface	81
22	Capillarograph on glass	82
23	Distribution of adhesion tension on polished *[111]* and *[110]*	84
24	Effect of oxidation on contact angles and adhesion tension	86
25	Recovery from hydrophilic state	87
26	Effect of attrition on oxidized surface	87
27	Effect of chromic acid and attrition	90
28	Effect of hydrogen on contact angles and adhesion tension	91
29	Effect of attrition on hydrogenated surface	92
30	Zisman plots for [111]H and [110]Int	92
31	Photographs from optical contact angle studies	97
32	Relative wettability of natural surfaces	99
33	RBS spectra	101
34	Composite RBS spectra for [111]Int and [111]H	102
35	LEED pattern on [111] 1X1	106
36	X-ray Photoelectron spectra	109
37	Ideal one third monolayer coverage by oxygen on the [111] surface	116
38	Simulation of randomized surface coverage	118
39	Hydration effect in water	122
40	Effect of pH on contact angles and adhesion tension	124
41	Effect of temperature on γ_{lv} and adhesion tension	126

TABLES

Table		Page Number
1	Previously reported contact angles for *diamond:water*	8
2	Contact angles of newly cleaved hydrophobic minerals : water	9
3	Classification of wetting behaviours by contact angles	14
4	Results of Laue crystal orientation analysis	54
5	Reagents used in this study	62
6	Reagents used for cleaning purposes	63
7	Wettability of mechanically cleaned diamond surfaces	83
8	Effect of attrition on oxidized [111] surface	85
9	Hydrogenation by lithium aluminium hydride in ethereal solution	88
10	Effect of chromic acid and attrition on the [111] surface	89
11	Classification of wetting behaviour	93
12	Adhesion tension of the different classifications	94
13	Data for Zisman plots	95
14	Optical contact angle measurements on natural faces	96
15	Surface coverages calculated from RBS spectra	104
16	Adatoms detected by RBS	105
17	Oxygen surface analysis by XPS	108
18	Estimation of strain energies	113
19	Simulated random surface coverage	117
20	Hydration during a standard test with three cycles of wetting	120
21	Acid strengths of various *OH containing* groups	125
22	Oxidation by aqueous oxidants	128
23	Analysis of Venetia shaft 5 water.	130

CHAPTER 1 - INTRODUCTION

1.1 Diamond

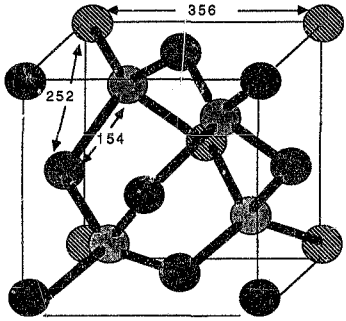
The Diamond Crystal

Diamond is the ultimate polymer, an extensive three dimensional lattice of carbon with sp^3 hybridization of the bonding orbitals (McKervey 1980). A unit cell, showing the interatomic spacing of 154 pm, appears as Figure 1 and a photograph of a model crystal appears as Figure 2 (100 pm = 1 Angstrom unit). Because the unit cell is drawn to show the diamond face-centred cubic cell, it is less easy to see the [111] plane, illustrated in this figure by the crosshatched carbon atoms. This is called the octahedral face, and has the lowest number of carbon atoms per unit area, and the lowest number of bonds broken on rupture of the crystal and is therefore the most frequent cleavage face (Bansal and Vastola 1972). It has been suggested (Wilks 1973) that diamond polishing proceeds by the breaking out of microfragments with [111] faces. Figure 3 shows the surface geometry of [111], [110] and [100] faces. The positions of the dangling bonds, those formed by rupture of the crystal along the particular crystal plane, and the spacing between surface atoms is shown.

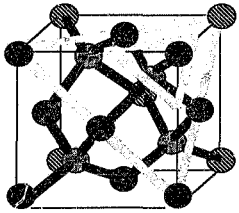
Reactivity of Diamond

Diamond is thermodynamically unstable with respect to graphite at normal temperatures and pressures. The standard free energy of graphitization is -2,89 kJ/mol. Diamond owes its existence, outside the laboratory or the upper mantle of the earth, to the kinetic restriction on graphitization. Davies and Evans (1972) have estimated the activation energy for graphitization at between 700 and 1050 kJ/mol, depending upon the crystal face at which the conversion occurs, and conclude that the mechanism requires the detachment of a triply or doubly bonded atom at the [111] and [110] surface respectively. In vacuum or an inert atmosphere, this starts only at 1500 K (Davies and Evans 1972).

fig 1 the diamond unit cell

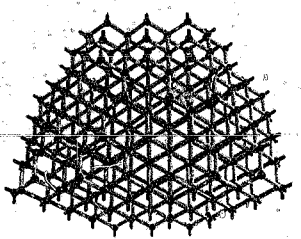


dimensions in picometres

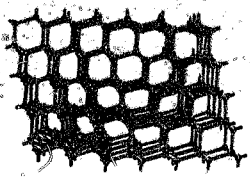


sections on [111] planes

fig 2 two views of the diamond lattice



looking down [111]

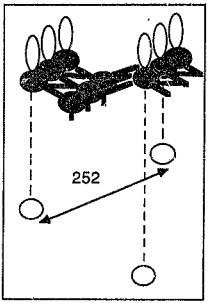


looking across [111] i.e. along [211]

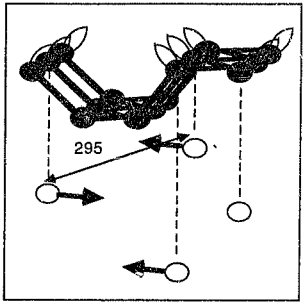
note "double layers" parallel to [111]

fig 3 surface views on low index planes

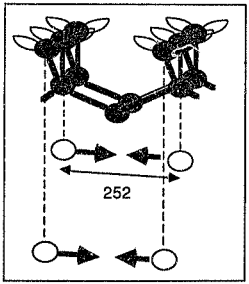
[111]



[110]



[100]



the dotted lines show the projection of top layer nearest neighbours and the direction of the dangling bond orbitals

all dimensions are pm

Similarly, although formation of the oxides from diamond is thermodynamically favoured, the standard free energy changes being -399 kJ/mol to CO_2 and -141 kJ/mol to CO, combustion of diamond does not start below 900 K (Field 1979). The oxidation proceeds by a surface corrosion or etching mechanism, producing triangular etch pits on the [111] surface. During polishing of diamonds, stones which are run too hot develop a frosty finish which is also seen on stones which have been set in a ring with too high a flame temperature. This is ascribed to "burning" (Watermeyer 1980). The carbon atoms in the surface layer of a diamond will have one or more bonding orbitals available for reaction with hetero-atoms. Barrer (1936) has shown that chemisorption of oxygen on vacuum outgassed diamond powder starts at 273 K. Apparently the surface of diamond is moderately reactive, but the perfection of the crystal prevents extensive bulk reaction.

Diamond Hydrophobicity

Isaac Newton (reported in Davies 1984) was reputedly the first to suggest that diamond was a "coagulated unctuous substance" on the basis of its optical properties. Diamond, amber and other waxes disobeyed his hypothesis for a simple relation between refractive index and density. The use of the term unctuous (oil-like) was perceptive since the term organic did not come into use until later. This was even before Lavoisier ignited diamonds in a belljar and concluded that the gas produced was carbon dioxide.

Given that the diamond is more than 99,5 % carbon, the hydrophobic (non wettable) behaviour of most diamond surfaces has sometimes been explained as a natural consequence of their "carbon character" :

"Adhesion of the diamonds to grease is no doubt related to their nonpolar structure and to the likewise nonpolar structure of the hydrocarbon molecules of which the grease is made "(Gaudin 1939), and, "Diamond, since it is carbon, is oil-wetted without chemical reaction" (Defoe 1985).

And yet Gaudi· et al (1957) suggest that minerals will exhibit natural hydrophobicity only when : "at least some fracture or cleavage surfaces form without rupture of interatomic bonds other than residual bonds". Diamond cannot fall into this category.

In practice there are situations where diamonds are found to be largely hydrophilic. Most coastal and alluvial deposits produce diamonds with wettable surfaces. Even in kimberlite (the igneous rock in which diamond was transported to the surface of the earth) there is a trend of more hydrophilic behaviour in diamonds found in the "weathered" ground near the surface (Davies 1985). Several possible explanations have been offered and are discussed below.

Because the behaviour was often seen with diamonds from beach deposits it was thought to be the result of adsorbed surface layers of "salt" (Weavind 1952). Alternatively, the high surface energy of the crystal (Rebinder 1952) and the coverage of the surface by a monolayer of oxygen (Kuryenkov 1963) were suggested as explanations. These theories do not address the easily observed hydrophobicity of most diamond crystals. The high theoretical surface energy of diamond, cited by Rebinder, has been calculated from bond energies and the areal density of ruptured bonds at 5650 mJ/m^2 (Adamson 1967). According to Zisman (1964) diamond represents one of the good examples of a hard, high melting solid which, because of the great interatomic forces in the crystal, will produce a high surface energy when sheared. This surface ought then to be very well wetted by ordinary liquids (excluding liquid metals) which have a surface energy of less than 100 mJ/m^2. Tabor (1975) also makes this point when remarking on the apparently low adhesion of diamond to diamond. As will be apparent from the analysis in Chapter 2, it is important to distinguish between the total surface energy formed by shearing a covalent solid and that due to the forces which can operate between the diamond surface, water molecules and the vapour phase. Since these forces operate over a range of a few atomic diameters, the composition of the topmost layer of the diamond surface has an overriding effect on hydrophobicity. Synthetic diamonds have been found to be predominantly lyophilic (hydrophilic) but this is most probably caused by the high level of metal impurities in the crystal

(Shilo et al 1986). This is not the case for natural diamonds, where the only major crystal impurity is nitrogen. The reason for deviation from hydrophobic behaviour must lie in modification of the surface composition or structure.

Reconstruction

The existence of a modified structure for the surface atoms of diamond, a phenomenon well established for silicon, which has the same bulk structure, was first proposed by Lander and Morrison (1966). A surface reconstruction of diamond occurs after vacuum outgassing at 1400 K, leading to a structure with periodicity at twice the lattice spacing. This is detected by Low Energy Electron Diffraction (LEED). Lander and Morrison proposed a surface layer of "puckered benzene rings" although there are various other models which could explain the same observations (Pandey 1982). Derry et al (1986) conclude that the π-bonded chain of Pandey best fits the data from ion scattering experiments. The existence of π-bonds on the diamond surface could presumably impart hydrophobic behaviour, by analogy with the hydrophobic graphite basal planes. However, LEED studies of natural and polished diamond surfaces show no reconstruction before heating to 1400 K, so this explanation can be dismissed. Recently, Pate (1986, Pate et al 1982, Pate et al 1983) and others (Himpsel et al 1980 and 1981, Vidali et al 1983, Derry et al 1983, Waclawski 1982, Lowther 1985) have shown that the bulk-like surface structure invariably seen by researchers using mechanically polished diamond surfaces in ultravacuum is terminated by hydrogen atoms. This is considered in more detail below. However, There is no self evident reason why hydrogen should be preferred to oxygen.

Oxygen and Hydrogen on the Diamond Surface

Since the surface atoms appear to occupy their bulk-like positions, and since the frequency of unreacted "dangling" bonds has been estimated by electron spin resonance study to be less than 1/1000 (Schlossin 1966) it seems feasible that the surface bonds are taken up by bonding with oxygen from the atmosphere.

Sappok and Boehm (1968) concluded that diamond was either hydrophilic, if most recently reacted with oxygen, or hydrophobic if most recently reacted with hydrogen, and the natural surface was assumed to have an initially hydrogen covered surface which reverted to an oxygen covered surface after prolonged exposure to atmospheric oxygen. A current theory of diamond genesis (Mitchell and Crockett 1974) provides some support for this. The fugacity of oxygen in the molten rock at the level where diamond growth is assumed to occur is estimated at 10^{-12}, so that the equilibration of free carbon and water would lead to the formation of methane, hydrogen and carbon monoxide. However, there is strong evidence that conditions nearer the surface become oxidizing, with etching and even complete resorption of the diamond crystals. (Dawson 1975).

The carbon-oxygen surface compounds (groups) responsible for the hydrophilic behaviour have been described as hydroxyls >COH, carbonyl >C=O, oxirane type >COC< and, on surfaces oxidized at high temperatures, where CO_2 desorption had begun, carboxylic acid groups, -COOH. Hartley (1978) and Shergold and Hartley (1982) provide additional evidence for the existence of multiple oxygen groups but Hartley considers the hydroxyl group to be the major oxygen containing group, rather than the oxirane COC preferred by Sappok and Boehm. Shergold and Hartley (1982) report values for the contact angle (wettability) of natural diamond surfaces which are considerably lower than had been previously reported. A low contact angle indicates hydrophilic behaviour, as will be discussed in Chapter 2.

TABLE 1 - PREVIOUSLY REPORTED CONTACT ANGLES FOR DIAMOND:WATER

Reference	Technique	Contact Angle (degrees)
Lurie and Ristic 1972	Optical, sessile drop	60
Nassau & Schonhorn 1977	Optical, sessile drop	47-55
Tabor 1975	Optical, sessile drop	60 (approx)
Hartley & Shergold 1982	Optical, captive bubble	11-25

For comparison, the contact angles of other naturally floatable minerals, measured by the sessile drop method are shown in Table 2.

TABLE 2 - CONTACT ANGLES OF NEWLY CLEAVED HYDROPHOBIC MINERALS:WATER

Reference	Mineral	Contact Angle (degrees)
Arbiter 1975	Graphite	80
Arbiter 1975	Molybdenite	89
Guiterrez 1984	Bituminous coal	40-72

This discrepancy in the diamond results may be because of the difference in techniques.

The hydrophobic component of the surface is ascribed by Shergold and Hartley to ringlike reconstruction of the surface carbon atoms (Lander et al 1966) and possibly oxirane groups by analogy with the hydrophobic ≡Si-O-Si≡ bond on heat treated silica (Laskowski et al 1969). The strongly acidic carboxyl and carbonyl groups are found on less than 10 % of the surface atoms, on a powder which must contain a mixture of all crystal faces. By inference, the major oxygen containing group is the hydroxyl group. The existence of ≡CH, ≻CH_2 and -CH_3 (methyl) groups on the natural surface is not discussed despite the large body of work on diamond surface analysis by vacuum techniques, which have pointed to hydrogen termination in almost every case. Pate (1986) provides the most recent analysis and many references, some of which were mentioned on page 4. The photon stimulated ion desorption analysis by Pate leaves open the possibility that the hydrogen is present as part of a surface hydroxyl. These results show an adsorbed species at mass number 16 which was assigned to CH_4^+, or

possibly O^+. The study by Waclawski et al (1982) apparently rules out the possibility of hydrogen present as hydroxyl. The High Resolution Electron Energy Loss Spectrum for ≡C-H on diamond matches the ≡C-H in ethane.

In addition there have been several studies of the diamond surface using molecular modelling theories. These include Linear Combination of Atomic Orbitals and ab initio Hartree Fock methods. (Lopez et al 1981, Bambakidis et al 1984, Barone et al 1985). These calculations all involve hydrogen as the surface adatom, possibly because of the more tractable calculations with the simpler atomic orbitals involved. There is apparently reasonable agreement with experimental observations of bond energy and bond lengths though little can be deduced from these studies about the relative reactivity of oxygen and hydrogen towards the surface carbon atoms.

Adsorption on Diamond Powders

The early work of Barrer (1936) and the comprehensive surface analyses of Sappok and Boehm (1968) were conducted with finely ground diamond powder. Barrer remarks on the apparent microporosity of his diamond powder, and it is clear that there will be a far higher frequency of edge sites and even internal surfaces on a powder than on a macroscopic crystal. More recently, Matsumoto et al (1977 and 1979) have studied the uptake of oxygen and hydrogen from the respective molecular gases and water on diamond powders by thermal desorption mass spectrometry. The powders were first outgassed at 1420 K. Temperatures higher than this produced unreactive surfaces, possibly by reconstruction of the surface. On this surface, temperatures of higher than 670 K were required to chemisorb hydrogen, although oxygen was chemisorbed even at room temperature. By contrast water vapour induced the adsorption of hydrogen through decomposition, even at room temperature, and the atomic ratio of oxygen to hydrogen was 1:2. At higher exposure temperatures, the oxygen was lower - i.e. replaced by hydrogen.

If the outgassing did not produce reconstruction, then presumably the dangling bonds were preserved, as in the newly cleaved state, and we could expect water vapour (or liquid) to react towards diamond surfaces in the same way producing a mixed hydrogen:oxygen surface. This augments the work of Bansal et al (1972) using an ultrasensitive pressure measurement technique to follow the uptake of oxygen. They concluded that up to 1,03 x 10^{19} atoms of O per m^2 could adsorb on an outgassed powder by exposure at up to 414 K, 0,07 mbar pressure.

These results were found for powders which had been activated by high temperature vacuum outgassing. The upper limit temperature of 1420 K was imposed to prevent the reconstruction of the diamond surface. A reconstructed surface is unreactive towards molecular oxygen and hydrogen, although potentially reactive towards atomic or microwave excited hydrogen, oxygen and nitrous oxide (Thomas 1979).

To conclude, there is conflicting evidence for the existence of both surface hydrides and a variety of surface oxides, or functional groups and, evidently, controversy as to the most frequent occurrence. Most of the definitive chemical analysis has been done using powders, which have a surface atypical of a large crystal because of the severe mechanical stressing required to pulverize diamond (Barrer 1936).

The natural hydrophobicity of diamond in nature, an oxygen rich atmosphere, remains a puzzle if we assume that oxygen groups on the surface will interact strongly with water, to produce a hydrophilic surface.

1.2 Wetting

Definition

In everyday usage, wetting means that water spreads completely over a solid surface, or alternately, that on withdrawing a solid surface from water, an unbroken film of the liquid persists (Adamson 1967). This definition does not require the use of the concept of a contact angle but for that reason it permits identification of only two classes of solids :

wettable - an unbroken film can be seen on the surface after removing from the bulk water, with no droplets

non-wettable - discrete droplets appear on the surface of the solid.

Because of the hysteresis of wetting, a droplet of water may be formed on a surface when dry, but after immersion, the surface may be covered by a film which will then absorb any droplets placed on the surface. A quantitative measure is provided by contact angles. For most surfaces, with microscopic roughness, the contact angle must be qualified by specifying whether the surface is being immersed (*advancing angle*) or drained (*receding angle*).

The Contact Angle

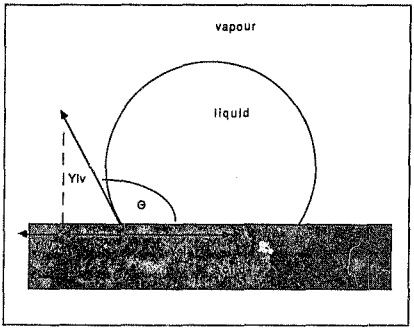
Young (1805) provided the first analysis of the interaction between solids and liquids, which in many cases gave constant observable angles of contact between the liquid and the solid. Figure 4 shows the droplet, with obtuse angle of contact, used by Young in his argument, which was essentially a mechanical force balance. Although Young's presentation is in rather archaic prose, which makes interpretation of the mathematics difficult, he is credited (Bikerman 1970) with recognizing the following equation :

$$\gamma_{sv} = \gamma_{sl} + \gamma_{lv} \cos\theta \qquad \ldots\ldots \qquad (1)$$

where the γ's are surface tensions ("attractive forces" in Young's terminology) acting between two of the three phases s,l and v representing solid, liquid and vapour respectively and θ is the angle of contact of the liquid on the solid, measured through the liquid phase.

The development of the same equation using surface energies, which are thermodynamically more acceptable quantities, is covered in Appendix 1. The contact angle provides a measure to characterize the wetting behaviour of a surface more effectively. The point at which a surface is classed as non-wettable may depend upon the application. Wetting behaviour has application in many fields :

fig 4 the mechanical equillbrium of Thos Young (1804)



$$Ysv = Ysl + Ylv \cos\Theta$$

note that θ is obtuse - cos θ is negative

TABLE 3 - CLASSIFICATION OF WETTING BEHAVIOURS BY CONTACT ANGLES

Application	Contact Angle for Non-Wettability (degrees)	References
Waterproofed cloth	greater than 90 advancing	Adamson 1967
Gluing	greater than zero advancing	Zisman 1964
Powder mixing (pastes)	greater than 45 advancing	Bikerman 1970
Flotation	greater than 0 receding	Rao 1974
Tertiary Oil Recuperation	greater than 90 (vs oil)	de Gennes' 85

Apparently there is no universal definition of a wettable surface, and even the contact angle must be qualified by specifying whether the surface is being immersed (advancing angle) or drained (receding angle). In mineral recovery by flotation, a bubble must make contact with a submerged particle, so the receding angle is important. In the case of the diamond surface, the native non-wetting behaviour of many diamond crystals permits separation from the ore by a process of selective adhesion to a "grease" or petroleum jelly phase. This apparently unsophisticated process - similar to methods described by Herodotus in 425 BC (Dasher et al 1943)- is still in use as an effective technique for the separation of diamonds. However, the process is inapplicable in some locations because of alteration of the diamond surface which gives rise to wettable or "refractory" behaviour. Better understanding of the causes of this alteration will assist in the improvement of diamond recovery efficiency.

There are other applications of finished diamond where the low wettability, and low friction, are important. Examples are diamond microtomes for eye surgery, styli for surface roughness gauges (Talysurf) and the domestic stereo record player (Davies 1984).

Contact angle measurement is the most direct method of characterizing wetting behaviour. However, the method is often criticised on the following grounds:

Geometrical Difficulties

The angle, being a geometrical measurement, is somewhat dependent upon the form of the liquid phase and the experimental method. Large discrepancies can occur. This is evident in some cases where sessile drop and captive bubble measurements on the same surface were in disagreement by up to 30 degrees (Gutierrez Rodriguez et al 1984). This can be explained to some extent by the difference in the stability of aqueous films when in hydrostatic equilibrium with a bulk reservoir of liquid, and when undergoing draining under gravity and evaporation (de Gennes 1985).

Thermodynamic Validity

There has been some controversy as to the existence of a true thermodynamic contact angle, one defined only by the free energies of the interfaces. This is covered in more detail by Neumann (1974) and a simpler approach is presented in Chapter 2.2.

Alternative Techniques

There are other methods for measuring the energy of interaction between a solid and a liquid, or two competing fluids. These are :

Adsorption Isotherms

The two dimensional "film pressure" of an adsorbing vapour is defined as :

$$\pi = (dG/dA)_{p,T,n} \qquad \ldots\ (2)$$

where G is the Gibbs free energy of the adsorbed film, A is the specific surface area of the adsorbent.

It has units of milliNewton per meter, or milliJoule per square metre, and so is dimensionally equivalent to a surface tension. The surface energy of a solid in equilibrium with a pure vapour is reduced by the surface pressure of the adsorbed film of that vapour, and so correctly, the solid surface tension used in the Young's equation should be adjusted by subtracting off the film pressure. Stasczuk (1986) has suggested that the thermodynamic relationship between the film pressure of an adsorbed vapour, below its critical point, and the work of adhesion of the liquid on the solid can be used to derive the wettability of the solid. He has used a plot of film pressure versus extent of adsorption of water to calculate the spreading coefficient :

$$S \text{ (water on graphite)} = \gamma_g - \gamma_{gw} - \gamma_w \qquad \ldots\ldots (3)$$

A positive spreading coefficient indicates a hydrophilic solid. For graphite, Stasczuk obtained a spreading coefficient of -53,7 mJ/m^2. By rearranging (3) and combining with (1) :

$$(\gamma_w + S)/(\gamma_w) = (\gamma_g - \gamma_{gw})/(\gamma_w) = \cos\theta = 0{,}25$$

This gives a contact angle of 75 degrees, reasonably close to the experimental value for graphite of 80 degrees.

Microcalorimetry

The adsorption of liquid at the solid surface, displacing a neutral gas or a less favoured liquid, produces a heat effect of the order of 10 to 100 mJ/m^2. This has been used by Sappok and Boehm (1968) in classifying diamond powders after hydrogen and chlorine treatment. The heat of wetting relates directly to the work of adhesion and hence wettability. Highly sensitive microcalorimetric apparatus is now commercially available (Microscal 1985).

Both these techniques require a fine powder, with a high surface area, in order to achieve measurable and reproducible results. In the case of diamond, the crushing and blending of the powder produces a very angular powder (Bansal et al 1972) with an unspecified mixture of true crystal faces. For this reason, and because previous surface chemical studies on diamond have made use of powders, a contact angle technique on macroscopic smooth surfaces of diamond was adopted for this study.

Wetting by Metals

Industrial diamonds are often bonded into an abrasive wheel using a metal phase or solder and in this case the metal must wet the surface of the diamond to create the adherent bond. The wear of diamond tools during machining is thought also to proceed by adhesion of the metal to the diamond. Experiments to determine the wetting and adhesion of several diamond:metal systems have been reported (Tanaka 1977, Naidich 1984, Miyoshi 1980). The conditions under which these experiments were conducted, i.e. ultravacuum, with argon ion etching of the surface, or at high temperatures and reducing conditions, makes the results of no use in determining the wetting of natural diamond by water.

Dynamics of Wetting

A review of the statics and dynamics of wetting of solids by water and other liquids has been given recently (de Gennes 1985). The author points out that, although the fundamentals of liquid spreading have been known for 180 years, poor preparation and characterization of surfaces has made experimentation difficult and only recently has spreading behaviour been adequately correlated with chemical composition of the phases. In particular, the phenomenon of hysteresis of contact angle, caused by physical roughness and chemical heterogeneity, affects all but the most ideal of systems. Exceptional cases, like highly purified polymer films on glass substrates, or polymers remelted between optical flats are often used in fundamental studies (Johnson et al 1977, Owens et al 1978). Realistic studies of mineral systems cannot be done in this way. Adamson (1967) suggests that hysteresis of contact angle is essential for efficient flotation of minerals. The effect of roughness on wetting and spreading has been reviewed by Mason (1978).

The recovery of mineral particles by flotation or adhesion occurs in fractions of a second. By contrast, some experimental techniques of contact angle measurement call for equilibration times of 10 minutes before reading the angle. The approach taken in this study involves the measurement of contact angles during interface advancement or recession, i.e. truly dynamic angles.

The objective in this work was to determine the wetting of diamond surfaces, using water or aqueous solutions. The surfaces of the diamonds would not be the vacuum desorbed, or argon ion etched surfaces most often used in Ultra High Vacuum studies, but mechanically prepared surfaces, with atmospherically stable surface adsorbed species. The need to approach the conditions applying in a real diamond plant ruled out the use of diamond powders. Techniques directed towards surface energy determination by, for instance, calorimetry or gas adsorption isotherms were not employed. With these, there is always the difficulty of translating results found with diamond powders to the practical situation of macroscopic surfaces. The planar surfaces of the test diamonds were well suited to the spectroscopic techniques used to detect surface adatoms and help explain changes in wetting behaviour.

1.3 Surface Forces

The interaction of a liquid with a solid surface leads to partial or total wetting. Young (1805) explained his observations of water and mercury on glass and metals by invoking two types of interatomic force :

1. an attractive force with a range of only one or two atomic diameters and "perfectly constant in its magnitude, throughout the minute distance to which it extends " and

2. a long range repulsive force with inverse linear relationship.

With this model he was able to show why menisci adopted the shapes they do, why capillary pressure existed and how the cosine of the contact angle should be related to the relative strengths of the interaction of the

elements of fluid and solid. The forces he incorrectly assumed to be dictated by the specific gravities of the phases only, so that the high surface tension of mercury follows from its high density.

In the one hundred and eighty years since then, colloid and interface scientists have refined this idea and classified a greater number of intermolecular forces of differing ranges (Israelachvili et al 1977). So for instance, the contribution of the gravitational forces is now known to be insignificant. Dispersion forces, which arise from the correlation of electronic motion in nearby atoms causes the attractive force in most liquids. In contrast to Young's analysis, it is the repulsive force which is short range, and the attractive force which is of greater range, giving rise to effects observable in the colloid size regime.

Surface Tension of a Pure Liquid

Bikerman (1970) provides a derivation for Laplace's equation :

$$\Delta P = \gamma_L \left(\frac{1}{R_1} + \frac{1}{R_2} \right) \qquad \ldots\ (4)$$

which relates the macroscopic pressure drop across a curved meniscus to the sum of the curvatures of the surface. The derivation proceeds by integration of the resultants of the forces of attraction of the elements of liquid in the meniscus for a point in the curved surface. The coefficient of proportionality, γ_L, which has the units of a tension, is shown to depend directly upon the mathematical function defining the intermolecular forces. Since this coefficient is known to be the surface tension, which can be observed experimentally, it follows that the surface tension depends directly upon the sum of the intermolecular forces which operate between molecules of the liquid. This is strictly true only for a liquid in equilibrium with its own saturated vapour. Usually the presence of air in the vapour phase causes an insignificant change because of the very weak dispersion forces which act between vapour phase molecules and liquid.

In water, for instance, the dipole moment of the molecule gives rise to additional polar attractive forces, hence a large increase in surface tension by comparison with nonpolar liquids, where only dispersion forces are present. The metallic bonding in mercury is now accepted to be the major component, 280 mJ/m^2 in a total of 480 mJ/m^2, in the interatomic attraction, and hence surface tension of mercury.

Interfacial Tension

When two liquids, or a liquid and a solid, are separated by an interface, a similar relationship between interfacial tension and the intermolecular forces between molecules in each phase, and across the phase boundary might be anticipated.

This has been shown by Fowkes (1971) for the case of liquids which interact by dispersion forces only :

$$\gamma_{12} = \gamma_1 + \gamma_2 - 2\sqrt{\gamma_{1d}\,\gamma_{2d}} \qquad \ldots\ldots (5)$$

where γ_1 and γ_2 are the surface tensions of the individual liquids, and γ_{1d} is the dispersion component of surface tension.

Good and Girifalco (1957) and Good and Elbing (1971) have developed a generalized theory for the estimation of interfacial energies of liquids which can interact by polar and induced polar forces :

$$\gamma_{12} = \gamma_1 + \gamma_1 - \phi\sqrt{\gamma_1\,\gamma_2} \qquad \ldots\ldots (6)$$

The factor ϕ, will vary for different liquid combinations because of the variable contribution due to hydrogen bonding, dipole and induced dipole effects, and even geometrical effects due to molecular shape. A similar relationship is expected for solid:liquid interfacial energy. In the case of diamond and water, the existence of polarizable hetero-atoms on the surface would give rise to additional interatomic forces, which would be

reflected in an increased value of ϕ in eqation (6) and a decreased interfacial energy of the liquid:solid interface. By Young's equation (1), this would increase the wettability.

The types of intermolecular forces possible, and the chemical groups most likely to give rise to these forces will be reviewed briefly.

London-Van der Waal's Forces (Dispersion Forces)

These derive from the Lennard Jones Potential, the interaction of electron clouds of neutral atoms. They have therefore a long range attraction (inverse sixth power) and a short range repulsion (inverse twelfth power) the attractive component is the major contributor to the liquefaction and surface tension of unpolarized molecules like hydrocarbons The repulsive component is of interest in defining the Van der Waal's radius, the shortest distance to which atoms which are not chemically bound to each other, will approach. This is important because it gives rise to a steric resistance to close packing of hetero-atoms on the relatively tightly spaced lattice of the diamond. The dispersion component of the surface tension of water is 21,8 mN/m, or less than one third of the total (Rao 1974). All atoms and molecules interact by dispersion forces to a varying degree, depending upon the magnitude of the Hamaker constant, A_i:

$$A_i = \pi^2 n_i^2 C_i \qquad \ldots\ (7)$$

where n_i is the number of centres (atoms or molecules) per unit volume, and C_i is the London constant for the atom.

Substitution of surface carbons on diamond by oxygen or even hydrogen will not cause a large change in the dispersion force interactions with liquids

Dipole-Dipole Interactions

These arise from the interaction of the Keesom potentials of two permanent dipoles. The force follows an inverse sixth power dependence, and is the important component in systems involving water and oxides. The formation

of surface oxides on diamond, particularly those with large polarization of the >C-O bond, as in a carboxylic group, should greatly increase this component and so also the wettability.

Dipole -Induced Dipole Interactions

Although less important than dipole-dipole forces, these arise from induction of a sympathetic dipole on a neutral atom or molecule in the field of a permanent dipole. The Debye potential leads to an inverse sixth power dependence of the force. This is important in many liquid-liquid systems. Again, polarized surface oxides on diamond should increase this type of interaction with water.

Hydrogen Bonds

These were considered by Pauling (1960) to be partly covalent and partly dipole-dipole in character, varying from bond to bond. π electrons can act as the donor (Fowkes 1971). They are highly short range and directional, so they cannot be included in continuum type models for interfacial energies. There is currently interest (Abraham et al 1986) in the characterising of molecules and functional groups as hydrogen bond donors of varying HBD acidity, and hydrogen bond acceptors, of varying HBA alkalinity. This allows the explanation and prediction of many phenomena, such as solvent effects on reaction rates, which had previously been poorly understood. It is likely that small electronegative atoms reacted with the diamond surface, such as oxygen or fluorine, will provide sites for hydrogen bonding of water molecules and thus decrease the solid:liquid interfacial energy, and increase the wettability.

Laskowski et al (1969) propose that the instability of water films on hydrophobic surfaces is due to the deficiency of hydrogen bonds in these films, as compared with bulk water, caused by the proximity of the non-hydrogen-bonding surface. Van Oss et al (1986) suggest that many effects involving bio-molecules and low energy surfaces, previously explained as "hydrophobic interactions" can be better explained in terms of the competition for hydrogen bonding. A similar argument may be applied to

explain the "structural" component of the disjoining pressure of a thin water film (Pashley 1978). The presence of oxygen or hydroxyl groups onthe diamond surface, as sites for hydrogen bonding of water molecules, will strongly affect the wettability. Hydrogen atoms on the diamond surface would create no site for hydrogen bonding because carbon is incufficierctiy electronegative.

Metallic Bonds

The metallic bond contributes to the high surface energy of mercury, and similarly, that of high temperature molten metals, but plays no part in the wetting of diamond by water.

In conclusion, a solid which has surface groups which can participate in hydrogen bonding with water will appear hydrophilic. Conversely, the presence of non-polar surface compounds will lead generally to hydrophobic behaviour.

CHAPTER 2 - THEORY OF WETTING

2.1 Capillarity and Buoyancy

When a solid is partially immersed in a liquid, or when a liquid droplet is placed on the surface of a solid, there are macroscopic forces which act between them. These are obviously, at the most fundamental level, caused by interactions between the material constituents, atoms or molecules of the two phases, but in the continuum model, and at the level at which physical measurements are made, it is useful to separate the forces into buoyancy and capillarity, or equivalently, "body forces" and "surface forces".

The analysis is made more complex because the surface tension can be viewed in one of three ways (Hiemenz 1977) :

1. as a force per unit length of a line in the surface of the fluid- most easily visualized by lifting the liquid surface on a wire frame as in the surface tension method of Lenard (1924).

2. as a surface energy per unit of surface area, which allows for a thermodynamically rigorous derivation showing that the surface tension is the increment in the Gibbs free energy per unit increment in area, i.e. a state variable.

3. as a reduced pressure in a surface zone of thickness approximately 10 Angstroms. This follows from the derivation of surface free energy (above), and the thermodynamic identities which, for a single phase, lead to :

$$\hat{G}_i = \frac{1}{\hat{V}} (F_i - F_\infty) = P_\infty - P_i \qquad \ldots\ (7)$$

$\hat{G}_f$ = Free energy per unit volume
$\hat{V}$ = molar volume
F = free energy per mol
P = pressure
∞ = in the bulk (at infinity)
i = in the interface.

Jameson and del Cerro (1976) have pointed out that although the reduced pressure in the interface is a scalar property, it takes its direction from the inclination of the interface at every point.

The existence of a reduced pressure over a microscopic line width must create very large stresses at three phase boundaries and has lead to criticism of the "force balance" method of deriving Young's equation and Neumann's triangle law (Lester 1961). However, it is shown that, where the Young's * modulus of a solid substrate is greater than 10^9 N/m^2, the surface deformation is unimportant. Diamond has the value 10^{12} N/m^2.

The appearance of surface tension as a pressure creates difficulties, because buoyancy forces are transmitted to the solid by the pressure exerted over all the immersed surfaces. However, by the use of a simple convention, it is possible to separate the effects of buoyancy and capillarity.

Buoyancy

Buoyancy i that component of the force which would vanish in a zero gravity field. It arises because of the gravitational potential energy field, which in turn leads to a hydrostatic pressure gradient in a body of liquid. Where this body of liquid impinges on a solid, a vector integration of the product of the pressure field with the unit inward

[* This is the same Young. It is a mark of the genius of the man, Thomas Young, that he made the most significant discoveries in at least three fields, being the mechanics of solids, and optics, as well as the field of fluid wetting, under study here.]

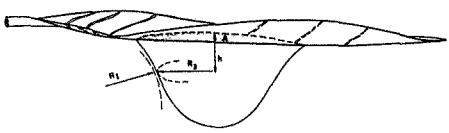
normal to the surface gives the net thrust. Thus Archimedes' principle can be proven in an elegant way by the use of the divergence theorem. Since there is a pressure gradient in only the vertical direction, of magnitude *equal to the density of the liquid*, the net thrust becomes an upward force equal to the density of the liquid multiplied by the volume of the body immersed below the planar surface of the liquid (Batchelor 1967).

To be consistent, forces due to hydrostatic pressure which act downwards on a solid must be classified as buoyancy forces, with appropriate sign. An interesting example is that of a rain droplet on the underside of a leaf, as shown in Figure 5. It is common to hear that it is hanging "by surface tension". And yet an identical droplet on the upper surface of the leaf is not accused of levitating the leaf, although its coordinate system is a simple inversion of the pendant drop. In the case of the pendant drop, its weight appears as the product of the wet area, and the reduced pressure at the plane of contact with the leaf. The pressure here is reduced by the hydrostatic head from the leaf bottom surface down to that point in the droplet where its two radii of curvature cancel out at which plane the pressure in the droplet is equal to *atmospheric pressure, by Laplace's* equation. An interesting thought experiment can be done by taking the leaf into zero gravity - in a space capsule. The droplet would still adhere to the leaf, because the surface energies which cause wetting are not affected by gravity, but there would be no net force on the leaf caused by the presence of the droplet. The component of the surface tension acting normal to the leaf surface at the perimeter of the droplet is opposed by the excess pressure within the droplet caused by its curvature, as explained by Lester (1961). The components parallel to the surface are at equilibrium according to Young's equation [1].

In the case where a body penetrates the surface of a liquid, with distortion of the liquid surface so that a meniscus is formed, the buoyancy forces are calculated from the volume of the body which is immersed below the plane of the liquid surface far from the meniscus.

Similarly, if a body of finite cross-section is well wetted and lifted clear from the surface of the liquid, a negative buoyancy, or downthrust

fig. 5 a droplet hanging from a leaf



The droplet does not hang "by surface tension"
The weight of the droplet is transmitted to the leaf hydrostatically, being the product of the droplet area, A, and the hydrostatic head -h*ρ*g.
h is the height to that plane in the droplet where the radii of curvature, R1 and R2, are equal in magnitude and opposite in sign. The pressure on this plane is atmospheric pressure.
The normal component of the surface tension is balanced by an increase in pressure inside the droplet due to curvature. This could be verified by releasing the leaf in a space capsule at zero gravity. The droplet would then exert no nett force on the leaf.

results, and this must be corrected for in any calculation of the capillary force.

Capillarity

When a condensed phase is sufficiently fluid so that its molecules can re-arrange to reduce their interfacial energy, this appears as capillary action or capillarity. Examples are water droplets forming spheres, or even oscillating jets, water being drawn up by a porous cloth, or in a fine tube, and oil droplets floating in the form of lenses on a water surface. Solid surfaces have a free energy of formation, but the bulk phase cannot flow so as to change the exposed area. Stresses which exist in the surface, which reflect work done in the creation of the surface, cannot be relieved in the same way as for a liquid surface. The surface energy of importance in the wetting of the solid becomes apparent only indirectly, when one or more fluid phases interact to form droplets of various shapes on the solid surface. Fortunately, Young's equation (1 above) involves the *difference* in surface energy between the dry and wet state, so these additional energy terms subtract out of the equation.

The first equation of capillarity, named after Laplace (1806) and listed above as equation (4), relates the excess pressure within a droplet to the surface tension and the curvature of the droplet.

Young quotes the same equation in his paper of December 1804, introducing it by saying "It is well known.." and presents a derivation based on a similarity to the two dimensional case of line tension and curvature. There is a more formal derivation by Bikerman (1970).

The term "capillary" derives from the fine bore (*capillus = hair*) tubes used by researchers of the 19th century in measuring surface tensions by the method of capillary rise :

$$\rho g h = 2\gamma/r \qquad \ldots\ (9)$$

ρ = density
g = *gravitational constant*
h = height of meniscus rise in capillary
γ = surface tension

This method assumes a zero contact angle and a hemispherical meniscus, neither of which is likely to to be true excert in special cases. A more general analysis can be done for a planar meniscus, i.e. the liquid surface near a semi-infinite vertical wall (Bikerman 1970). For any fluid, a constant with the dimensions of length can be defined :

$$a = \sqrt{\frac{2\gamma}{\rho g}} \qquad \ldots\ (10)$$

and it can be shown that this is the height to which the fluid would rise, opposing gravity, against a fully wettable vertical wall. The meniscus formed at such a wall has a shape which is defined only by the capillary constant. Using the height and the angle of inclination of the surface as parameters it is written :

$$z^2/a^2 = (1-\cos\phi)$$

where ϕ is the slope of the meniscus at the line of contact with the vertical wall, the slope is shown to be :

$\phi = 90-\theta$ where θ is the contact angle.

This is the basis of the planar capillary rise method of measuring contact angle (*Cain et al 1983*). *In theory, for a totally wettable surface, the* same technique could be used to measure surface tension, instead of a force measurement. In practice total wetting leads to a very indistinct three phase line, even a precursor film of visible thickness, (de Gennes 1985) which makes this non-useful.

There is thus a difficulty in the analysis of forces when a liquid phase interacts at a solid. The surface tension can be simplified to a force per unit length. But in addition to the action at the three phase line, there will be a change in the pressure distribution of the liquid because of the curvature in the liquid interface. In many instances the effect is to cancel the normal component of the surface tension at the three phase line, as in the example of the droplet in space mentioned above. A further interesting example is the supposed *perpetuum mobile* formed by a floating body which has one or more sides with poorer wettability than the others, so that the meniscus is more nearly horizontal on that side. By surface tension components alone, this side should then drag the body across the surface of the water. (Not to be confused with a camphor driven "boat", which uses the spreading pressure of the camphor to move, and comes to rest when the water surface is covered with camphor). In practice, the liquid in the meniscus on the well wetted side is below atmospheric pressure and the combination of the normal component of the surface tension and the "suction" of the meniscus is equivalent to the surface tension acting horizontally around the body. After integrating this around the whole body there is no nett force in the plane of the liquid surface.

In zero gravity, the capillary forces are all important and wetting effects have been underestimated during the design of experiments (Noma et al 1985).

Capillary forces are identified as those forces which vanish when the surface tension of the liquid phase tends to zero. Then the capillary constant goes to zero, we expect no meniscus rise or depression, and the undisturbed fluid will exert only buoyancy forces.

The distinction between buoyancy and capillary forces is important in the determination of contact angle by measuring the capillary weight or force. (see section 4.2). The term capillarography has been proposed by Mason (1978) for this technique.

2.2 The Thermodynamic Contact Angle

When the contact angle appears in an equation relating surface tensions, its meaning is consistent with Newtonian mechanics. Forces can be resolved along orthogonal axes. However, the surface tension of a solid is an ill-defined concept. If we choose to regard the interface terms in Young's equation as surface free energies, then the concept of cos θ as a component of a scalar property becomes untenable. In the simpler "energy derivation", excluding gravitational potential energy terms, the cosine term appears as the ratio of two incremental surface areas in the minimization of the sum of the free energies. Various assumptions about the preservation of the shape of the droplet on the solid must hold for this to be true.

Alternately, by rearranging equation (1)

$$\cos\theta = (\gamma_{sv}-\gamma_{sl})/\gamma_{lv} \qquad \ldots. (11)$$

The RHS is the ratio of two energy terms. The numerator, being the difference between the surface energies of the same element of surface before and after immersing in the liquid, is free of surface stress energies, and is a thermodynamically sound quantity. The denominator is the well defined surface tension (or surface free energy) of the liquid vapour interface. Their ratio is then a valid thermodynamic property. Since the product $\gamma\cos\theta$ is known as the "adhesion tension" (Bendure 1973), we might call it the dimensionless adhesion tension for wetting by water. It has the advantage over the contact angle, in that it can assume values greater than 1 ($\theta = 0^0$). This is the state of spontaneous wetting, when the liquid spreads over the solid. On a large horizontal surface, a *droplet of such a liquid will spread so as to thin the film of liquid* formed until the liquid:vapour interface starts to approach the liquid: solid interface. At these small distances, additional forces come into play, giving rise to a "disjoining" pressure, so that the final droplet shape is a flat pancake, as described by de Gennes (1985) and not a monomolecular film.

When the dimensionless adhesion tension is less than 1, but greater than -1, a wetting droplet or meniscus forms. The angle at the edge of this droplet is regarded as the arc-cosine of the quotient in equation (10).

There has been doubt whether this geometrical measurement should be used as the angle which truly represents the desired thermodynamic property. Some objections follow :

Core Region

Bikerman (1970) and Jameson and del Cerro (1976), argue that the use of the two phase interfacial energies cannot be correct near the three phase line, where the proximity of the third phase will affect the potential of molecules in the interface. To refute this, Neumann (1974) and de Gennes (1985) concede that there may well be a core region where the contact angle has a different value, but the observed contact angle, at distances of tenths of a millimetre from the solid surface, is dictated by macroscopic energy terms and follows from Young's equation.

Gravitational and Curvature Energy Terms

The usual derivations, either by force or energy arguments, ignore gravitational forces and energies, and the energy associated with curvature of the droplet. Derivations which ignore gravitational energy terms can be replaced by particular cases where they can be included. Pethica and Pethica (1957) give a derivation for a large flat topped droplet, with gravitational potential energy, and show by a macroscopic energy minimization that the Young equation still holds good. De Gennes (1985) shows that the energy associated with curvature of the meniscus can be *neglected for menisci of millimetre dimension and liquids of low* compressibility. This might not be the case in space, for example, where menisci may extend for large distances because of the reduced gravity.

The meniscus weight method of measuring adhesion tension can be shown to include gravitational potential energy in its derivation (Appendix 1). In addition, there is little curvature for a flat plate, and principally in the dimension normal to the face of the plate.

The greatest attraction of the capillary weight technique, is that the adhesion tension appears automatically as a force per unit length, so assumptions about droplet slope and shape are not required. Allowing for effects of hysteresis and dynamics of wetting (Bayramli et al 1981), this would appear to be the most noncontroversial method of extracting a thermodynamic reading from a wetted surface.

2.3 Kinetic and Hysteresis Effects

Approach to Equilibrium

The true contact angle, a state of free energy minimization, may not be attained in practice.

If the spreading of the liquid is occurring slowly, by for example spontaneous creeping of a vertical meniscus, there may be energy barriers associated with the progress of the wetting line. Consequently the advancing angle may be more obtuse than the equilibrium value. The receding angle may similarly be more acute than the equilibrium value because of similar energy barriers to movement of the wetting line. The origin of these barriers in rugosity (physical roughness) is described by Johnson and Dettre (1964), and the effect of chemical heterogeneity, microscopic areas of greater or lesser hydrophobicity, has been discussed by Neumann (1974), and by Oliver et al (1980).

The viscosity of the liquid will tend to slow the spontaneous spreading and so some researchers (Gutierrez Rodriguez 1984) advise the use of a ten minute equilibration time, or even light tapping of the stage on which the experiment is occurring. Presumably the mechanical energy of the tapping helps to surmount small energy barriers.

This author has noted another effect with highly wettable ($\theta \longrightarrow 0$) surfaces when testing by the meniscus rise method. On first touching of the solid platelet by the ascending water surface, there is a rapid drawing up of the meniscus to a position of almost total wetting. The rate of wetting of the surface is so fast, that kinetic energy is imparted to the water near the

wetting front. Presumably there is a driving force until the wetting line reaches the position of the equilibrium contact angle, so that there is still some momentum (or kinetic energy) available to cause an overshoot. This can be seen in the capillarographic apparatus by withdrawing the meniscus, but without detachment, and then returning to the zero height datum - the level at which first contact was made. The value of the meniscus rise after inching up is lower than the value after first contact, or equally the contact angle is larger. This is in opposition to the usual hydration effect, i.e. a lower contact angle after prolonged exposure to water, and so the inference must be that the kinetic energy of the meniscus, which is present only during the first rapid advance, is responsible.

The left-hand-side of Young's equation as written in equation (1), represents the free energy change on wetting a unit area of surface. By the definition of free energy, this is the maximum possible non-PV work which can be released by the wetting process. By this argument, the state reached by rapid advance is probably a better measure of the thermodynamic contact angle than the state reached by inching up the three phase line. There is presumably a similar process when a drop of liquid is brought into contact with a horizontal dry surface for the first time. The spreading front must achieve considerable velocity, and hence kinetic energy, which would be dissipated by further advance after the driving force for wetting had reached zero. Nevertheless, the accepted method for contact angle measurement demands that the droplet must be formed and then slowly inflated or deflated to produce the advancing and receding angles.

Neumann (1974) and Hiemenz (1977) advocate the use of the average of the advancing and receding angles (presumably at the same velocity) as the best approximation to the thermodynamic value. This will to some extent correct for the kinetic effect mentioned above. In this work I have adopted the cosine average, since this gives equal weighting to the errors which may arise through weighing or buoyancy correction in advancing or receding directions respectively :

$$\theta_{th} = \text{arc cos } ((\cos\theta_a + \cos\theta_r)/2) \quad \ldots\ldots (12)$$

Multiplying the cosine of this angle by the surface tension of the liquid phase gives the adhesion tension, or in energetic terms, the (negative) free energy of wetting of the surface. This has a range of 0 to 72,5 (approx) mJ/m^2 for aqueous systems. Negative values (i.e. positive free energy changes) are possible, on for instance paraffin wax surfaces, but these values were rarely seen with diamonds.

CHAPTER 3 - EXPERIMENTAL METHODS FOR CONTACT ANGLE MEASUREMENT

3.1 Optical Methods

Optical methods of measurement of contact angle are performed on small droplets or on small bubbles, often with the aid of microscopy and photographic enlargement to improve the accuracy (Billett et al 1968, Lubetkin 1985).

Recently (Huh et al 1983), a method of numerical regression for determination of the contact angle from the profile of the entire droplet has been discussed. This method makes use of electronic aids for digitization of photographic profiles and an iterative method of solution of the differential equations for the drop profile. Apparently this allows the measurement of sessile drops with contact angles below 20 degrees, something which is rarely reported confidently by direct observation.

Allain et al (1985) have used a laser for measuring the contact angle of a liquid droplet on a transparent substrate. The beam is directed down through the droplet and diffraction at the droplet edge produces a circle on a screen below the droplet. The geometry of the system, along with refractive index data, permits direct calculation of the contact angle, averaged around the droplet perimeter.

Although these indirect methods can improve the accuracy of measurement of the angle, there remain objections to the technique because of the arbitrary way in which droplets are formed, so-called equilibration times, and even the selection of the site on which the droplet is to be placed.

The use of a bubble instead of a droplet removes some of the problems of contamination of solid surfaces open to the atmosphere, but raises a further question. The interfacial energy of the bubble to solid interfaces complicated by the existence of a pressurized liquid film (de Gennes 1985). Guttierez-Rodriguez et al (1984) found consistently different values for captive bubble contact angles than sessile drop values on the same (coal) substrate. The captive bubble results were always lower - more hydrophilic.

Because of the ease of the experimental method, a first estimate of the wettability of a surface can be found from a sessile droplet measurement.

The major results of this study are for polished diamond surfaces. The nature of the diamond surface as it occurs in the host rock (kimberlite) cannot be directly deduced from these results. For this reason, a small number of optical measurements were made on the unpolished surfaces of Premier mine diamonds. Previously (Hartley 1978), measurements have been made on natural diamonds, but after rigorous chemical cleaning. In this instance, the diamonds were selected from the production of partially liberated "diamonds-in-kimberlite" which are currently recovered by X-ray machines. This is a recent development, and such diamond surfaces have not been commonly available before. The exposed faces were painted with Tipp-Ex, the composite carefully crushed using a controlled hydraulic ram, and the liberated diamond caught on filter paper. The previously embedded surface was then dusted off, first with filter paper wet with milli-Q water and then with dry filter paper. The diamond was positioned on an adhesive tape on a microscope slide, with the painted face down, and the microscope slide was mounted on modelling clay so that it could be swivelled to obtain the best levelling of a particular crystal surface.

The diamonds were viewed using a WILD MSA stereo microscope (type 374590) with a 45 degree mirror attachment in a thermostatted microscope laboratory. The surface was illuminated with a VOLPI cold light source and the droplets were photographed using the WILD MPS 45 35mm photosystem. Overall magnification of x9 was achieved, and by using slide film, further enlargement was possible.

Droplets of milli-Q water were formed using a syringe and square ground hypodermic needle, allowed to inflate until advancing angles were seen (approx 2 mm size) and then drained by means of fine ribbons of filter paper, so as to achieve receding angles. As far as possible, angles were measured (subsequently off projected slides) on both sides of the horizontal axis of the droplet, and where a reasonable estimate of the direction of the tangent plane to the diamond surface could be seen. To offset prejudice by the author, a second independent party did the same

constructions on a drawing board, onto which the slides were projected, and measured off the angles.

Apart from this testwork, all contact angles measured in this study were calculated from capillarographs.

3.2 Capillary Pressure

The pressure drop across a bed of powder, when water is being forced through the bed, is related to the capillary force exerted by the water in the small channels between particles (Dunstan and White 1986). Provided that data for the powder size are adequate, this can be related to the contact angle. The method appears to have merit where the subject of the wetting study is already a powder, for instance a paint pigment (Crow and Wooldridge 1968). Apparently the method is useful for powders of nearly round particles, but poor for jagged particles. For this reason, and because of the problems associated with characterization of diamond powders, this approach was not adopted.

3.3 Capillarography - Wilhelmy Plate

The weight of the meniscus formed around a prism with vertical sides is numerically equal to the product of the wetted perimeter, on a horizontal crossection, the liquid surface tension and the contact angle, averaged around the perimeter :

$$W_{capill} = p\,\gamma_{lv}\cos\theta \qquad \ldots\ (13)$$

This was first recognized by Wilhelmy (1863), who used totally wettable glass plates of well known dimensions and so measured the liquid surface tension. Provided the liquid surface tension is known, the contact angle can be calculated from an accurate weighing of the meniscus, with appropriate correction for buoyancy. The superiority of this technique on theoretical grounds is discussed in Appendix 1 and has been argued by Mason (1978) and Bayramli et al (1981).

Figure 6 shows the orientation of the capillary forces and buoyancy at a plate during immersion.

The most attractive experimental feature of this technique is the high precision, even for very small angles. The terms, p, perimeter and γ_{lv} the surface tension of water, can be measured independently to precision levels of 0,4 % respectively, even for relatively small test plates. This allows measurement of contact angles as small as 5 degrees with confidence, and at more typical angles of 50 to 90 degrees, the precision is better than 0,3 degrees. The non-linearity of the cosine function detracts to some extent in the low angle range, but this is still very much better than optical techniques, where measurement below 20 degrees is virtually impossible.

Other attractive [illegible] the technique are :

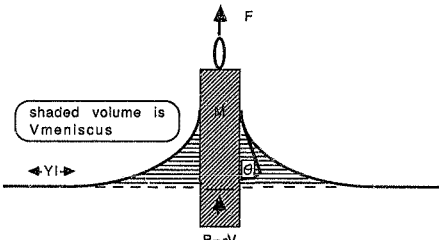
Each measurement at [illegible]ght datum is an automatic average of the contact angle around a perimeter. This perimeter is not necessarily at the same height as the datum, since there is usually meniscus rise, but for a prism or plate the perimeter is constant.

Measurements can be made at many heights up the face of the plate, so in effect an area-average contact angle can be extracted, the average of the perimeter averages over a range of heights. This is less subjective than the methods of averaging usually employed in optical studies.

Velocity effects can be standardized. The rate of meniscus advance or recede can be controlled closely and reproduced from test to test.

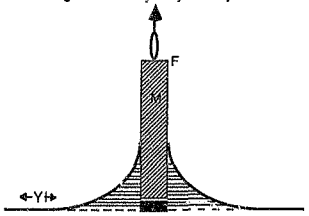
Hysteresis effects can be detected from the slope of the capillary force curve. This is discussed below in Chapter 7.1. Stable contact angle values are obtained from those sections of the capillarograph plot where the slope of the line is equal to the buoyancy slope. (The immersion of a body of uniform cross-section causes a constant increase in upthrust per unit depth immersed, conveniently called the buoyancy slope). This eliminates the need for subjective assessment of the behaviour of a droplet.

fig 6 Basis of the capillarographic method



Yl cos Θ . perimeter = ρgVmeniscus = F - Mg + Bg

an instance of negative buoyancy - hydrostatic downthrust



Slow changes arising from surface reactions can be followed by repeated traversals of the same surface. For instance, Kendig and Fadner (1985) have used the technique to study the effect of the electrochemical potential of a copper plate on its wettability.

There are some difficulties which need to be addressed :

Test Plate Shape

The test prism or plate must have vertical walls. Most cross-sections can be allowed (Herb et al 1983). In previous optical and electrical studies, natural diamonds have been polished into blocks and plates for ease of analysis, (Bharadwaj et al 1983), so this was feasible. Some materials, because of their friability, would not be suitable, although Johnson (1976) has used coated glass slides for the study of polymers. In use the platelet must be caused to hang with its major face vertical and its sides square. This can be proven by consideration of a thin plate of length l hanging vertically. The capillary force will be :

$F = 2l\gamma\cos\theta$ ... where θ is the contact angle - equal on both sides

When a platelet is inclined away from the vertical by the small angle $d\theta$, and since the contact angle on each side will remain constant with respect to the face of the plate, not the true vertical, the vertical component of the surface tension becomes :

$$F = l\gamma\cos(\theta + d\theta) + l\gamma\cos(\theta - d\theta)$$

this is transformed using a trigonometric identity :

$$F = 2l\gamma\cos\theta\cos(d\theta)$$

Since the cosine of a small angle, $d\theta$, whether positive or negative, is less than one, the maximum force occurs when the plate is vertical, and this gives the true contact angle.

Liquid Level Disturbance

The wetting liquid must be moved up to immerse the prism in a steady and uniform way. The vessel containing the liquid must be large enough to prevent interference between the wall meniscus and the wetting meniscus of the test plate.

The parametric equation for meniscus shape at a flat plate developed by Laplace (1805) is :

$$\frac{z^2}{a^2} = (1 - \cos\phi) \qquad \text{.... (eqn 14)}$$

by making the substitution $dz/dx = \tan\phi$ and re-arranging, the following differential equation arises :

$$\frac{dx}{dz} = \frac{B}{\sqrt{1 - B^2}} \qquad \text{where } B = 1 - \frac{z^2}{a^2}$$

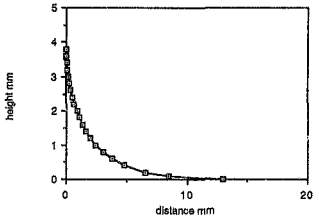
This differential equation can be solved numerically, taking care to use sufficiently small step size near the two asymptotes z=0 and z=a to develop the meniscus profile.
This has been done using a fourth order Runge-Kutta technique (Ralston et al, 1960) written for an Apple IIE computer.

The resulting profile appears as Figure 7.

It appears that the meniscus height is less than 0,01 mm at a distance of 12 mm from a fully wetted wall. A vessel diameter of 52 mm, with the test plate at the centre of the vessel, effectively separates the test meniscus and the wall meniscus.

Evaporation must be minimized, particularly during long experiments.

fig 7 numerical solution of meniscus curve for water



(exaggerated height scale)

Liquid Interface Cleaning

The liquid:vapour interfacial tension appears explicitly in the calculation of the contact angle. Water surfaces in contact with the air become contaminated by dust particles, some of which carry surfactants. The effect is to reduce the surface tension, hence causing an error in the contact angle measurement. There may be further complications caused by surfactant adsorption at the solid surface. The capillarographic cell must have a facility for excluding dust and laboratory air, and a system for renewing the water surface. This can be done by sweeping (as in a Langmuir trough) or vacuum cleaning the surface.

CHAPTER 4 - CAPILLAROGRAPHIC APPARATUS AND REAGENTS

4.1 Cell and Weighing Linkage

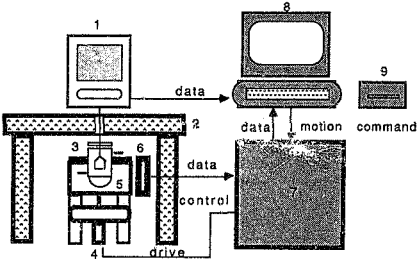
A schematic diagram of the capillarographic apparatus used in this study is shown in Figure 8. The elements are listed in a key to the drawing and more details are provided below. Figure 9 shows the cell with the close fitting lid used to exclude laboratory air. A trickle of high purity nitrogen (Air Products HP) was admitted to the cell through a distributor, aimed to avoid the liquid surface. The nitrogen was passed through a hydrocarbon trap (J & W Scientific, Rancho Cordova, California) and a Drechsel bottle containing reagent grade water at 25 °C. This was to inhibit evaporation in the test cell and was found to be effective. A fully wetting meniscus could be drawn onto a clean platinum plate and maintained at fixed meniscus weight for more than 8 hours.

The cell was thermostatted, normally at 25 °C, to a precision of approx 0,2 °C using a Labotec Julabo water bath. For low temperature tests, the water was diverted through a chiller.

MilliQ water was added to the cell through a small glass funnel which was drawn down to a tip. The tip retained a droplet of water and so provided a gas seal. Reagents to modify pH and ionic strength could be added through the same funnel. A feature of the cell, after a suggestion by Lubetkin (1985), is the facility for vacuum cleaning the interface. A hypodermic needle with a square cut tip protrudes through the lid to the level of the undisturbed planar water surface. This is attached to a vacuum line with a collection flask. The surface of the water can be drawn off in a "tornado" like effect, whilst adding clean water slowly through the funnel. This has the effect of sweeping surface impurities from the cell and allowed the maintenance of water surface tensions above 72 mN/m during long experiments.

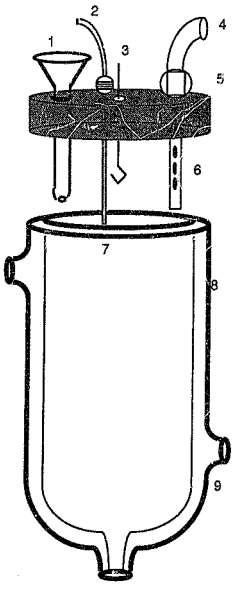
Figure 10 shows the type of clip used to hold the diamond test plate. The diamond was polished in the form of a spade, with a triangular peak which allowed positioning of the diamond in the clip in a reproducible manner.

fig 8 capillarographic apparatus - schematic



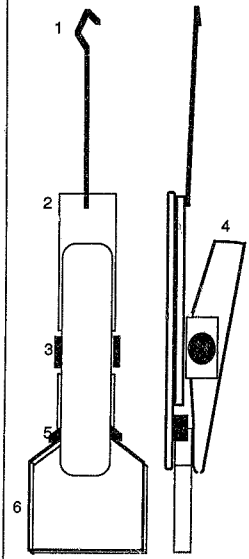
1. Mettler transmitting electrobalance
2. Balance table for underpan weighing
3. Introl precision positioning table (vertical)
4. DC motor with reduction box
5. Thermostatted glass cell with level reset and N2 atmosphere
6. Anilam 10 micron digital displacement transducer
7. Galil motion controller
8. Apple IIe microcomputer for motion and data processing
9. 5 1/4 " floppy disk data storage

fig 9 detail of capillarographic cell and lid



1. filling & addition funnel
2. sampling & cleaning extraction line
3. weighing linkage through 3 mm hole in lid
4. moist N2 supply
5. machined aluminium lid
6. low pressure N2 distributor
7. square needle tip for interface cleaning
8. 52 mm ID thermostatted glass cell
9. thermostat water inlet
10. test water drain.

fig 10 detail of clip for diamond test plates



1. hanger wire 0.4 mm brass
2. clip body, platinum
3. axle and rivet, brass
4. spring, hidden, steel
5. fitted vee-shoulder, platinum
6. diamond test plate

fig 11 capillarographic apparatus



fig 12 capillarographic cell

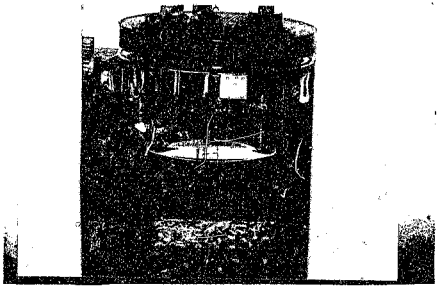
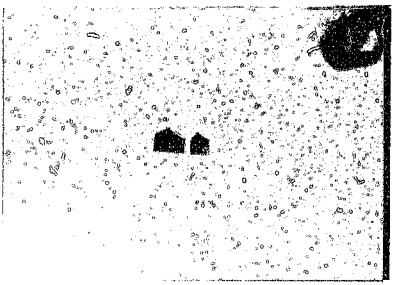


fig 13 diamonds used in wetting tests



The verticality of the diamond in the clip was adjusted by bending the hanger wire attached to the diamond so that the reflection of the diamond, when the diamond was suspended over a horizontal mirror, was collinear with the sides of the diamond. Two clips were made, one for the diamond with [111] major face, and one for the diamond with [110] major face. The body of the clip is platinum, to prevent corrosion product from affecting the water in the cell. The clips were cleaned by ultrasound in Contrad detergent (also called Decon in some countries), followed by three changes of milliQ water, and stored in a desiccator over silica gel when not in use.

Figures 11 and 12 show the apparatus and a close-up view of the diamond in the cell. The liquid surface has not reached the bottom edge of the diamond in Figure 12, so no meniscus can be seen.

4.2 Displacement and Force Transducers

Displacement Measurement and Control

The cell was mounted in a specially fitted anodized aluminium clamping plate which assured good verticality and no slip during elevation. The clamping plate was bolted to the platform of a precision positioning table (single axis table 2080-1, Introl, Edenvale, RSA), driven by a Unimatic MT2115 DC servomotor with 18:1 reduction box. The table was operated in the vertical mode, attached to a massive support frame of powder coated steel. The servomotor was powered by a Digiplan PWM4 servo drive, with 20 amp peak motor current and slewrate of 500Hz. The position of the table was detected by a digital linear displacement transducer (Anilam A10, Anilam Electronics, Milton Keynes, England) to an accuracy of 0,01 mm and a reproducibility of 0,01 mm in 150 mm. The displacement signal was processed by a motion controller (Galil DMC 100, Mountain View, California). This "card" communicates upwards with the Apple IIe microcomputer used to sequence the experiment, via an RS232 data link. A position or velocity command from the Apple computer causes the Galil card to generate the appropriate motor drive signal to the servo drive, depending upon the deviation from the desired position. This system

allowed accurate and repeatable traversals with direct data logging of the position. The accuracy of the displacement transducer and motion controller was tested using a machinist's clock gauge mounted rigidly on the weighing table (Figure 8) with a 6 mm steel bracket, and found to be within specification, less than 0,01 mm error after repeated traversals of 100mm.

Force Measurement

The weight of the diamond and support clip was measured using a Mettler AE163 electrobalance, with 0,01 milligram resolution, and using the underpan weighing facility. The digitally encoded weight was transmitted via a Mettler 011 data transfer module to the Apple IIe supervisory computer. The front of the weighing table, below the plinth, was enclosed to exclude drafts, and a window of 200 x 80 mm in clear perspex was installed to allow viewing The electrobalance system is well suited to capillarography because of the null deflection principle (Bayramli et al 1981). The maximum data transmission rate achieved was once in 600 milliseconds. For faster weighing than this, a strain gauge or piezo-electric system could be used, with compensation for deflection in the buoyancy calculation, but this was not necessary in these tests.

4.3 Water Preparation

The water used in all experiments was prepared from distilled water using a Milli-Q 3-cartridge (Continental Water Systems, El Paso Texas) water purifier followed by reboiling to remove air. The conductivity was always less than 0,05 µS. Surface tension was measured using a platinum plate of dimensions very similar to that of one of the diamonds used in the testwork, supported in the same way. The platinum was flamed in a low blue hydrogen flame until glowing and tested within 10 minutes. The surface tension was found to be 72,4 ± 0,1 mN/m at 298K. This is somewhat higher than normally found by force measuring techniques (71,9 mN/m), but Bayramli et al (1981) have reported the same value, with higher standard deviation, for triply distilled water. If this is because of a geometry effect (the end-correction of Padday (1964)), then apply equally to the diamonds testpieces, which are of similar shape.

4.4 Data Capture

Data-Logging Computer

The data from the electrobalance and from the Galil motion controller were already in digital form. Routines for interfacing the data string transmitter of the Mettler balance with a BASIC operating program were provided by Protea Laboratory Services. The routines for sending motion commands to the motion controller, and extracting position information during execution of the supervisory program were developed by the author in consultation with Ivy Systems, Craighall Park, RSA. The supervisory programs, which include the routines for detecting the bottom edge of the testplate, recognizing the buoyancy slope and accumulating averages of the contact angles, were written by the author. A flow sheet of a typical supervisory program appears in Appendix 2, and a listing of one of the programs appears in Appendix 3.

4.5 Shaping and Orientation of Diamonds

Test diamonds were made by conventional polishing of diamond crystals taken from the production of Premier Mine, Transvaal. There is a certain proportion of diamonds which form as flattish triangles (macles) or irregular shapes. This occurs as a result of "twinning", the simultaneous growth of two crystals, with one crystal rotated through 180 degrees on an octahedral plane (Bruton 1978).

The diamonds were marked, in discussion with a diamond polisher at the Diamond Research Centre, so as to derive the largest possible square sided plate, with Vee-shaped peak, which would be free of surface flaws such as exposed non-diamond inclusions. The major faces were then polished, as near to the [111] plane as could be achieved. This is a very slow process, because the [111] surface is notoriously difficult to polish, and excessive loading causes burning of the diamond. This has been discussed by Watermeyer (1980).

Once two large and flat parallel faces had been obtained, with a thickness of 1,0 to 1,5 mm, the sides, base and peak were formed. A photograph of two finished diamond plates appears as Figure 13.

After the first polishing, the remains of the epoxy setting cement were removed in hot chromic acid, followed by distilled water rinses and extraction in toluene (similar to the technique of Hartley (1978), but using the more environmentally acceptible toluene, rather than benzene). Because of the possibility of oxidation by the chromic acid, and adsorption of the toluene, a method of physical cleaning using alumina abrasive powder on a glass disc, was used after subsequent polishings. This is discussed in more detail in section 4.6 below.

Crystal Orientation

The crystal orientation of the major faces was determined by Laue photography. The Laue photograph for the testplate used predominantly in the RBS analysis is shown in Figure 14. The position of the centre of the diffraction pattern, together with the d - screen distance, was used to determine how far from the true [111] plane the major face was in each case.

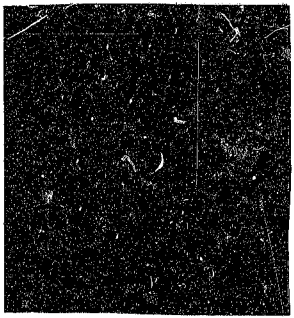
The results are shown in Table 4.

TABLE 4 - RESULTS OF LAUE CRYSTAL ORIENTATION ANALYSIS

Test Plate Number	Orientation Degrees off [111]	Comment
TP0 (oval)	19	Large, unsuitable for capillary measurements
TP1	3,5	Medium sized
TP2	5	Small
TP3	40	Large, 7 degrees off [110]

TP2 was used largely for RBS, although characterized by capillarography after polishing.

fig 14 x-ray diffractometer (' aue) photograph of polished [111] diamond



TP1 and TP3 were used extensively for capillarography, and TP3 was assumed to represent the behaviour of the dodecahedral face, [110]. It is possible that a macroscopic dodecahedral face is composed, on a microscopic scale, of terraces of [111] planes, but this will in any case give a higher frequency of edge sites, with more labile carbon atoms, so the suspected trend of greater reactivity of the true [110] may be preserved.

TPO was used in LEED and XPS experiments, because of the greater available flat area.

4.6 Cleaning Techniques

The cleaning of mineral surfaces prior to analysis is contentious. Dust and organic contaminants such as skin oils must be removed, and some techniques, such as accurate contact angle studies, call for planar surfaces.

Polishing and Cleaving

Soft minerals such as graphite and coal can be polished on abrasive papers, ending up with a final polish on filter paper or degreased linen (Gutierrez Rodriguez et al 1984). Arbiter et al (1975) showed that organic rinsing (in alcohol and ether) of graphite and stibnite specimens polished on filter paper produces a sessile drop contact angle some 15 degrees greater than water rinsing. Cleaving graphite in air produced a value intermediate between these two. Cleaving is the most reasonable approach for minerals since it simulates the process of liberation from the ore. Kelebek and Smith (1985) have used this approach for molybdenite and sulphur, both soft minerals. Hartley (1978) attempted to do the same for diamond but with *little success. The cleaving of diamond requires considerable skill, and* would be virtually impossible as a routine procedure in a glovebox or similar clean environment. Polishing is assumed to proceed by cleavage on a microscopic scale. Janczuk et al (1985) polished graphite in water using a graphite powder, followed by ultrasonic rinsing to remove polishing debris. The same technique is theoretically possible for diamond, using *diamond* powder on a conventional polishing wheel or "skaif", but in

practice there are two complications. Firstly, the diamond powder must be held on the polishing wheel, which rotates at high speed, and conventionally olive oil is used. This introduces organic impurities, which, arguably, may be removed by a series of organic rinses using progressively more volatile solvents. Secondly, the diamond itself must be fixed rigidly in a polishing tool or "dop", using epoxy cement or inorganic cement containing asbestos. Because of the high forces and temperatures transmitted to this bond during the polishing, a tough coating forms, and a vigorous chemical cleaning step is needed subsequently. Strong oxidizing acids, such as chromic (chromosulphuric) acid are used in the industry. A less severe polishing on a slow disc with mechanical clamping of the diamond, is possible, but the same effect can be achieved using a softer abrasive - see below.

Chemical Cleaning

Pate (1986) used the sequence halocarbon:acetone:alcohol after polishing diamonds and before analysis in ultrahigh vacuum. He also used a "heat cleaning anneal" at 770 K in UHV before making measurements on the diamond surface. This would probably desorb any organic molecules still present from the rinsing step.

In the case of wettability measurements, the chemical effects of strong acids or organic solvents may mask entirely the intrinsic behaviour. Sappok and Boehm (1968) were obliged to use an acid rinse on the diamond powders in their studies because the process of pulverizing diamond produces metal debris which must be dissolved out of the product. The possible effects on their results will be discussed in section 7.3. Hartley (1978) used a series of hot and cold organic rinses, culminating in *hot extraction for 6 hours with benzene. No mechanical cleaning of the* diamond surface is discussed, although most researchers, as listed above, feel the need for a final wipe with filter paper or lens paper, or an ultrasonic cleaning. Early experiments in these laboratories using a cruder form of capillarographic apparatus than discussed here, revealed clearly that organic rinsing (toluene, n-heptane, methanol) prior to testing had a hydrophobizing effect and chromic acid had a slight hydrophilizing effect.

Soft Polishing

Pashley (1978) produced quartz surfaces for ellipsometric measurements of smoothness in the nanometre range by a long process of polishing, ending up with ceric oxide powder on a Pellon pad. The ceric oxide is softer than quartz, by the usual hardness tests, and it seems surprising that this should work. Pashley remarks that the surface left after polishing with diamond powder, even the finest grades, had surface marks and subsurface stresses which interfered with the ellipsometric technique. The soft polishing removed these features. Two previous studies have suggested the use of alumina powder as a cleaning agent for the study of diamond surfaces. Miyoshi and Buckley (1980) used alumina polishing to prepare diamond flats for the measurement of metal:diamond friction. Nassau and Schonhorn (1977) used alumina polishing to produce a fresh surface on diamonds for contact angle measurement by sessile drop. They suggest that these diamonds had undergone surface modification by exposure to radiation, making them exceptionally hydrophilic. A different reason may be suggested (see section 7.3). It appears that polishing with a soft abrasive can remove the topmost layers, particularly if these have been modified by some chemical reaction.

A polishing technique using alumina abrasive (Norton 1 micron powder) in water was used in this study for cleaning the diamond surface prior to contact angle measurements. Initially this was done in the laboratory atmosphere, but later the entire polishing and rinsing stage was installed in a glove box which was slightly overpressurized with nitrogen. No attempt was made to exclude oxygen, but only to reduce interference from dust and airborne organics. Polishing was performed on a 90 mm glass disc fitted in an aluminium wheel and rotating at up to 400 rpm. The polishing holders for the diamonds were made of stainless steel and were designed so that the diamond was retained by virtue of its shape alone. The diamond was traversed along an arc during polishing to achieve a uniform surface.

The procedure for preparing the diamonds was then :

1. An initial diamond polishing to form the plates
   This was repeated after surface damage

2. Washing with toluene and acetone under ultrasound.

3. Polishing with levigated alumina (< 1 micron) on a glass disc of 90 mm diameter at approximately 300 rpm for 3 minutes per face. The disc was irrigated and rinsed with milliQ water.

4. Jet cleaning of the diamond with pressurized milliQ water in a PTFE beaker.

5. Ultrasonic rinsing in a PTFE beaker, under milliQ water for 10 minutes.

6. On withdrawing from the milliQ water the major faces emerged dry. Any droplets on the edges were drained using wicks of filter paper. The diamond was further dried in nitrogen over a heated ceramic wafer for 120 seconds.

After chemical contamination, or a period of no use, steps 3 to 6 were employed.

The integrity of this cleaning step was assessed by cleaning a glass test plate of dimensions similar to those of TP3. Chromic acid cleaning of such a glass surface gives contact angles of zero, advancing and receding. (See Figure 22). Alumina polishing of the glass did not cause an increase in the contact angles. As a further precaution, the alumina was calcined in an oven at 770 K for 12 hours before being introduced into the glove box.

Cleaning of the Cell

The glass cell and associated glass fittings were cleaned by pickling in hot chromic acid. This was repeated whenever the inner surface of the cell showed signs of "beading" by water droplets. The chromic acid was rinsed off with cold milliQ water and the inner surface of the cell was then steam extracted for several hours in an upside down position. Cooling water was passed through the jacket and the condensate was diverted from the reboiler. The inner surface was judged clean when uniform film condensation was seen.

Cleaning of Tweezers and Hanger Wires

Tweezers, used to handle the diamond testplates between cleaning and loading into the cell, as well as clips and hanger wires were cleaned using Contrad, a laboratory detergent, in an ultrasonic bath. This was followed by three changes of MilliQ water to rinse, and drying in an oven at 70 °C. When not in use, clips and tweezers were stored in a desiccator. The author wore gloves during all operations on the cell and diamond holders, to prevent skin oils from being transmitted to the test surfaces or glassware.

4.7 Surface Reaction

Changes in the surface properties of the test plates were brought about by reactions with gases and with aqueous reagents.

Reaction with Gases

The diamond surface was modified by reaction [illegible] in a tube furnace. Details of the apparatus used are given in Fig [illegible] he gases used were :

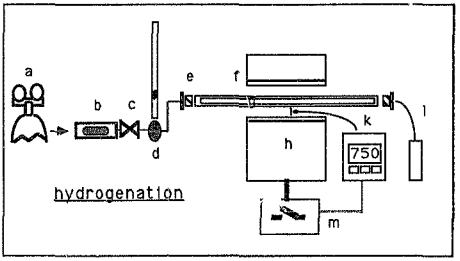
Oxygen	Afrox 99,5 %
Hydrogen	Afrox ultra high purity
Nitrogen	Air Products high purity
Argon	Air Products high purity

Reaction with Aqueous Reagents

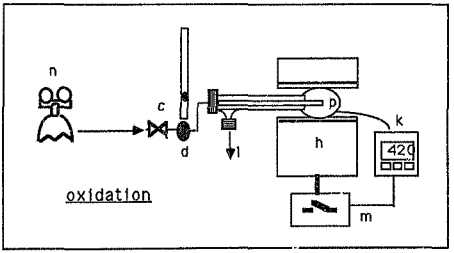
Reaction with aqueous reagents was conducted both outside the cell (prior to testing) and by addition of the chosen reagent to the cell volume through a filling funnel.

In the latter case, the concentration in the cell and the pH were monitored by extracting small volumes of the cell liquid through the surface cleaning needle and analysing in a micro-conductivity cell and a micro-pH cell. The conductivity cell was by Amber Science (San Diego, Ca) and the pH system by Markson (Phoenix, Arizona). For pH modifiers, titrimetric ampoules of

fig 15 tube reactor for gas reaction



a	high purity H2	i	thermocouple
b	indicating oxygen trap	k	RKC 1000 controller
c	isolating valve	l	gas bubbler
d	needle valve & rotameter	m	contactor
e	brass end plug	n	pure O2, Ar ..
f	outer tube (s/steel)	p	glass reactor tube
g	inner tube (silica)		
h	ceramic tube furnace		



sodium hydroxide and hydrochloric acid (Carlo Erba) were used. The surface tension coefficient, K, defined by the equation :

$$\gamma - \gamma_0 = K \cdot [M] \qquad \ldots\ (15)$$

where γ is surface tension at conc m
γ_0 is water surface tension
M is molar concentration (< 0,1 M)

was found using the Platinum Wilhelmy plate in the cell. Bikerman (1970) reports values of 1,7 for alkali metal hydroxides, 1,6 for chlorides, and 2,6 for alkaline earth salts. Experimental values are shown in Table 5 . A negative value would indicate a surface active impurity. Note that the trivalent ions, Fe^{+++}, Cr^{+++} and Al^{+++} give considerably higher K values than do the di- and monovalent cations.

TABLE 5 - REAGENTS USED IN THIS STUDY

Reagent	Formula	Grade	Manufacturer	K
Potassium chloride	KCl	Aristar	BDH	1,2
Hydrochloric acid	HCl	Normex AR	Carlo Erba	2,3
Sodium hydroxide	NaOH	Normex AR	Carlo Erba	1,4
Sulphuric acid	H_2SO_4	AR	PAL	2,5
Sodium chloride	NaCl	AR	Protea	
Calcium chloride	$CaCl_2.6H_2O$	AR	PAL	2,8
Ferric chloride	$FeCl_3.6H_2O$	AR	PAL	62
Chromic chloride	$CrCl_3.6H_2O$	AR	Carlo Erba	33
Aluminium sulphate	$Al_2(SO_4)_3.16H_2O$	Analar	BDH	28
Sodium perchlorate	$NaClO_4.H_2O$	Analar	Carlo Erba	(1,4)
Sodium borate	$Na_2B_4O_7.10H_2O$	AR	PAL	
Boric acid	H_3BO_3	AR	H&W	
Sodium metasilicate	$Na_2SiO_3.9H_2O$	AR	J.T. Baker	
Potassium dichromat	$K_2Cr_2O_7.2H_2O$	AR	BDH	
Sodium borohydride	$NaBH_4$	Synthesis	Merck	
Lithium Aluminium - Hydride	$LiAlH_4$	Synthesis	Merck	
Methanol	CH_3OH	AR	PAL	γ = 22,1

Apart from these reagents, a selection of solvents and etchants were used to clean the diamond testplates and the glass cell.

TABLE 6 - REAGENTS USED FOR CLEANING PURPOSES

Reagent	Grade	Supplier
Toluene	Analar	BDH
Acetone	GP Reagent	BDH
Methanol	AR	PAL
Trichloroethylene	AR	BDH
Sodium dichromate	CP) "chromic acid"	PAL
Sulphuric acid	CP)	Protea
Contrad	Laboratory detergent	Hickman & Kleber

Contrad has been recommended for the cleaning of diamond prior to UHV work (Derry et al 1983). It was found to be an extremely alkaline agent (at 10% v/v in water) and was not used in diamond cleaning before wettability measurements because of the possible effect of pH on the surface groups.

CHAPTER 5 - SPECTROSCOPIC TECHNIQUES

5.1 Surface Analysis

Several different states of wettability were identified by means of capillarographic techniques, and the nature of the pretreatment suggested that changes in the types of surface adatoms induced by the treatment could be important. In order to resolve some of the possibilities, three surface analytical techniques were used. These were :

1. Rutherford Backscattering Spectroscopy (RBS)

2. Low Energy Electron Diffraction (LEED)

3. X-ray Photo-electron Spectroscopy (XPS or ESCA)

The basis of these techniques is outlined briefly in the following sections. There is a precedent for use of vacuum techniques to probe surfaces along with aqueous chemical studies. Kozlowski and Sherwood (1986) have combined XPS studies with electrochemical studies of the oxidation of carbon fibres.

5.2 Rutherford Backscattering

Theory

Rutherford Backscattering Spectroscopy utilizes the scattering or reflection of positive ions, of suitable high energy, by the nucleus of an atom in the target. A typical geometry for large angle Rutherford Backscattering is shown in Figure 16. In these experiments, a helium ion of 1,0 MeV energy was used as the scattered ion. The selection of helium is not arbitrary, Derry (1978) has shown that helium, with a mass number of four, gives the optimum resolution of surface adatoms with mass number near 12, the value for the carbon atom. The technique is based on the detection of peaks in a spectrum of backscattered ion counts vs energy. A surface barrier detector is used, which produces voltage pulses of height

Page 65 omitted in the pagination.

proportional to the energy of the backscattered particle. The number of pulses at a given voltage, after counting a certain large number of total pulses, represents the fractional occurrence of nuclei of a given mass number. For a single plane (thin film) of a single element, the spectrum would consist of one steep peak at an energy calculated by the following relation :

$$\frac{E_{scat}}{E_{inc}} = \left[\frac{M_1 \cos\theta_2 + \sqrt{M^2_2 - M^2_1 \sin^2\theta_1}}{M_1 + M_2} \right]^2 \qquad \ldots\ (16)$$

where M_1 = mass number of incident ion (4 for He)
M_2 = mass number of scattering atom (12 for C)
θ_1 = scattering angle - position of detector relative to incident beam - 25 degrees in this set up

or by rearrangement to permit the calculation of the mass number of the target atom :

$$M_2 = M_1 \frac{\varepsilon - 2\sqrt{\varepsilon \cos\theta_1} + 1}{1 + \varepsilon} \qquad \ldots\ (17)$$

where $\varepsilon = \frac{E_{scat}}{E_{inc}}$

In practice, this type of film does not exist, although a surface layer of adsorbed atoms on a planar surface of a substrate with lighter nucleus is a good approximation. Oxygen on the surface of diamond is an example. There will be a far greater frequency of bombarding ions which miss the nuclei of the oxygen layer completely, and penetrate the diamond crystal to some depth before being scattered. The ion will lose energy both on penetration and escape from the crystal so the spectrum becomes a plateau or shoulder, with a well defined high energy edge.

Meyer et al (1970) have developed the method for calculating the area density of target atoms from the counts in the peak for a particular adatom, and the number of counts per unit depth due to scattering by the substrate - in this case carbon (diamond).

$$\frac{P}{\Delta S}\,\Delta E_2\,\frac{dz}{dE_2}\left(\frac{Z_i}{Z_c}\right)^2\,\frac{\rho_{dia}\,N_{av}}{M_c}\cos\theta_1$$

where
- P = counts in surface layer peak
- ΔS = counts per channel in substrate spectrum
- $\Delta E2$ = channel width (energy units)
- dz/dE_2 = energy to depth conversion factor = 14 A/keV for 1,0 MeV He
- Zc = atomic number of carbon
- Zi = atomic number of adatom under investigation
- ρ_{dia} = density of diamond 3,52 g/cm^3
- N_{av} = Avogadro's number 6,023.10^{23}
- M_c = mass number of substrate = 12 for carbon.

The calculation yields the numbers of atoms per cm^2 on the surface. With suitable assumptions about the state of the surface, and on a defined crystal plane such as [111], the number of carbon atoms in the immediate surface layer can be calculated and the count of adatoms converted to an equivalent monolayer. For instance, the carbon atoms in the topmost layer of an ideal [111] plane occur with a frequency of 1 per 55 000 square picometres, or 1,82.10^{19} per m^2.

Experimental Details

The 1,0 MeV particle Cockcroft accelerator at the Schonland Centre for *Nuclear Sciences of the University of Witwatersrand* was used to provide the particle beam. Further details of the system are given by Annegarn (1976). The diamond testplate was mounted in a holder with an additional beryllium shield over the front face of the holder to reduce stray reflections, which otherwise lead to a noisy background in the spectrum.

Meyer et al (1970) have developed the method for calculating the area density of target atoms from the counts in the peak for a particular adatom, and the number of counts per unit depth due to scattering by the substrate - in this case carbon (diamond).

$$\frac{P}{\Delta s}\,\Delta E_2\,\frac{dz}{dE_2}\left(\frac{Z_i}{Zc}\right)^2\,\frac{\rho dia\ N_{av}}{M_c}\cos\theta 1$$

where
- P = counts in surface layer peak
- ΔS = counts per channel in substrate spectrum
- $\Delta E2$ = channel width (energy units)
- dz/dE_2 = energy to depth conversion factor = 14 A/keV for 1,0 MeV He
- Zc = atomic number of carbon
- Zi = atomic number of adatom under investigation
- ρ_{dia} = density of diamond 3,52 g/cm^3
- N_{av} = Avogadro's number 6,023.10^{23}
- M_c = mass number of substrate = 12 for carbon.

The calculation yields the numbers of atoms per cm^2 on the surface. With suitable assumptions about the state of the surface, and on a defined crystal plane such as [111], the number of carbon atoms in the immediate surface layer can be calculated and the count of adatoms converted to an equivalent monolayer. For instance, the carbon atoms in the topmost layer of an ideal [111] plane occur with a frequency of 1 per 55 000 square picometres, or 1,82.10^{19} per m^2.

Experimental Details

The 1,0 MeV particle Cockcroft accelerator at the Schonland Centre for Nuclear Sciences of the University of Witwatersrand was used to provide the particle beam. Further details of the system are given by Annegarn (1976). The diamond testplate was mounted in a holder with an additional beryllium shield over the front face of the holder to reduce stray reflections, which otherwise lead to a noisy background in the spectrum.

The holder was positioned in a special goniometer equipped with an electron flood to inhibit charging of the non conducting diamond. The vacuum in this section of the ion beam line was maintained at better than 10^{-5} millibar.

Test Diamond

The ion beam induced surface damage, evident as a black spot after the experiment, was removable only by heavy polishing. Because this adversely affected parallel testing by capillarographic methods, a third diamond platelet, of slightly smaller dimension than the [111] platelet used for wetting, and with major face near the [111] plane, was used for the RBS testwork. Both sides were used, allowing normally 4 to 8 beam spots, before the surface needed repolishing to remove the radiation damage. A Laue X-ray diffraction analysis of the diamond revealed that the major faces were 5 degrees off true [111] planes.

5.3 Low Energy Electron Diffraction

Electrons of sufficiently low energy (100 eV for instance) will have a wavelength, according to the particle/wave duality of de Broglie (1924) of the order of 100 pm. They may be expected to create interference patterns with periodic structures such as crystals, which have a lattice spacing of the same order. Also, because of their low energy, the depth within a crystal from which elastically scattered electrons emerge, is very small. This makes them useful probes for the lattice structure of the surface of crystal. Ertl and Kuppers (1974) describe the development of the techniques of low energy electron bombardment and detection and the geometrical theory of diffraction. The possibility of surface reconstruction after reaction with hydrogen or oxygen, or the generation of surface groups with a fixed periodicity, could be detected by this technique.

The Geometrical Theory of Diffraction

The elastic interaction of the impinging electrons, with one or two topmost layers of the crystal, may be viewed as the scattering of monochromatic

waves by a two dimensional lattice or mesh. All regular surface arrangements can be classed into 5 two-dimensional Bravais lattices by the use of two basis vectors, a_1 and a_2. These are the sides of the smallest parallelogram, which by translation generates the surface mesh. In the case of diamond [111], the two vectors are of equal length and at an angle of 60 degrees, the co-called hexagonal mesh. The vector length is 252 pm.

The defining equations for the angles are :

$$\lambda = \frac{h}{mv} \qquad \ldots. (19)$$

$$d\ (\sin \phi - \sin \phi_0) = n\lambda \qquad \ldots. (20)$$

d = lattice spacing
ϕ = angle of constructive interference
ϕ_0 = incident beam angle (to normal)
n (integer)= diffraction order

Usually the surface atoms can be considered as equally spaced rows, of row spacing d, and where the incident beam is normal $\sin \phi_0 = 0$

$$\text{then } \sin \phi = \frac{n\lambda}{d} = \frac{n}{d} \cdot 1417 \cdot \frac{1}{\sqrt{U}} \qquad \ldots. (21)$$

where U = accelerating voltage of the electron beam
d = row spacing in pm.

see Appendix 4.

In practice, the reflected beams with constructive interference fall on a hemispherical screen centred on the diamond sample. This is an image of the reciprocal space mesh. The matrix equations defining the coordinate transformation from real space to reciprocal space are given in Appendix 4. The symmetry of the diamond surface mesh gives a hexagonal lattice in reciprocal space too, but the spacing of the spots is in inverse proportion

to the spacing of the real scattering centres. Thus, a surface adatom which is attached at every second carbon surface atom, with a consequent lattice constant of 2 x 252 pm, will generate a superlattice with defining vectors twice the length of the diamond lattice. In reciprocal space this will form a lattice which has beamspots midway between the spots of the original pattern (Pate 1986).

This effect was used to determine whether there was reconstruction, or a periodic adsorption of hydroxyl groups or oxygen atoms on the surface of the test diamonds.

Experimental Details

LEED patterns of two of the test diamonds were obtained using the SOLAR 300 UHV chamber with Vacuum Generators LEED system at the Schonland Research Centre for Nuclear Sciences. The system is shown in Figure 17. The patterns were obtained at several voltages, but the most intense patterns occured near 220 volts. In some experiments a digital readout of the voltage appears on the photographs.

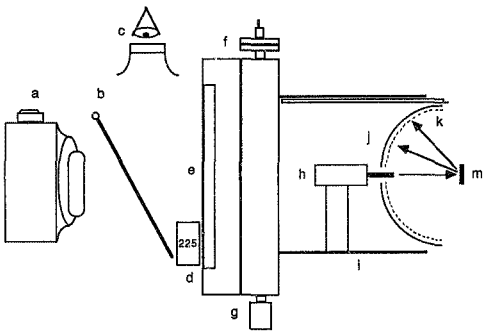
Diamonds TP1 and TP2 were tested after the standard cleaning step, and including a period of bake-out in the UHV chamber at 473 K. Sample TP2 (surface 5 degrees off [111]) was heated to 673 K in UHV and the LEED pattern examined again.

5.4 X-ray Photo-electron Spectroscopy

Theory

The excitation of atoms near the surface of the diamond crystal by mono-energetic X-rays results in absorption of a photon of characteristic energy, and prompt emission of a photo-electron. Electrons from all the orbitals which have binding energies lower than the photon energy will be excited, but the kinetic energy of the emitted electron will be reduced for orbitals of higher binding energy. This is expressed by the relation :

fig 17 low energy electron diffraction apparatus



a 35 mm camera
b swivelling mirror
c eyepiece
d digital voltage display
e viewport 200 mm on standard UHV flange
f grid feedthrough
g electron gun feedthrough
h electron gun
i mu-metal shield
j hemi-spherical cathodoluminescent screen 145 mm
k grids
m specimen

$$E_{kin} = h\upsilon - E_b - e_{\phi sp} \quad \ldots\ (22)$$

E_{kin} is the kinetic energy of the detected electron
E_b is the binding energy of the detected electron
$e_{\phi sp}$ is the work function for the sample

When the spectrum of energies of emergent electrons is scanned by a suitable analyzer, a series of peaks at energies characteristic of the atoms present in the surface region will appear. The techniques of Carley and Roberts (1977) was used for the calibration and interpretation of the peak heights and shifts.

The relevant equation is shown as equation 23.

$$\sigma = \frac{Y_m}{Y_s} \cdot \frac{N \cos \theta\ \mu_s\ \rho_s\ \lambda}{\mu_m\ M_s} \quad \ldots\ (23)$$

where σ = surface coverage by (oxygen) adatoms atoms/cm^2
Y_m = integrated XPS peak area for adsorbed atoms (oxygen) corrected for the increase in analyser sensitivity with decreasing kinetic energy
Y_s = integrated peak area for substrate carbon
N = Avogadro's Number
θ = system geometrical constant, 25 °
μ_s = photoionization cross-section for carbon = 1.0
μ_m = photoionization cross-section for oxygen
= 2,92 (Schofield 1976)
ρ = diamond density, 3,52 g/cm^3
λ = photoelectron escape depth (AlK_α)
= 10 x 10^{-8}cm (Pate 1986)
M_s = Mass number of carbon
= 12,01

Depth Sensitivity

The depth of the crystal probed is governed by the depth from which electrons can escape. This is called the mean free path or escape depth and has been determined for diamond by Pate et al (1983) using a range of primary energies up to 1250 eV. On the [111] plane, this depth is of the order of 1000 pm, or approximately five double sheets. (The structure of the [111] planes is such that side view reveals alternately closely spaced and more distantly spaced sheets of atoms, conveniently regarded as double sheets, at a spacing of 204 pm (See Figure 2)).

Although this is not a purely surface sensitive technique, the surface layer will contribute more to the signal because of shielding and attenuation effects. The attraction of the technique is that it provides not only identification of the atomic species present, since each element has a unique combination of electron energy levels, but also some information about the relative frequency of each species and even the chemical environment in which hetero-atoms are bound. This last effect is due to the "chemical shift", the small change in the electrostatic potential of an atom, and so on the binding energy of even the core electrons, when involved in a covalent bond with a heteroatom of different electronegativity.

The most attractive feature of XPS is the non-destructive nature of the interrogation. Ion beams tend to desorb or destroy the surface during analysis, but only very unstable surface compounds are susceptible to damage by X-rays. Obviously, the use of an ultrahigh vacuum technique will force desorption of physically adsorbed molecules, but this is so for almost all the surface spectroscopies.

It is possible to combine analysis of the surface with more severe treatments, like heating, desorption and ion etching in order to obtain information about the type of bonding employed by the surface adatoms.

The major disadvantage found in these experiments was the rather broad analyzed area. In all cases, some signal was detected off the sample holder. This arises because of the difficulty in focussing the X-ray beam, and collimating the emitted electrons, on a target as small as these test diamonds.

Experimental Details

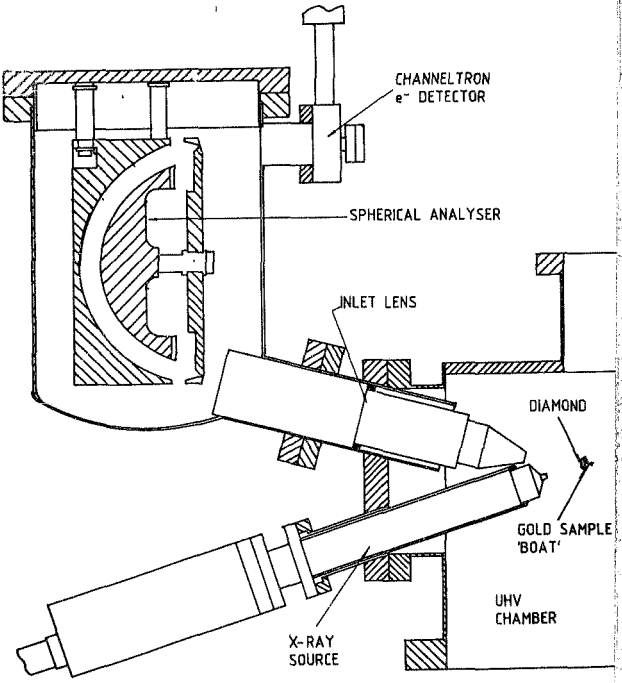
The elements of the Vacuum Generators CLAM system mounted on a SOLAR 300 UHV chamber are shown in Figure 18.

A choice of target material is possible. This changes the energy of the incident X-rays, hence the position of the XPS peaks in the analyzed spectrum. The emergent electron beam is analyzed using a hemispherical retarding lens analyzer, with digital display of the analyser voltage for good location of peaks. In practice, there was a slight drift in the analyzer datum, so that the carbon (1s) peak appeared between 1198 and 1203 eV on the kinetic energy scale. This is not important, as both the carbon and oxygen (1s) peaks are obvious, and cannot be confused with other species. The spectrum is recorded on an analog chart recorder.

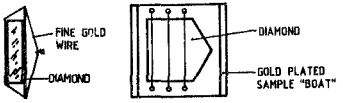
In the early stages of this experimental program, the only method for introducing the sample (diamond) was by removing the top plate of the UHV chamber. *This plate carries the sample manipulator and heater contacts.* Because this procedure allowed moist air into the UHV chamber, the entire system required baking at 473 K before a reasonable vacuum could be obtained. A vacuum of better than 10^{-8} millibar is required for XPS. The diamond was thus subjected to temperatures of 473 K for several hours, which could have caused desorption of surface oxygen groups.

Early in 1987, a Leybold Heraus sample introduction rod was fitted to the UHV system. This allows the movement of the sample, on a specially designed "boat", from atmosphere, through a chamber where gas reactions can be conducted, onto the sample manipulator. No bake-out is then required and the surface can be analysed without delay. The boat fits into a clip in the rod which allows passage of electrical current through the stainless

FIG. 18 XPS APPARATUS



DETAIL OF HOLDER



steel plate supporting the diamond. This allows heating of the diamond in the reaction chamber. In this way oxidation of the diamond could be achieved. The temperature attainable were not high enough for useful hydrogenation experiments in this chamber. Hydrogenation was performed remotely, in a silica tube furnace.

A number of mechanisms for mounting the diamonds on the boat were attempted. An important consideration was the amount of oxygen signal generated by X-rays impinging on the sample holder. This was gold plated because gold has a low retention of adsorbed oxygen in UHV.

The best approach was found to be strapping of the diamond to the holder using a system of fine holes and 0,3mm gold wire. The diamond was positioned for analysis on the manipulator by minimizing the gold (4f) peak, whilst maximizing the carbon (1s) peak, and the blue (X-ray induced) luminescence of the diamond, which could be seen through an upper viewing port.

The sample manipulator has a built in heater for thermal desorption experiments. There is a thermocouple for readout of sample temperature.

CHAPTER 6 - RESULTS

6.1 Capillarographs

The result of an individual experiment is a capillarograph which is a plot of force vs depth of immersion. The computer data retrieval technique allows instantaneous calculation of a contact angle from the basic equation shown in Figure 4. Not every contact angle is an equilibrium (dynamic) angle because of the phenomenon of "hingeing". Figure 19 shows the phases of an experiment of three cycles of immersion. Hingeing occurs at the end of a pass, where the three phase line is stationary and the contact angle swings from an advancing to a receding value. This is seen as the steep (and smooth) sides of a capillarograph. By a simple numerical differentiation of the data to detect the slope, these data can be excluded from calculation of the true advancing and receding contact angles. Figure 20 shows an actual capillarograph plotted from data stored during an experiment with TP1, in the cleaned state. Since this state is intermediate between an extremely hydrophobic state and a hydrophilic state, it is designated "INT" (discussed more fully below, Section 6.4)

It is possible to extract a value for the advancing and receding contact angles by a graphical construction which is illustrated in Figure 20. Two lines are drawn to be the best fits to the groups of lines in the stable advancing and receding sections of the loop. These lines (or their extrapolations) will intersect the vertical line corresponding to zero immersion depth. At this point, the force is solely due to the meniscus weight, since dry weight has been tared off electronically by the balance. In this example the construction gives 21 mgf in the advancing mode and 91 mgf in the receding mode. The perimeter of this diamond is 1,388 cm. The surface tension (in mgf - the author begs leave to forsake the pure SI system for just this one example, and until the balance manufacturers start to provide direct readings in Newtons), is 73,8 mg/cm and hence :

advancing contact angle = arc cos (21/1,388.73,8) = 78 degrees
receding contact angle = arc cos (91/1,388.73,8) = 28 degrees

The measure adopted to combine these values into a single index of wettability is the average adhesion tension :

fig 19 stages in the wetting hysteresis loop

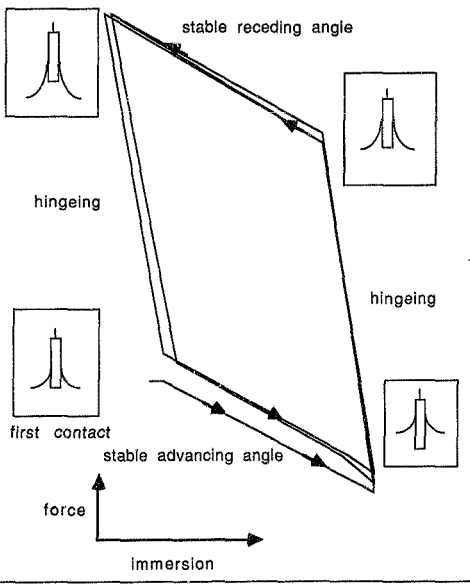


fig 19 stages in the wetting hysteresis loop

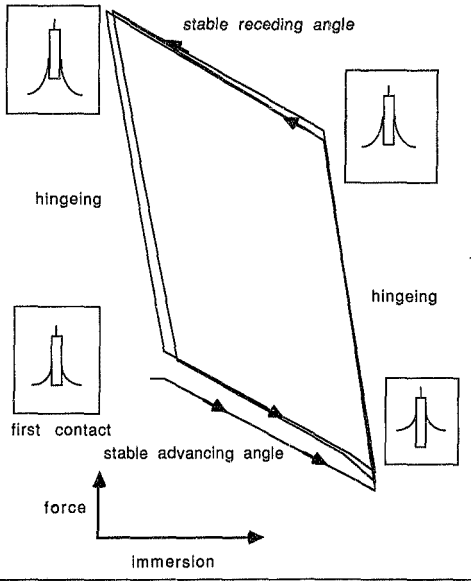
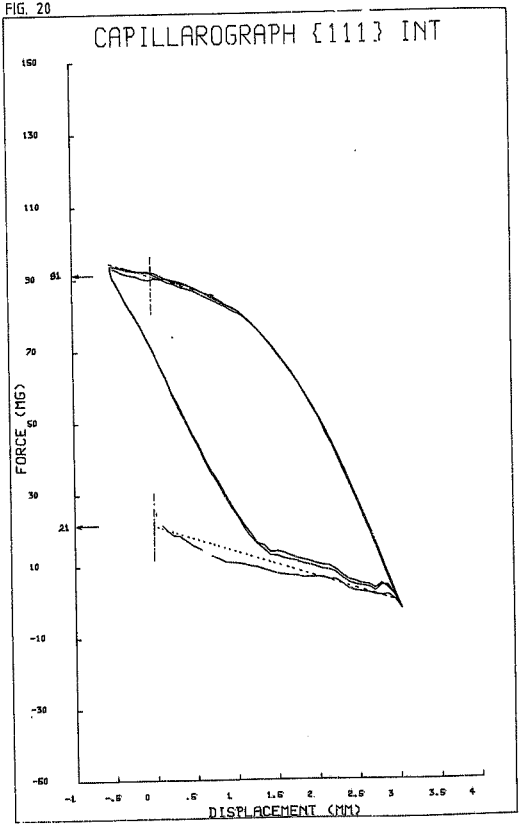


FIG. 20


CAPILLAROGRAPH {111} INT
150
130
110
90
70
50
30
10
-10
-30
-50
81
21
FORCE (MG)
-1
-.5
0
.5
1
1.5
2
2.5
3
3.5
4
DISPLACEMENT (MM)
J.O.HANSEN UW CHEM

adhesion tension = 72,4 (cos θa + cos θr)/2 = 39,5 dyn/cm or mN/m.

In operation under computer control, the graphical construction is replaced by calculations at 50 (approx) points on the stable advancing or receding sections, with averaging of the results at the end of each pass.

Figure 21 shows the superimposed capillarographs for one diamond after three different treatments :

1. Oxidation at 693 K in oxygen

2. Normal attrition cleaning

3. Hydrogenation at 1023 K in UHP hydrogen.

The capillarographs are progressively displaced downwards (lower wetting force or adhesion tension) and the differentiation between the states is clear, even though the hysteresis loops overlap. This is because the advancing angle on, say, an intermediate surface, is still higher than the receding angle on an hydrogenated surface.

Because the capillarograph is not a very condensed method of displaying the data, all further results will be presented as either :

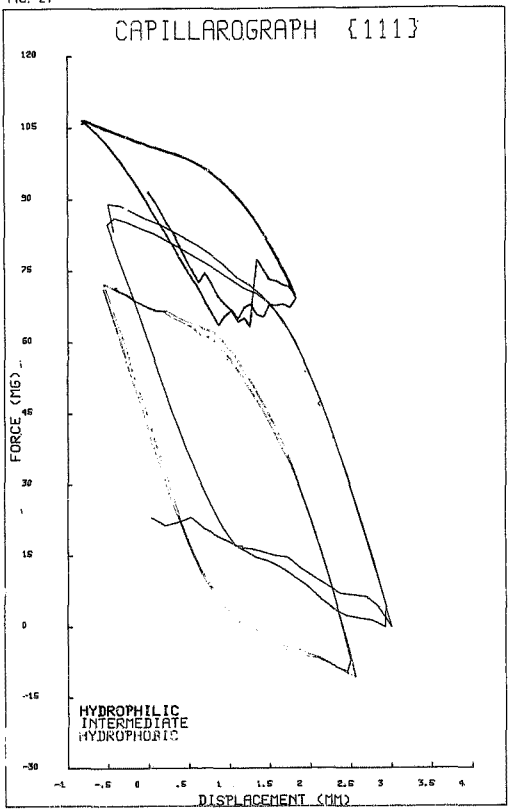
1. A single adhesion tension

2. A pair of contact angles from the average of three passes.

Each full pass takes 0,2 hours, therefore this result refers to a surface in contact with the test solution for 0,3 hours.

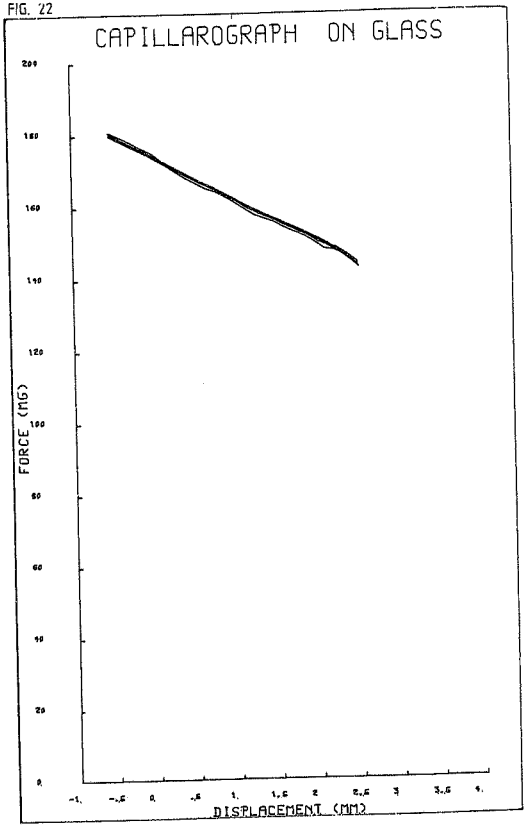
Figure 22 is a capillarograph obtained with a glass plate of perimeter 2,350 cm, matching the shape of diamond TP3 as far as possible. A very shallow hysteresis loop (virtual absence of hysteresis) was obtained. The graphical method gives a mean meniscus force (advancing and receding) of 173 mg, and hence a contact angle of less than 4 degrees - effectively

FIG. 21



J.O.HANSEN UW CHEM

FIG. 22



J. D. HANSEN, UW CHEM.

zero. This test was used to monitor contaminant ingress into the cell, and cleaning techniques.

6.2 Polished Diamond Surfaces

Appendix 5 contains the results of experiments on TP1, major face [111] and TP3, major face [110] using alumina attritioning as a cleaning step. These experiments were conducted over a period of two years. Some of the earlier results for TP1 were obtained by polishing manually on a microscope slide. Later results were obtained by polishing in the glove box on a glass disc at approximately 200 rpm using three minutes per side. Histograms showing the distribution of adhesion tension for the two surfaces are shown in Figure 23. The results show considerable scatter, but this is thought to be a real effect deriving from the variability of surface composition of the diamond surface following various chemical treatments in prior experiments, rather than experimental errors. This is discussed in Section 8.3.

The major results may be presented in this abbreviated table, showing the average advancing and receding angles, and the adhesion tension, for [111] and [110] faces :

TABLE 7 - WETTABILITY OF MECHANICALLY CLEANED DIAMOND SURFACES

	Advancing Angle Degrees	Receding Angle Degrees	Adhesion Tension mN/m
TP1 [111] Surface	76 ± 5	29 ± 5	40 ± 4
TP3 [110] Surface	71 ± 4	25 ± 5	45 ± 3

fig 23a distribution of adhesion tension on polished [111]

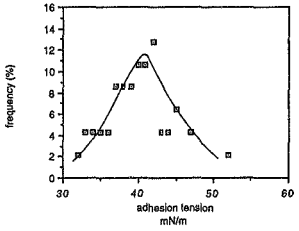
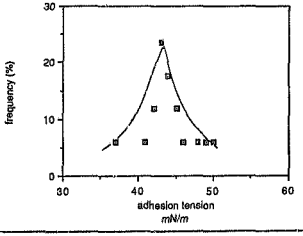


fig 23b distribution of adhesion tension for polished [110]



6.3 Oxidized Diamond Surfaces

Figure 24 shows the effect of treatment of [111] and [110] surfaces in oxygen, at approximately 90 kPa absolute pressure, and progressively higher temperatures. The time of exposure was 0,5 hours at the stated temperature, with progressively longer heating up and cooling times at the higher temperatures.

These figures show that oxidation of the surface, evident as increased wettability or adhesion tension and lower contact angles, begins at approximately 470 K and progresses virtually to completion at 720 K. The adhesion tension approaches 70 mN/m at this point, only slightly less than that for clean glass (72,4). Sappok and Boehm (1968) demonstrate the same effect for diamond powders at 690 K. The [110] surface appears to be more susceptible to oxidation than the [111] surface. The [110] diamond approaches total wettability at a temperature some 50 K lower than does the [111] surface.

The extremely hydrophilic state appeared to be unstable, with a slow but reproducible reversion towards more hydrophobic behaviour. This is shown in Figure 25. This process is more pronounced if the surface is attritioned with alumina. Table 8 shows the results of tests performed on the [111] diamond, immediately after oxidation at 690 K, and then after progressively longer periods of attrition cleaning, using alumina abrasive in a glovebox.

TABLE 8 - EFFECT OF ATTRITION CLEANING ON THE OXIDIZED [111] SURFACE

State	adv angle degrees	rec angle degrees	adh tension mN/m
Oxidized 690 K	37,3	11,6	64,2
Reclean 3 mins	62,4	23,2	50,0
Reclean 6 mins	70,1	28,0	44,3
Reclean 9 mins	69,0	25,2	45,7
Reclean 12 mins	73,4	28,6	42,1

fig 24a oxidation effects on contact angles

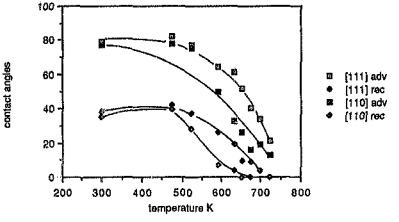


fig 24b oxidation effects on adhesion tension

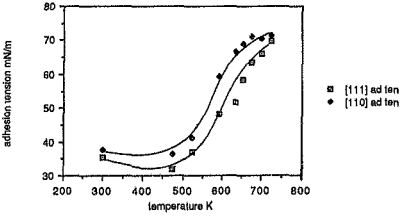


fig 25 recovery from hydrophilic state

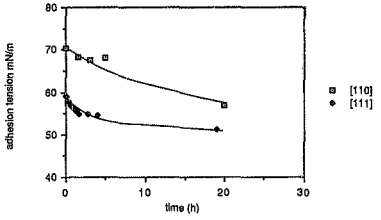
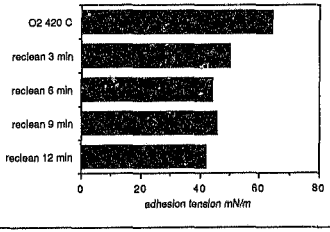


fig 26 effect of attrition on oxidized surface



The trend is shown in Figure 26. Apart from an anomaly at the third cleaning step, which may have been caused by inadvertent contamination, the surface tends towards the value seen for the clean polished surface in Section 6.2. This effect helps to explain the scatter seen in the results for the mechanically cleaned surface. If we conclude that the process of polishing removes microfragments of oxidized surface, and replaces them by new surface which then equilibrates with the aqueous environment at the time of polishing, then there may be areas of the diamond surface which are protected from polishing, because of orientation or rugosity, and therefore persist after a few stages of cleaning. Chemical modification, by for instance, reduction with hydrogen at 1020 K, will not be impeded by surface roughness.

Hydrogenation in Solution

Hydrogenation of surface oxides by an organic hydrogenating agent, lithium aluminium hydride in diethyl ether, was attempted. The technique was first performed on a polished surface, and then on a surface which had been oxidized. An acid rinse is required to decompose aluminium reaction products on the surface.

TABLE 9 - HYDROGENATION BY LITHIUM ALUMINIUM HYDRIDE IN ETHEREAL SOLUTION

State	Adhesion Tension mN/m
Intermediate - polished	46,3
$LiAlH_4$ + acid rinse	45,0
Oxidized	63,9
$LiAlH_4$ + acid rinse	49,4

The acid rinse may have had the effect of decomposing surface oxirane type groups. There is a clear decrease in the wettability, but it is not possible to say whether the hydrophilic species destroyed was a surface carboxylic acid or an epoxide group. Note that there is no significant effect on the wettability of the polished surface, after treatment with lithium aluminium hydride.

Oxidation by Chromic Acid

Oxidation by hot concentrated chromic acid produces a less severe increase in wettability than gaseous oxidation. The [111] surface was exposed to chromic acid (Lelah et al 1979) for ten minutes at 90 °C. This was followed by rinsing with ultrasound and drying in the glovebox.

TABLE 10 - EFFECT OF CHROMIC ACID AND ATTRITION ON THE [111] SURFACE

State	Advancing Angle Degrees	Receding Angle Degrees	Adhesion Tension mN/m
Polished, clean	79	33	37,3
Chromic acid	62	22,5	50,4
Reclean 3 mins	64,7	27,8	47,5
Reclean 6 mins	73,2	27,3	42,6
Reclean 9 mins	73,6	28,9	41,9

This is shown in Figure 27. The chromic acid appears to be less strongly oxidizing than the high temperature oxygen, and the (intermediate) hydrophobic state is achieved with limited attritioning.

6.4 Hydrogenated Diamond Surfaces

Diamonds with [111] and [110] major faces were exposed to hydrogen at progressively higher temperatures. Figure 28 shows that there is no effect until 720 K, at which point the surface becomes significantly more hydrophobic, reaching a maximum at 1020 K. The surfaces were partially oxidized at the start of the series, which accentuates the transition, and the [110] surface started considerably more hydrophilic than the [111] surface. The change is most pronounced at approximately 770 K, which is the range of temperature where the most rapid thermal desorption of CO and CO_2 from diamond powders has been seen (Matsumoto et al 1977). It is possible that the hydrogenation process requires the desorption of a CO group, exposing a reactive surface carbon atom for hydrogenation, rather than splitting of the C-O bond.

fig 27 effect of chromic acid and attrition

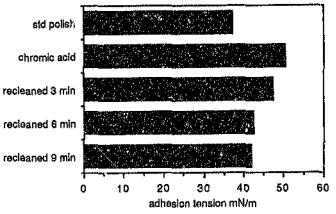


fig 28a effect of hydrogen on contact angles

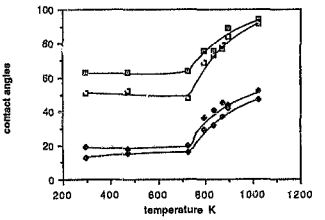


fig 28b effect of hydrogen on adhesion tension

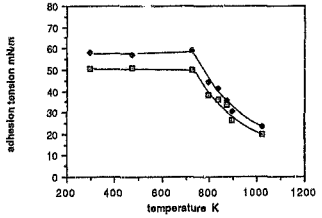


fig 29 effect of attrition on hydrogenated surface

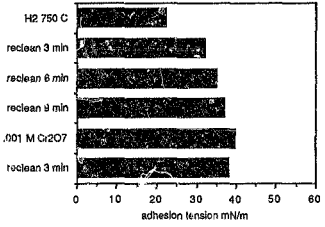
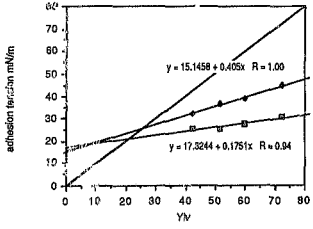


fig 30 Zisman plots for [111]H and [110]Int



The [111] surface appears to be more susceptible to hydrogenation, after partial oxidation, than does the [110] surface. This may be a result of the more favourable sites for oxygen chemisorption on a net [110] face.

The hydrogenated surface was very stable. The diamonds were stored in a desiccator for 10 days and retested, with no significant change in the adhesion tension characteristic of the strongly hydrophobic state.

The hydrogenated surface could be removed by attrition cleaning. Figure 29 shows the result of progressively longer polishing with alumina. After three stages of polishing the adhesion tension approached that of the standard intermediate surface (40 mN/m). At this stage a chemical treatment, with acidified potassium dichromate, was applied. There was a small increase in wettability, indicating that some surface groups were susceptible to mild oxidants. Alternatively this may have been caused by adsorption of a hydrated cation (see Section 9.7) because a subsequent polishing stage produced a slightly more hydrophobic state.

An examination of Figure 26 in conjunction with Figure 29 demonstrates that there is a continuum of states of wettability for the diamond surface, ranging from : very hydrophilic, but relatively unstable, after oxidation at 670 K, with adhesion tension near 70 mN/m,

through a more hydrophobic range, most usually seen on mechanically polished surfaces, with a median adhesion tension at 40 mN/m,

and on to a very hydrophobic state, after hydrogenation at 1000 K, stable against chemical attack at room temperature, with adhesion tension 20 mN/m.

In further discussion the following identification of these states is proposed :

TABLE 11 - CLASSIFICATION OF WETTING BEHAVIOUR

H	The very hydrophobic state
O	The hydrophilic state
Int	The intermediate state

To some extent the intermediate state is a range of states, depending upon the direction of the most recent treatment, oxidation or hydrogenation.

These states can be classed according to adhesion tension :

TABLE 12 - ADHESION TENSION OF THE DIFFERENT CLASSIFICATIONS

State	Adhesion Tension (mN/m)
H	18-25
Low Int	25-40
High Int	40-55
O	55-72

The median of the results for the polished [111] and [110] surfaces (Section 6.2) provides the boundary between low intermediate and high intermediate values. Nassau and Schonhorn (1977) give a contact angle for the polished diamond surface of 47 -55 degrees. If we assume that this is a reasonable average of receding and advancing values, then this corresponds to an adhesion tension of 49-42 mN/m. This is in fair agreement with the present work, particularly since the top face of a brilliant cut diamond (as tested by them) will not be a [111] face, but something closer to [100], likely to have a higher frequency of surface oxides (Verwoerd 1986) and hence potentially more hydrophilic.

6.5 Zisman Plot

The Zisman plot is a recognized tool for characterizing the surface energy of a solid, independent of a particular wetting liquid (Zisman 1964). A method for determination of γc, the critical surface tension of wetting of minerals, using solutions of methanol in water has been given by Kelebek and Smith (1985).

Tests were performed with diamond TP1, with [111] major face in an hydrogenated state and diamond TP3, with [110] major face in an intermediate state.

The results are shown in Table 13 and the Zisman plots appear as Figure 30.

TABLE 13 - DATA FOR ZISMAN PLOTS

[111] Hydrogenated				
Volume % Methanol	γ mN/m	Advancing Angle Degrees	Receding Angle Degrees	Adhesion Tension mN/m
0	72,4	85	41	30,5
5	60,0	82	39	27,5
10	51,4	81	34	25,3
25	42,4	72	26	25,6
100	22,5	0	0	22,5 * excluded
[110] Intermediate				
Volume % Methanol	γ mN/m	Advancing Angle Degrees	Receding Angle Degrees	Adhesion Tension mN/m
0	72,4	72	26	44,6
5	60,0	69	20	38,9
10	51,4	65	0	36,6
25	42,4	59	0	32,1
100	22,5	0	0	22,5 * excluded

* data excluded from plot because total wetting occurred.

Linear regression gives the following equations for the Zisman plots in Figure 30 :

[111] hydrogenated : $\gamma \cos \theta = 0{,}175\ \gamma_{lv} + 17{,}3$
[110] intermediate : $\gamma \cos \theta = 0{,}405\ \gamma_{lv} + 15{,}2$

hence by setting cos θ to 1 and solving we find the critical surface tensions of wetting :

[111] hydrogenated : $\gamma_{crit} = 21$ mN/m
[110] intermediate : $\gamma_{crit} = 26$ mN/m

This can be seen again from the intercept with the diagonal on the plot. Kelebek and Smith (1985) find values of 40 - 45 for coals, 29 for the cleavage plane of molybdenite and 27 for a sulphur crystal face. Zisman quotes 22 for a surface of methyl groups, i.e. a paraffin wax. We conclude that the hydrogenated surface has a character essentially similar to a paraffin wax, and that even the polished surface is mainly composed of hydrophobic, low energy sites.

6.6 Optical Contact Angle Measurement

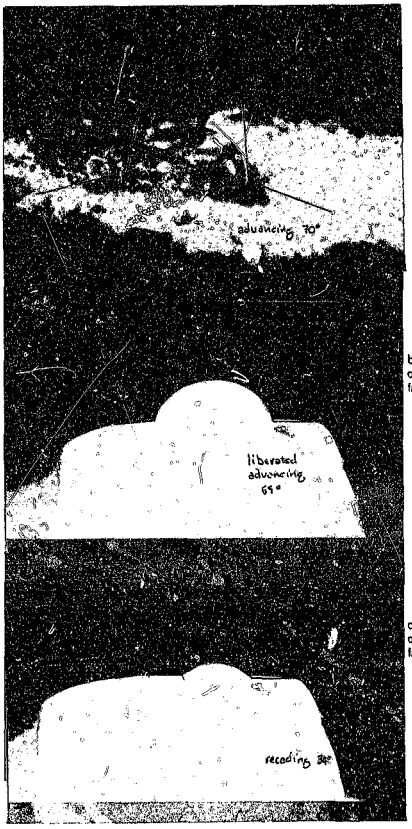
The optical or photographic technique was used to find the advancing and receding contact angles on the surface of good "near octahedral" diamond crystals. Figure 31a shows a diamond still "locked in the kimberlite", Figure 31b shows the advancing angle on the newly liberated surface and 31c shows the receding angle.

Table 14 shows the results found by the author and another independent party of constructions to find the contact angles at the left and right edges of the droplets.

TABLE 14 - OPTICAL CONTACT ANGLE MEASUREMENTS ON NATURAL FACES

	Author's Measurements				Independent Measurements			
	Exposed Surface		Fresh Surface		Exposed Surface		Fresh Surface	
	adv degrees	rec degrees	adv degrees	rec degrees	adv degrees	rec degrees	adv degree	rec degrees
	70	36	76	39	74	37	78	50
	55	34	68	27	52	34	57	24
	78	27	67	25	58	33	57	24
	52	26	77	30	80	32	69	32
	67	35	73	26	78	37	69	30
	78	38	65	30	81	45	80	36
	75		67	32	74	60	69	36
	65		69	34	68		65	
			70	29			81	
			61				62	
							68	
Averages	67,50	32,67	69,30	30,22	70,63	39,71	68,64	34,43

fig 31 photographs from optical contact angle studies

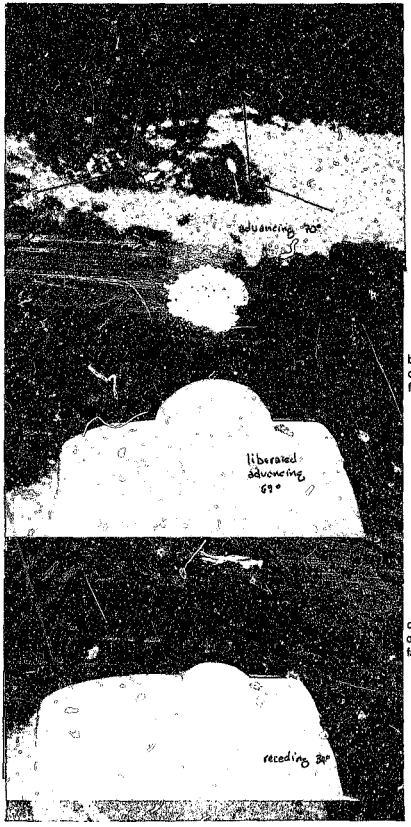


a) advancing angle on a diamond still partially locked in *kimberlite rock*

b) advancing angle on a freshly liberated face

c) receding angle on a freshly liberated face

fig 31 photographs from optical contact angle studies



a) advancing angle on a diamond still partially locked in kimberlite rock

b) advancing angle on a freshly liberated face

c) receding angle on a freshly liberated face

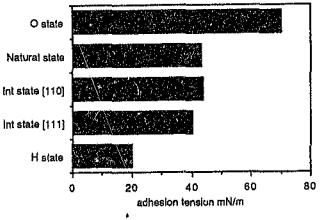
The adhesion tensions calculated from these results are :

exposed surface: 40,0 - 44,3 mN/m
fresh surface : 43,0 - 44,1 mN/m

which are in the range seen for the intermediate state of mechanically polished surfaces.

The advancing angles were generally lower, and the receding angles generally higher, than found by capillarography. This is in part due to relaxation during the time required to make an optical measurement, where capillarographic angles are measured instantaneously, and in part due to evaporation from the droplet. Fortunately the errors tend to cancel in calculating the adhesion tension.

fig 32 relative wettability of natural surface



CHAPTER 7 - RESULTS OF SPECTROSCOPIC METHODS

7.1 Sequence of Experimentation

Historically, the XPS technique was attempted before the RBS or LEED techniques. Because of difficulties with an O(1s) signal derived from the sample holder during XPS, which made quantitative measurement of the oxygen coverage of the surface difficult, the RBS technique was used. There were initial difficulties even here, because of a high background caused by secondary scattering of ions. After solving this problem by the use of a beryllium shield, better quantitative results were obtained from the surface. This indicated an approximately 1/3 monolayer coverage by oxygen, which was then followed up using the XPS technique, using a larger diamond, a goldplated holder for the diamond, and introduction of the diamond by means of a UHV transfer system (see 5.4).

7.2 Rutherford Backscattering Results

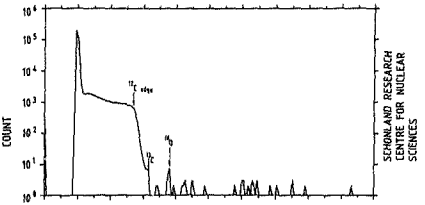
7.2.1 Oxygen Analysis

Experiments with mechanically polished and oxidized surfaces in the early stages were characterized by a high background in the spectra, and no significant difference between polished or oxidized surfaces. Oxygen levels of 0,6 to 0,7 monolayer were calculated. There was often significant level of Fe and Si (up to 0,4 ML). This suggested changes in the cleaning equipment, longer ultrasonic rinsing, and the use of a beryllium shield on the sample holder. The low atomic weight of beryllium causes very little secondary scattering.

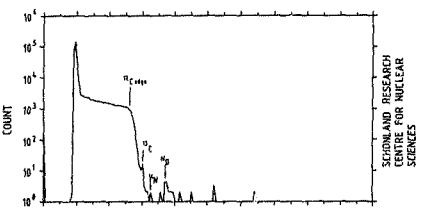
After the inclusion of the beryllium shield, better spectra were obtained. Examples are shown in Figure 33. The use of a logarithmic scale in these spectra, to allow inclusion of the high carbon signal, causes some distortion of the smaller peaks, and zero suppression which obscures the low level background signals. The region of the oxygen peak, channels 70 to 80, was replotted on a linear scale and this is shown in Figure 34. The oxygen peak can be seen, clear of the background.

FIGURE 33 R B SPECTRA

(a) POLISHED 0,32 ML 0



(b) HYDROGENATED 0,07 ML 0



(c) ADSORBED SPECIES

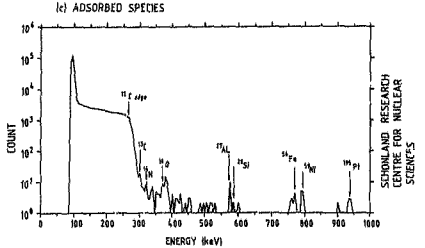


fig 34a composite RB spectrum for [111] Int

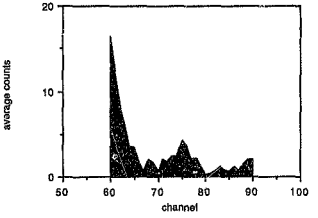
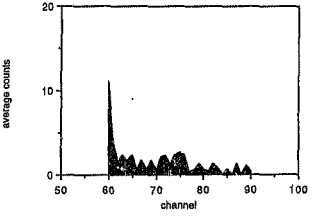


fig 34b composite RB spectrum for [111] H



CHAPTER 4 - CAPILLAROGRAPHIC APPARATUS AND REAGENTS

4.1 Cell and Weighing Linkage

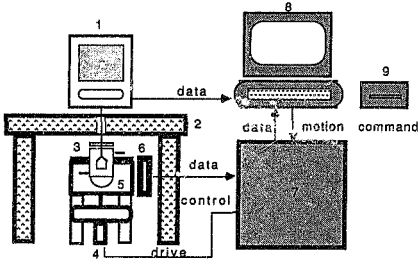
A schematic diagram of the capillarographic apparatus used in this study is shown in Figure 8. The elements are listed in a key to the drawing and more details are provided below. Figure 9 shows the cell with the close fitting lid used to exclude laboratory air. A trickle of high purity nitrogen (Air Products HP) was admitted to the cell through a distributor, aimed to avoid the liquid surface. The nitrogen was passed through a hydrocarbon trap (J & W Scientific, Rancho Cordova, California) and a Drechsel bottle containing reagent grade water at 25 °C. This was to inhibit evaporation in the test cell and was found to be effective. A fully wetting meniscus could be drawn onto a clean platinum plate and maintained at fixed meniscus weight for more than 8 hours.

The cell was thermostatted, normally at 25 °C, to a precision of approx 0,2 °C using a Labotec Julabo water bath. For low temperature tests, the water was diverted through a chiller.

MilliQ water was added to the cell through a small glass funnel which was drawn down to a tip. The tip retained a droplet of water and so provided a gas seal. Reagents to modify pH and ionic strength could be added through the same funnel. A feature of the cell, after a suggestion by Lubetkin (1985), is the facility for vacuum cleaning the interface. A hypodermic needle with a square cut tip protrudes through the lid to the level of the undisturbed planar water surface. This is attached to a vacuum line with a collection flask. The surface of the water can be drawn off in a "tornado" like effect, whilst adding clean water slowly through the funnel. This has the effect of sweeping surface impurities from the cell and allowed the maintenance of water surface tensions above 72 mN/m during long experiments.

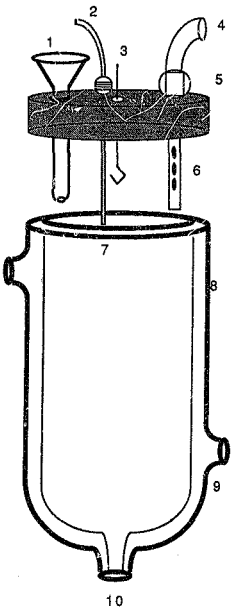
Figure 10 shows the type of clip used to hold the diamond test plate. The diamond was polished in the form of a spade, with a triangular peak which allowed positioning of the diamond in the clip in a reproducible manner.

fig 8 capillarographic apparatus - schematic



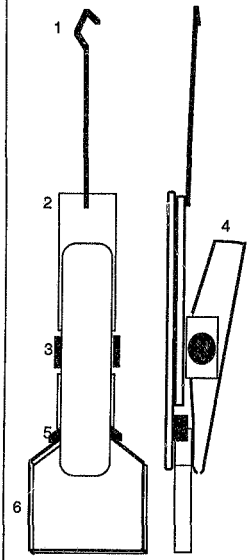
1. Mettler transmitting electrobalance
2. Balance table for underpan weighing
3. Introl precision positioning table (vertical)
4. DC motor with reduction box
5. Thermostatted glass cell with level reset and N2 atmosphere
6. Anilam 10 micron digital displacement transducer
7. Galil motion controller
8. Apple IIe microcomputer for motion and data processing
9. 5 1/4 " floppy disk data storage

fig 9 detail of capillarographic cell and lid



1. filling & addition funnel
2. sampling & cleaning extraction line
3. weighing linkage through 3 mm hole in lid
4. moist N2 supply
5. machined aluminium lid
6. low pressure N2 distributor
7. square needle tip for interface cleaning
8. 52 mm ID thermostatted glass cell
9. thermostat water inlet
10. test water drain.

fig 10 detail of clip for diamond test plates



1. hanger wire 0.4 mm brass
2. clip body, platinum
3. axle and rivet, brass
4. spring, hidden,steel
5. fitted vee-shoulder, platinum
6. diamond test plate

fig 11 capillarographic apparatus



fig 12 capillarographic cell

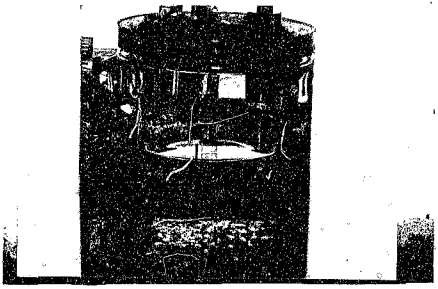
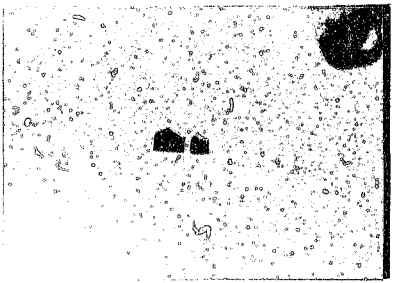


fig 13 diamonds used in wetting tests



The verticality of the diamond in the clip was adjusted by bending the hanger wire attached to the diamond so that the reflection of the diamond, when the diamond was suspended over a horizontal mirror, was collinear with the sides of the diamond. Two clips were made, one for the diamond with [111] major face, and one for the diamond with [110] major face. The body of the clip is platinum, to prevent corrosion product from affecting the water in the cell. The clips were cleaned by ultrasound in Contrad detergent (also called Decon in some countries), followed by three changes of milliQ water, and stored in a desiccator over silica gel when not in use.

Figures 11 and 12 show the apparatus and a close-up view of the diamond in the cell. The liquid surface has not reached the bottom edge of the diamond in Figure 12, so no meniscus can be seen.

4.2 Displacement and Force Transducers

Displacement Measurement and Control

The cell was mounted in a specially fitted anodized aluminium clamping plate which assured good verticality and no slip during elevation. The clamping plate was bolted to the platform of a precision positioning table (single axis table 2080-1, Introl, Edenvale, RSA), driven by a Unimatic MT2115 DC servomotor with 18:1 reduction box. The table was operated in the vertical mode, attached to a massive support frame of powder coated steel. The servomotor was powered by a Digiplan PWM4 servo drive, with 20 amp peak motor current and slewrate of 500Hz. The position of the table was detected by a digital linear displacement transducer (Anilam A10, Anilam Electronics, Milton Keynes, England) to an accuracy of 0,01 mm and a reproducibility of 0,01 mm in 150 mm. The displacement signal was processed by a motion controller (Galil DMC 100, Mountain View, California). This "card" communicates upwards with the Apple IIe microcomputer used to sequence the experiment, via an RS232 data link. A position or velocity command from the Apple computer causes the Galil card to generate the appropriate motor drive signal to the servo drive, depending upon the deviation from the desired position. This system

allowed accurate and repeatable traversals with direct data logging of the position. The accuracy of the displacement transducer and motion controller was tested using a machinist's clock gauge mounted rigidly on the weighing table (Figure 8) with a 6 mm steel bracket, and found to be within specification, less than 0,01 mm error after repeated traversals of 100mm.

Force Measurement

The weight of the diamond and support clip was measured using a Mettler AE163 electrobalance, with 0,01 milligram resolution, and using the underpan weighing facility. The digitally encoded weight was transmitted via a Mettler 011 data transfer module to the Apple IIe supervisory computer. The front of the weighing table, below the plinth, was enclosed to exclude drafts, and a window of 200 x 80 mm in clear perspex was installed to allow viewing The electrobalance system is well suited to capillarography because of the null deflection principle (Bayramli et al 1981). The maximum data transmission rate achieved was once in 600 milliseconds. For faster weighing than this, a strain gauge or piezo-electric system could be used, with compensation for deflection in the buoyancy calculation, but this was not necessary in these tests.

4.3 Water Preparation

The water used in all experiments was prepared from distilled water using a Milli-Q 3-cartridge (Continental Water Systems, El Paso Texas) water purifier followed by reboiling to remove air. The conductivity was always less than 0,05 µS. Surface tension was measured using a platinum plate of dimensions very similar to that of one of the diamonds used in the testwork, supported in the same way. The platinum was flamed in a low blue hydrogen flame until glowing and tested within 10 minutes. The surface tension was found to be 72,4 ± 0,1 mN/m at 298K. This is somewhat higher than normally found by force measuring techniques (71,9 mN/m), but Bayramli et al (1981) have reported the same value, with higher standard deviation, for triply distilled water. If this is a geometry effect (the end-correction of Padday (1964)), it should apply equally to the diamonds testpieces, which are of similar shape.

4.4 Data Capture

Data-Logging Computer

The data from the electrobalance and from the Galil motion controller were already in digital form. Routines for interfacing the data string transmitter of the Mettler balance with a BASIC operating program were provided by Protea Laboratory Services. The routines for sending motion commands to the motion controller, and extracting position information during execution of the supervisory program were developed by the author in consultation with Ivy Systems, Craighall Park, RSA. The supervisory programs, which include the routines for detecting the bottom edge of the testplate, recognizing the buoyancy slope and accumulating averages of the contact angles, were written by the author. A flow sheet of a typical supervisory program appears in Appendix 2, and a listing of one of the programs appears in Appendix 3.

4.5 Shaping and Orientation of Diamonds

Test diamonds were made by conventional polishing of diamond crystals taken from the production of Premier Mine, Transvaal. There is a certain proportion of diamonds which form as flattish triangles (macles) or irregular shapes. This occurs as a result of "twinning", the simultaneous growth of two crystals, with one crystal rotated through 180 degrees on an octahedral plane (Bruton 1978).

The diamonds were marked, in discussion with a diamond polisher at the Diamond Research Centre, so as to derive the largest possible square sided plate, with Vee-shaped peak, which would be free of surface flaws such as exposed non-diamond inclusions. The major faces were then polished, as near to the [111] plane as could be achieved. This is a very slow process, because the [111] surface is notoriously difficult to polish, and excessive loading causes burning of the diamond. This has been discussed by Watermeyer (1980).

Once two large and flat parallel faces had been obtained, with a thickness of 1,0 to 1,5 mm, the sides, base and peak were formed. A photograph of two finished diamond plates appears as Figure 13.

After the first polishing, the remains of the epoxy setting cement were removed in hot chromic acid, followed by distilled water rinses and extraction in toluene (similar to the technique of Hartley (1978), but using the more environmentally acceptible toluene, rather than benzene). Because of the possibility of oxidation by the chromic acid, and adsorption of the toluene, a method of physical cleaning using alumina abrasive powder on a glass disc, was used after subsequent polishings. This is discussed in more detail in section 4.6 below.

Crystal Orientation

The crystal orientation of the major faces was determined by Laue photography. The Laue photograph for the testplate used predominantly in the RBS analysis is shown in Figure [illegible] position of the centre of the diffraction pattern, together with the diamond - screen distance, was used to determine how far from the true [111] plane the major face was in each case.

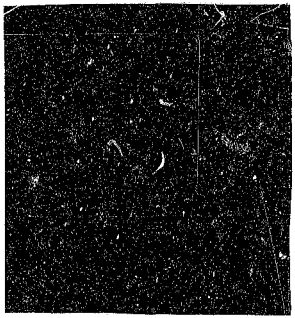
The results are shown in Table 4.

TABLE 4 . RESULTS OF LAUE CRYSTAL ORIENTATION ANALYSIS

Test Plate Number	Orientation Degrees off [111]	Comment
TP0 (oval)	19	Large, unsuitable for capillary measurements
TP1	3,5	Medium sized
TP2	5	Small
TP3	40	Large, 7 degrees off [110]

TP2 was used largely for RBS, although characterized by capillarography after polishing.

fig 14 x-ray diffractometer (Laue) photograph of polished [111] diamond



TP1 and TP3 were used extensively for capillarography, and TP3 was assumed to represent the behaviour of the dodecahedral face, [110]. It is possible that a macroscopic dodecahedral face is composed, on a microscopic scale, of terraces of [111] planes, but this will in any case give a higher frequency of edge sites, with more labile carbon atoms, so the suspected trend of greater reactivity of the true [110] may be preserved.

TP0 was used in LEED and XPS experiments, because of the greater available flat area.

4.6 Cleaning Techniques

The cleaning of mineral surfaces prior to analysis is contentious. Dust and organic contaminants such as skin oils must be removed, and some techniques, such as accurate contact angle studies, call for planar surfaces.

Polishing and Cleaving

Soft minerals such as graphite and coal can be polished on abrasive papers, ending up with a final polish on filter paper or degreased linen (Gutierrez Rodriguez et al 1984). Arbiter et al (1975) showed that organic rinsing (in alcohol and ether) of graphite and stibnite specimens polished on filter paper produces a sessile drop contact angle some 15 degrees greater than water rinsing. Cleaving graphite in air produced a value intermediate between these two. Cleaving is the most reasonable approach for minerals since it simulates the process of liberation from the ore. Kelebek and Smith (1985) have used this approach for molybdenite and sulphur, both soft minerals. Hartley (1978) attempted to do the same for diamond but with *little success. The cleaving of diamond requires considerable skill, and* would be virtually impossible as a routine procedure in a glovebox or similar clean environment. Polishing is assumed to proceed by cleavage on a microscopic scale. Janczuk et al (1985) polished graphite in water using a graphite powder, followed by ultrasonic rinsing to remove polishing debris. The same technique is theoretically possible for diamond, using diamond powder on a conventional polishing wheel or "skaif", but in

practice there are two complications. Firstly, the diamond powder must be held on the polishing wheel, which rotates at high speed, and conventionally olive oil is used. This introduces organic impurities, which, arguably, may be removed by a series of organic rinses using progressively more volatile solvents. Secondly, the diamond itself must be fixed rigidly in a polishing tool or "dop", using epoxy cement or inorganic cement containing asbestos. Because of the high forces and temperatures transmitted to this bond during the polishing, a tough coating forms, and a vigorous chemical cleaning step is needed subsequently. Strong oxidizing acids, such as chromic (chromosulphuric) acid are used in the industry. A less severe polishing on a slow disc with mechanical clamping of the diamond, is possible, but the same effect can be achieved using a softer abrasive - see below.

Chemical Cleaning

Pate (1986) used the sequence halocarbon:acetone:alcohol after polishing diamonds and before analysis in ultrahigh vacuum. He also used a "heat cleaning anneal" at 770 K in UHV before making measurements on the diamond surface. This would probably desorb any organic molecules still present from the rinsing step.

In the case of wettability measurements, the chemical effects of strong acids or organic solvents may mask entirely the intrinsic behaviour. Sappok and Boehm (1968) were obliged to use an acid rinse on the diamond powders in their studies because the process of pulverizing diamond produces metal debris which must be dissolved out of the product. The possible effects on their results will be discussed in section 7.3. Hartley (1978) used a series of hot and cold organic rinses, culminating in hot extraction for 6 hours with benzene. No mechanical cleaning of the diamond surface is discussed, although most researchers, as listed above, feel the need for a final wipe with filter paper or lens paper, or an ultrasonic cleaning. Early experiments in these laboratories using a cruder form of capillarographic apparatus than discussed here, revealed clearly that organic rinsing (toluene, n-heptane, methanol) prior to testing had a hydrophobizing effect and chromic acid had a slight hydrophilizing effect.

Soft Polishing

Pashley (1978) produced quartz surfaces for ellipsometric measurements of smoothness in the nanometre range by a long process of polishing, ending up with ceric oxide powder on a Pellon pad. The ceric oxide is softer than quartz, by the usual hardness tests, and it seems surprising that this should work. Pashley remarks that the surface left after polishing with diamond powder, even the finest grades, had surface marks and subsurface stresses which interfered with the ellipsometric technique. The soft polishing removed these features. Two previous studies have suggested the use of alumina powder as a cleaning agent for the study of diamond surfaces. Miyoshi and Buckley (1980) used alumina polishing to prepare diamond flats for the measurement of metal:diamond friction. Nassau and Schonhorn (1977) used alumina polishing to produce a fresh surface on diamonds for contact angle measurement by sessile drop. They suggest that these diamonds had undergone surface modification by exposure to radiation, making them exceptionally hydrophilic. A different reason may be suggested (see section 7.3). It appears that polishing with a soft abrasive can remove the topmost layers, particularly if these have been modified by some chemical reaction.

A polishing technique using alumina abrasive (Norton 1 micron powder) in water was used in this study for cleaning the diamond surface prior to contact angle measurements. Initially this was done in the laboratory atmosphere, but later the entire polishing and rinsing stage was installed in a glove box which was slightly overpressurized with nitrogen. No attempt was made to exclude oxygen, but only to reduce interference from dust and airborne organics. Polishing was performed on a 90 mm glass disc fitted in an aluminium wheel and rotating at up to 400 rpm. The polishing holders for the diamonds were made of stainless steel and were designed so that the diamond was retained by virtue of its shape alone. The diamond was traversed along an arc during polishing to achieve a uniform surface.

The procedure for preparing the diamonds was then :

1. An initial diamond polishing to form the plates
   This was repeated after surface damage

2. Washing with toluene and acetone under ultrasound.

3. Polishing with levigated alumina (< 1 micron) on a glass disc of 90 mm diameter at approximately 300 rpm for 3 minutes per face. The disc was irrigated and rinsed with milliQ water.

4. Jet cleaning of the diamond with pressurized milliQ water in a PTFE beaker.

5. Ultrasonic rinsing in a PTFE beaker, under milliQ water for 10 minutes.

6. On withdrawing from the milliQ water the major faces emerged dry. Any droplets on the edges were drained using wicks of filter paper. The diamond was further dried in nitrogen over a heated ceramic wafer for 120 seconds.

After chemical contamination, or a period of no use, steps 3 to 6 were employed.

The integrity of this cleaning step was assessed by cleaning a glass test plate of dimensions similar to those of TP3. Chromic acid cleaning of such a glass surface gives contact angles of zero, advancing and receding. (See Figure 22). Alumina polishing of the glass did not cause an increase in the contact angles. As a further precaution, the alumina was calcined in an oven at 770 K for 12 hours before being introduced into the glove box.

Cleaning of the Cell

The glass cell and associated glass fittings were cleaned by pickling in hot chromic acid. This was repeated whenever the inner surface of the cell showed signs of "beading" by water droplets. The chromic acid was rinsed off with cold milliQ water and the inner surface of the cell was then steam extracted for several hours in an upside down position. Cooling water was passed through the jacket and the condensate was diverted from the reboiler. The inner surface was judged clean when uniform film condensation was seen.

Cleaning of Tweezers and Hanger Wires

Tweezers, used to handle the diamond testplates between cleaning and loading into the cell, as well as clips and hanger wires were cleaned using Contrad, a laboratory detergent, in an ultrasonic bath. This was followed by three changes of MilliQ water to rinse, and drying in an oven at 70 °C. When not in use, clips and tweezers were stored in a desiccator. The author wore gloves during all operations on the cell and diamond holders, to prevent skin oils from being transmitted to the test surfaces or glassware.

4.7 Surface Reaction

Changes in the surface properties of the test plates were brought about by reactions with gases and with aqueous reagents.

Reaction with Gases

The diamond surface was modified by reaction [illegible]s in a tube furnace. Details of the apparatus used are given in Figu[illegible]. The gases used were :

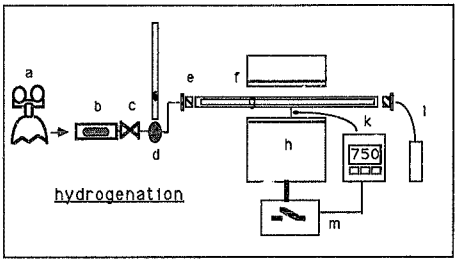
Oxygen	Afrox 99,5 %
Hydrogen	Afrox ultra high purity
Nitrogen	Air Products high purity
Argon	Air Products high purity

Reaction with Aqueous Reagents

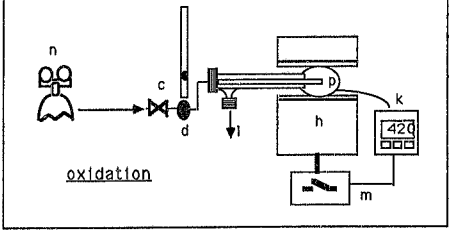
Reaction with aqueous reagents was conducted both outside the cell (prior to testing) and by addition of the chosen reagent to the cell volume through a filling funnel.

In the latter case, the concentration in the cell and the pH were monitored by extracting small volumes of the cell liquid through the surface cleaning needle and analysing in a micro-conductivity cell and a micro-pH cell. The conductivity cell was by Amber Science (San Diego, Ca) and the pH system by Markson (Phoenix, Arizona). For pH modifiers, titrimetric ampoules of

fig 15 tube reactor for gas reaction



	high purity H2	i	thermocouple
b	indicating oxygen trap	k	RKC 1000 controller
c	isolating valve	l	gas bubbler
d	needle valve & rotameter	m	contactor
e	brass end plug	n	pure O2, Ar ..
f	outer tube (s/steel)	p	glass reactor tube
g	inner tube (silica)		
h	ceramic tube furnace		



sodium hydroxide and hydrochloric acid (Carlo Erba) were used. The surface tension coefficient, K, defined by the equation :

$$\gamma - \gamma_0 = K \cdot [M] \qquad \ldots\ (15)$$

where γ is surface tension at conc m
γ_0 is water surface tension
M is molar concentration (< 0,1 M)

was found using the Platinum Wilhelmy plate in the cell. Bikerman (1970) reports values of 1,7 for alkali metal hydroxides, 1,6 for chlorides, and 2,6 for alkaline earth salts. Experimental values are shown in Table 5 . A negative value would indicate a surface active impurity. Note that the trivalent ions, Fe^{+++}, Cr^{+++} and Al^{+++} give considerably higher K values than do the di- and monovalent cations.

TABLE 5 - REAGENTS USED IN THIS STUDY

Reagent	Formula	Grade	Manufacturer	K
Potassium chloride	KCl	Aristar	BDH	1,2
Hydrochloric acid	HCl	Normex AR	Carlo Erba	2,3
Sodium hydroxide	NaOH	Normex AR	Carlo Erba	1,4
Sulphuric acid	H_2SO_4	AR	PAL	2,5
Sodium chloride	NaCl	AR	Protea	
Calcium chloride	$CaCl_2.6H_2O$	AR	PAL	2,8
Ferric chloride	$FeCl_3.6H_2O$	AR	PAL	62
Chromic chloride	$CrCl_3.6H_3O$	AR	Carlo Erba	33
Aluminium sulphate	$Al_2(SO_4)_3.16H_2O$	Analar	BDH	28
Sodium perchlorate	$NaClO_4.H_2O$	Analar	Carlo Erba	(1,4)
Sodium borate	$Na_2B_4O_7.10H_2O$	AR	PAL	
Boric acid	H_3BO_3	AR	H&W	
Sodium metasilicate	$Na_2SiO_3.9H_2O$	AR	J.T. Baker	
Potassium dichromat	$K_2Cr_2O_7.2H_2O$	AR	BDH	
Sodium borohydride	$NaBH_4$	Synthesis	Merck	
Lithium Aluminium - Hydride	$LiAlH_4$	Synthesis	Merck	
Methanol	CH_3OH	AR	PAL	γ = 22,1

Apart from these reagents, a selection of solvents and etchants were used to clean the diamond testplates and the glass cell.

TABLE 6 - REAGENTS USED FOR CLEANING PURPOSES

Reagent	Grade	Supplier
Toluene	Analar	BDH
Acetone	GP Reagent	BDH
Methanol	AR	PAL
Trichloroethylene	AR	BDH
Sodium dichromate	CP) "chromic acid"	PAL
Sulphuric acid	CP)	Protea
Contrad	Laboratory detergent	Hickman & Kleber

Contrad has been recommended for the cleaning of diamond prior to UHV work (Derry et al 1983). It was found to be an extremely alkaline agent (at 10% v/v in water) and was not used in diamond cleaning before wettability measurements because of the possible effect of pH on the surface groups.

CHAPTER 5 - SPECTROSCOPIC TECHNIQUES

5.1 Surface Analysis

Several different states of wettability were identified by means of capillarographic techniques, and the nature of the pretreatment suggested that changes in the types of surface adatoms induced by the treatment could be important. In order to resolve some of the possibilities, three surface analytical techniques were used. These were :

1. Rutherford Backscattering Spectroscopy (RBS)

2. Low Energy Electron Diffraction (LEED)

3. X-ray Photo-electron Spectroscopy (XPS or ESCA)

The basis of these techniques is outlined briefly in the following sections. There is a precedent for use of vacuum techniques to probe surfaces along with aqueous chemical studies. Kozlowski and Sherwood (1986) have combined XPS studies with electrochemical studies of the oxidation of carbon fibres.

5.2 Rutherford Backscattering

Theory

Rutherford Backscattering Spectroscopy utilizes the scattering or reflection of positive ions, of suitable high energy, by the nucleus of an atom in the target. A typical geometry for large angle Rutherford Backscattering is shown in Figure 16. In these experiments, a helium ion of 1,0 MeV energy was used as the scattered ion. The selection of helium is not arbitrary, Derry (1978) has shown that helium, with a mass number of four, gives the optimum resolution of surface adatoms with mass number near 12, the value for the carbon atom. The technique is based on the detection of peaks in a spectrum of backscattered ion counts vs energy. A surface barrier detector is used, which produces voltage pulses of height

Page 65 omitted in the pagination.

proportional to the energy of the backscattered particle. The number of pulses at a given voltage, after counting a certain large number of total pulses, represents the fractional occurrence of nuclei of a given mass number. For a single plane (thin film) of a single element, the spectrum would consist of one steep peak at an energy calculated by the following relation :

$$\frac{E_{scat}}{E_{inc}} = \left[\frac{M_1 \cos\theta_2 + \sqrt{M_2^2 - M_1^2 \sin^2\theta_1}}{M_1 + M_2} \right]^2 \qquad \ldots\ldots (16)$$

where M_1 = mass number of incident ion (4 for He)
M_2 = mass number of scattering atom (12 for C)
θ_1 = scattering angle - position of detector relative to incident beam - 25 degrees in this set up

or by rearrangement to permit the calculation of the mass number of the target atom :

$$M_2 = M_1 \frac{\varepsilon - 2\sqrt{\varepsilon \cos\theta_1} + 1}{1 + \varepsilon} \qquad \ldots\ldots (17)$$

where $\varepsilon = \dfrac{E_{scat}}{E_{inc}}$

In practice, this type of film does not exist, although a surface layer of adsorbed atoms on a planar surface of a substrate with lighter nucleus is a good approximation. Oxygen on the surface of diamond is an example. There will be a far greater frequency of bombarding ions which miss the nuclei of the oxygen layer completely, and penetrate the diamond crystal to some depth before being scattered. The ion will lose energy both on penetration and escape from the crystal so the spectrum becomes a plateau or shoulder, with a well defined high energy edge.

Meyer et al (1970) have developed the method for calculating the area density of target atoms from the counts in the peak for a particular adatom, and the number of counts per unit depth due to scattering by the substrate - in this case carbon (diamond).

$$\frac{P}{\Delta s}\,\Delta E_2\,\frac{dz}{dE_2}\left(\frac{Z_i}{Zc}\right)^2\,\frac{\rho_{dia}\,N_{av}}{M_c}\cos\theta_1$$

where P = counts in surface layer peak

ΔS = counts per channel in substrate spectrum

$\Delta E2$ = channel width (energy units)

dz/dE_2 = energy to depth conversion factor = 14 A/keV for 1,0 MeV He

Zc = atomic number of carbon

Zi = atomic number of adatom under investigation

ρ_{dia} = density of diamond 3,52 g/cm^3

N_{av} = Avogadro's number 6,023.10^{23}

M_c = mass number of substrate = 12 for carbon.

The calculation yields the numbers of atoms per cm^2 on the surface. With suitable assumptions about the state of the surface, and on a defined crystal plane such as [111], the number of carbon atoms in the immediate surface layer can be calculated and the count of adatoms converted to an equivalent monolayer. For instance, the carbon atoms in the topmost layer of an ideal [111] plane occur with a frequency of 1 per 55 000 square picometres, or 1,82.10^{19} per m^2.

Experimental Details

The 1,0 MeV particle Cockcroft accelerator at the Schonland Centre for Nuclear Sciences of the University of Witwatersrand was used to provide the particle beam. Further details of the system are given by Annegarn (1976). The diamond testplate was mounted in a holder with an additional beryllium shield over the front face of the holder to reduce stray reflections, which otherwise lead to a noisy background in the spectrum.

Meyer et al (1970) have developed the method for calculating the area density of target atoms from the counts in the peak for a particular adatom, and the number of counts per unit depth due to scattering by the substrate - in this case carbon (diamond).

$$\frac{P}{\Delta s}\,\Delta E_2\,\frac{dz}{dE_2}\left(\frac{Z_i}{Z_c}\right)^2\,\frac{\rho_{dia}\,N_{av}}{M_c}\cos\theta$$

where
- P = counts in surface layer peak
- ΔS = counts per channel in substrate spectrum
- $\Delta E2$ = channel width (energy units)
- dz/dE_2 = energy to depth conversion factor = 14 A/keV for 1,0 MeV He
- Zc = atomic number of carbon
- Zi = atomic number of adatom under investigation
- ρ_{dia} = density of diamond 3,52 g/cm^3
- N_{av} = Avogadro's number 6,023.10^{23}
- M_c = mass number of substrate = 12 for carbon.

The calculation yields the numbers of atoms per cm^2 on the surface. With suitable assumptions about the state of the surface, and on a defined crystal plane such as [111], the number of carbon atoms in the immediate surface layer can be calculated and the count of adatoms converted to an equivalent monolayer. For instance, the carbon atoms in the topmost layer of an ideal [111] plane occur with a frequency of 1 per 55 000 square picometres, or 1,82.10^{19} per m^2.

Experimental Details

The 1,0 MeV particle Cockcroft accelerator at the Schonland Centre for Nuclear Sciences of the University of Witwatersrand was used to provide the particle beam. Further details of the system are given by Annegarn (1976). The diamond testplate was mounted in a holder with an additional beryllium shield over the front face of the holder to reduce stray reflections, which otherwise lead to a noisy background in the spectrum.

The holder was positioned in a special goniometer equipped with an electron flood to inhibit charging of the non conducting diamond. The vacuum in this section of the ion beam line was maintained at better than 10^{-5} millibar.

Test Diamond

The ion beam induced surface damage, evident as a black spot after the experiment, was removable only by heavy polishing. Because this adversely affected parallel testing by capillarographic methods, a third diamond platelet, of slightly smaller dimension than the [111] platelet used for wetting, and with major face near the [111] plane, was used for the RBS testwork. Both sides were used, allowing normally 4 to 8 beam spots, before the surface needed repolishing to remove the radiation damage. A Laue X-ray diffraction analysis of the diamond revealed that the major faces were 5 degrees off true [111] planes.

5.3 Low Energy Electron Diffraction

Electrons of sufficiently low energy (100 eV for instance) will have a wavelength, according to the particle/wave duality of de Broglie (1924) of the order of 100 pm. They may be expected to create interference patterns with periodic structures such as crystals, which have a lattice spacing of the same order. Also, because of their low energy, the depth within a crystal from which elastically scattered electrons emerge, is very small. This makes them useful probes for the lattice structure of the surface of crystal. Ertl and Kuppers (1974) describe the development of the techniques of low energy electron bombardment and detection and the geometrical theory of diffraction. The possibility of surface reconstruction after reaction with hydrogen or oxygen, or the generation of surface groups with a fixed periodicity, could be detected by this technique.

The Geometrical Theory of Diffraction

The elastic interaction of the impinging electrons, with one or two topmost layers of the crystal, may be viewed as the scattering of monochromatic

waves by a two dimensional lattice or mesh. All regular surface arrangements can be classed into 5 two-dimensional Bravais lattices by the use of two basis vectors, a_1 and a_2. These are the sides of the smallest parallelogram, which by translation generates the surface mesh. In the case of diamond [111], the two vectors are of equal length and at an angle of 60 degrees, the co-called hexagonal mesh. The vector length is 252 pm.

The defining equations for the angles are :

$$\lambda = \frac{h}{mv} \qquad \ldots\ (19)$$

$$d\ (\sin \phi - \sin \phi_0) = n\lambda \qquad \ldots\ (20)$$

d = lattice spacing
ϕ " angle of constructive interference
ϕ_0 = incident beam angle (to normal)
n (integer)= diffraction order

Usually the surface atoms can be considered as equally spaced rows, of row spacing d, and where the incident beam is normal $\sin \phi_0 = 0$

$$\text{then } \sin \phi = \frac{n\lambda}{d} = \frac{n}{d} \cdot 1417 \cdot \frac{1}{\sqrt{U}} \qquad \ldots\ (21)$$

where U = accelerating voltage of the electron beam
d = *row spacing in pm.*

see Appendix 4.

In practice, the reflected beams with constructive interference fall on a hemispherical screen centred on the diamond sample. This is an image of the reciprocal space mesh. The matrix equations defining the coordinate transformation from real space to reciprocal space are given in Appendix 4. The symmetry of the diamond surface mesh gives a hexagonal lattice in reciprocal space too, but the spacing of the spots is in inverse proportion

to the spacing of the real scattering centres. Thus, a surface adatom which is attached at every second carbon surface atom, with a consequent lattice constant of 2 x 252 pm, will generate a superlattice with defining vectors twice the length of the diamond lattice. In reciprocal space this will form a lattice which has beamspots midway between the spots of the original pattern (Pate 1986).

This effect was used to determine whether there was reconstruction, or a periodic adsorption of hydroxyl groups or oxygen atoms on the surface of the test diamonds.

Experimental Details

LEED patterns of two of the test diamonds were obtained using the SOLAR 300 UHV chamber with Vacuum Generators LEED system at the Schonland Research Centre for Nuclear Sciences. The system is shown in Figure 17. The patterns were obtained at several voltages, but the most intense patterns occured near 220 volts. In some experiments a digital readout of the voltage appears on the photographs.

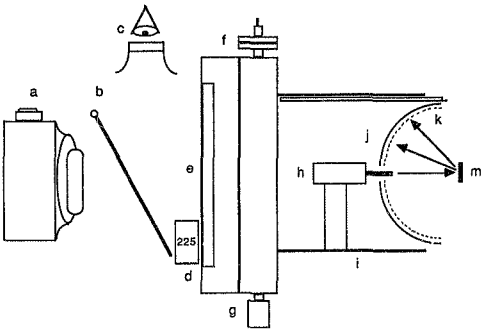
Diamonds TP1 and TP2 were tested after the standard cleaning step, and including a period of bake-out in the UHV chamber at 473 K. Sample TP2 (surface 5 degrees off [111]) was heated to 673 K in UHV and the LEED pattern examined again.

5.4 X-ray Photo-electron Spectroscopy

Theory

The excitation of atoms near the surface of the diamond crystal by mono-energetic X-rays results in absorption of a photon of characteristic energy, and prompt emission of a photo-electron. Electrons from all the orbitals which have binding energies lower than the photon energy will be excited, but the kinetic energy of the emitted electron will be reduced for orbitals of higher binding energy. This is expressed by the relation :

fig 17 low energy electron diffraction apparatus



a 35 mm camera
b swivelling mirror
c eyepiece
d digital voltage display
e viewport 200 mm on standard UHV flange
f grid feedthrough
g electron gun feedthrough
h electron gun
i mu-metal shield
j hemi-spherical cathodoluminescent screen 145 mm
k grids
m specimen

$$E_{kin} = h\nu - E_b - e\phi sp \qquad \ldots\ (22)$$

E_{kin} is the kinetic energy of the detected electron
E_b is the binding energy of the detected electron
$e\phi sp$ is the work function for the sample

When the spectrum of energies of emergent electrons is scanned by a suitable analyzer, a series of peaks at energies characteristic of the atoms present in the surface region will appear. The techniques of Carley and Roberts (1977) was used for the calibration and interpretation of the peak heights and shifts.

The relevant equation is shown as equation 23.

$$\sigma = \frac{Y_m}{Y_s} \cdot \frac{N \cos\theta\ \mu_s\ \rho_s\ \lambda}{\mu_m\ M_s} \qquad \ldots\ (23)$$

where σ = surface coverage by (oxygen) adatoms atoms/cm^2
Y_m = integrated XPS peak area for adsorbed atoms (oxygen) corrected for the increase in analyser sensitivity with decreasing kinetic energy
Y_s = integrated peak area for substrate carbon
N = Avogadro's Number
θ = system geometrical constant, 25°
μ_s = photoionization cross-section for carbon = 1.0
μ_m = photoionization cross-section for oxygen
= 2,92 (Schofield 1976)
ρ = diamond density, 3,52 g/cm^3
λ = photoelectron escape depth (AlK_a)
= 10 x 10^{-8}cm (Pate 1986)
M_s = Mass number of carbon
= 12,01

Depth Sensitivity

The depth of the crystal probed is governed by the depth from which electrons can escape. This is called the mean free path or escape depth and has been determined for diamond by Pate et al (1983) using a range of primary energies up to 1250 eV. On the [111] plane, this depth is of the order of 1000 pm, or approximately five double sheets. (The structure of the [111] planes is such that side view reveals alternately closely spaced and more distantly spaced sheets of atoms, conveniently regarded as double sheets, at a spacing of 204 pm (See Figure 2)).

Although this is not a purely surface sensitive technique, the surface layer will contribute more to the signal because of shielding and attenuation effects. The attraction of the technique is that it provides not only identification of the atomic species present, since each element has a unique combination of electron energy levels, but also some information about the relative frequency of each species and even the chemical environment in which hetero-atoms are bound. This last effect is due to the "chemical shift", the small change in the electrostatic potential of an atom, and so on the binding energy of even the core electrons, when involved in a covalent bond with a heteroatom of different electronegativity.

The most attractive feature of XPS is the non-destructive nature of the interrogation. Ion beams tend to desorb or destroy the surface during analysis, but only very unstable surface compounds are susceptible to damage by X-rays. Obviously, the use of an ultrahigh vacuum technique will force desorption of physically adsorbed molecules, but this is so for almost all the surface spectroscopies.

It is possible to combine analysis of the surface with more severe treatments, like heating, desorption and ion etching in order to obtain information about the type of bonding employed by the surface adatoms.

The major disadvantage found in these experiments was the rather broad analyzed area. In all cases, some signal was detected off the sample holder. This arises because of the difficulty in focussing the X-ray beam, and collimating the emitted electrons, on a target as small as these test diamonds.

Experimental Details

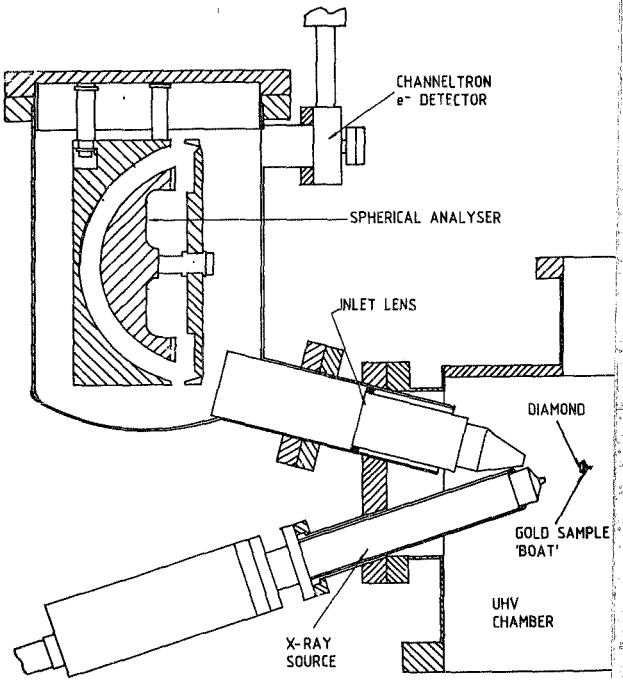
The elements of the Vacuum Generators CLAM system mounted on a SOLAR 300 UHV chamber are shown in Figure 18.

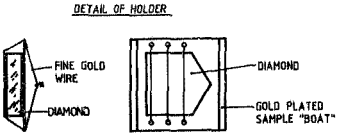
A choice of target material is possible. This changes the energy of the incident X-rays, hence the position of the XPS peaks in the analyzed spectrum. The emergent electron beam is analyzed using a hemispherical retarding lens analyzer, with digital display of the analyser voltage for good location of peaks. In practice, there was a slight drift in the analyzer datum, so that the carbon (1s) peak appeared between 1198 and 1203 eV on the kinetic energy scale. This is not important, as both the carbon and oxygen (1s) peaks are obvious, and cannot be confused with other species. The spectrum is recorded on an analog chart recorder.

In the early stages of this experimental program, the only method for introducing the sample (diamond) was by removing the top plate of the UHV chamber. This plate carries the sample manipulator and heater contacts. Because this procedure allowed moist air into the UHV chamber, the entire system required baking at 473 K before a reasonable vacuum could be obtained. A vacuum of better than 10^{-8} millibar is required for XPS. The diamond was thus subjected to temperatures of 473 K for several hours, which could have caused desorption of surface oxygen groups.

Early in 1987, a Leybold Heraus sample introduction rod was fitted to the UHV system. This allows the movement of the sample, on a specially designed "boat", from atmosphere, through a chamber where gas reactions can be conducted, onto the sample manipulator. No bake-out is then required and the surface can be analysed without delay. The boat fits into a clip in the rod which allows passage of electrical current through the stainless

FIG. 18 XPS APPARATUS





steel plate supporting the diamond. This allows heating of the diamond in the reaction chamber. In this way oxidation of the diamond could be achieved. The temperature attainable were not high enough for useful hydrogenation experiments in this chamber. Hydrogenation was performed remotely, in a silica tube furnace.

A number of mechanisms for mounting the diamonds on the boat were attempted. An important consideration was the amount of oxygen signal generated by X-rays impinging on the sample holder. This was gold plated because gold has a low retention of adsorbed oxygen in UHV.

The best approach was found to be strapping of the diamond to the holder using a system of fine holes and 0,3mm gold wire. The diamond was positioned for analysis on the manipulator by minimizing the gold (4f) peak, whilst maximizing the carbon (1s) peak, and the blue (X-ray induced) luminescence of the diamond, which could be seen through an upper viewing port.

The sample manipulator has a built in heater for thermal desorption experiments. There is a thermocouple for readout of sample temperature.

CHAPTER 6 - RESULTS

6.1 Capillarographs

The result of an individual experiment is a capillarograph which is a plot of force vs depth of immersion. The computer data retrieval technique allows instantaneous calculation of a contact angle from the basic equation shown in Figure 4. Not every contact angle is an equilibrium (dynamic) angle because of the phenomenon of "hingeing". Figure 19 shows the phases of an experiment of three cycles of immersion. Hingeing occurs at the end of a pass, where the three phase line is stationary and the contact angle swings from an advancing to a receding value. This is seen as the steep (and smooth) sides of a capillarograph. By a simple numerical differentiation of the data to detect the slope, these data can be excluded from calculation of the true advancing and receding contact angles. Figure 20 shows an actual capillarograph plotted from data stored during an experiment with TP1, in the cleaned state. Since this state is intermediate between an extremely hydrophobic state and a hydrophilic state, it is designated "INT" (discussed more fully below, Section 6.4)

It is possible to extract a value for the advancing and receding contact angles by a graphical construction which is illustrated in Figure 20. Two lines are drawn to be the best fits to the groups of lines in the stable advancing and receding sections of the loop. These lines (or their extrapolations) will intersect the vertical line corresponding to zero immersion depth. At this point, the force is solely due to the meniscus weight, since dry weight has been tared off electronically by the balance. In this example the construction gives 21 mgf in the advancing mode and 91 mgf in the receding mode. The perimeter of this diamond is 1,388 cm. The surface tension (in mgf - the author begs leave to forsake the pure SI system for just this one example, and until the balance manufacturers start to provide direct readings in Newtons), is 73,8 mg/cm and hence :

advancing contact angle = arc cos (21/1,388.73,8) = 78 degrees
receding contact angle = arc cos (91/1,388.73,8) = 28 degrees

The measure adopted to combine these values into a single index of wettability is the average adhesion tension :

fig 19 *stages in the wetting hysteresis loop*

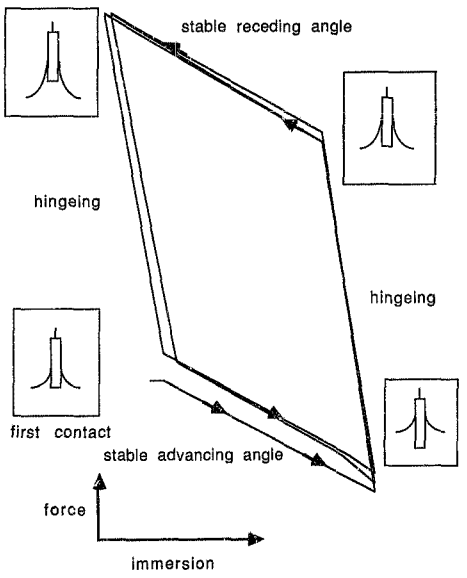


fig 19 stages in the wetting hysteresis loop

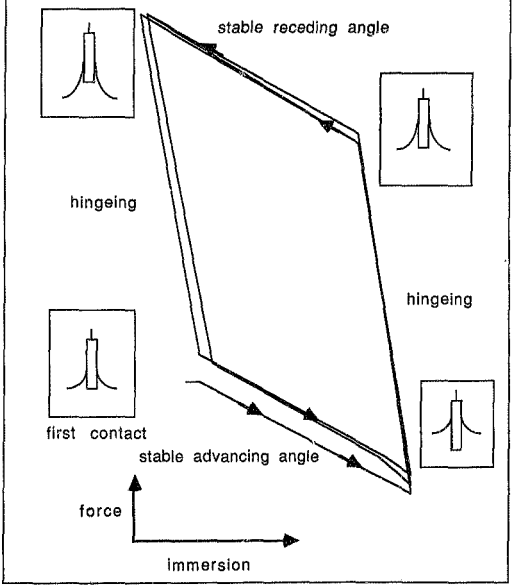
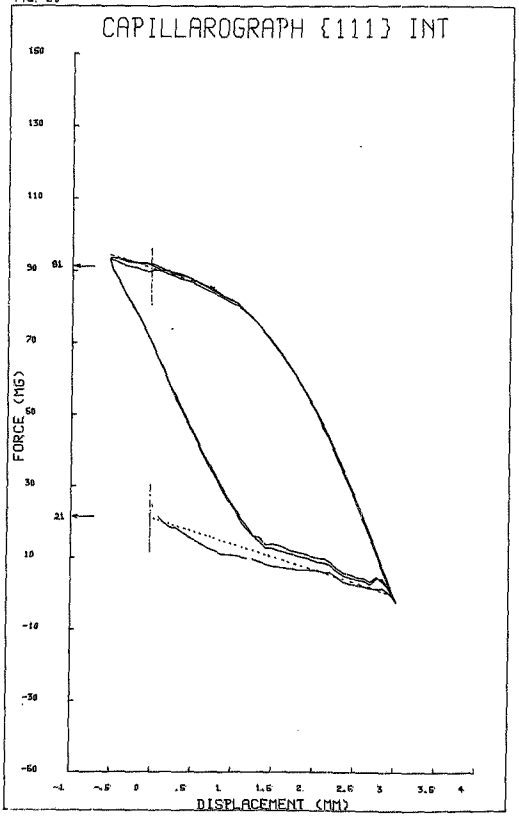


FIG. 20



J. D. HANSEN UW CHEM

adhesion tension = 72,4 (cos θa + cos θr)/2 = 39,5 dyn/cm or mN/m.

In operation under computer control, the graphical construction is replaced by calculations at 50 (approx) points on the stable advancing or receding sections, with averaging of the results at the end of each pass.

Figure 21 shows the superimposed capillarographs for one diamond after three different treatments :

1. Oxidation at 693 K in oxygen

2. Normal attrition cleaning

3. Hydrogenation at 1023 K in UHP hydrogen.

The capillarographs are progressively displaced downwards (lower wetting force or adhesion tension) and the differentiation between the states is clear, even though the hysteresis loops overlap. This is because the advancing angle on, say, an intermediate surface, is still higher than the receding angle on an hydrogenated surface.

Because the capillarograph is not a very condensed method of displaying the data, all further results will be presented as either :

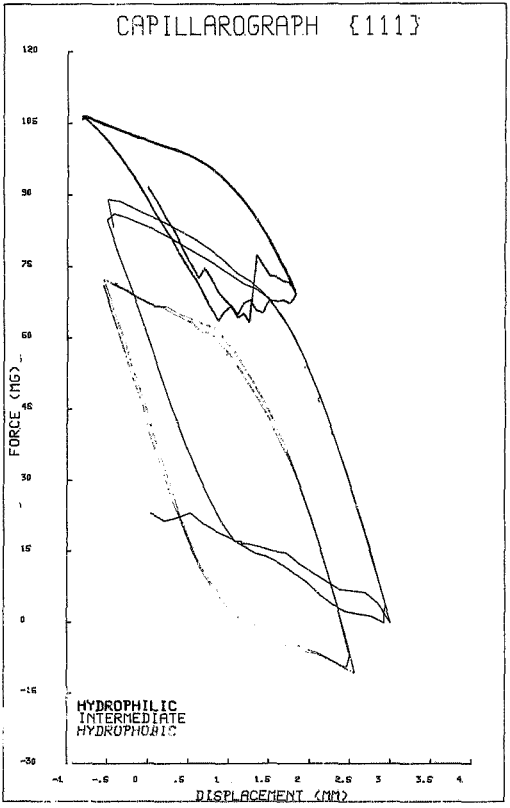
1. A single adhesion tension

2. A pair of contact angles from the average of three passes.

Each full pass takes 0,2 hours, therefore this result refers to a surface in contact with the test solution for 0,3 hours.

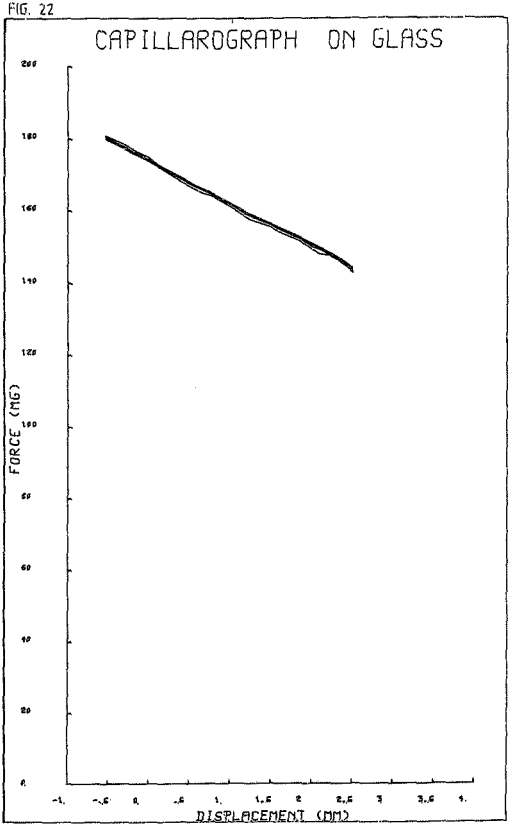
Figure 22 is a capillarograph obtained with a glass plate of perimeter 2,350 cm, matching the shape of diamond TP3 as far as possible. A very shallow hysteresis loop (virtual absence of hysteresis) was obtained. The graphical method gives a mean meniscus force (advancing and receding) of 173 mg, and hence a contact angle of less than 4 degrees - effectively

FIG. 21



J.O. HANSEN UW CHEM

FIG. 22


CAPILLAROGRAPH ON GLASS
FORCE (MG)
DISPLACEMENT (MM)
J. D. HANSEN, UW CHEM.

zero. This test was used to monitor contaminant ingress into the cell, and cleaning techniques.

6.2 Polished Diamond Surfaces

Appendix 5 contains the results of experiments on TP1, major face [111] and TP3, major face [110] using alumina attritioning as a cleaning step. These experiments were conducted over a period of two years. Some of the earlier results for TP1 were obtained by polishing manually on a microscope slide. Later results were obtained by polishing in the glove box on a glass disc at approximately 200 rpm using three minutes per side. Histograms showing the distribution of adhesion tension for the two surfaces are shown in Figure 23. The results show considerable scatter, but this is thought to be a real effect deriving from the variability of surface composition of the diamond surface following various chemical treatments in prior experiments, rather than experimental errors. This is discussed in Section 8.3.

The major results may be presented in this abbreviated table, showing the average advancing and receding angles, and the adhesion tension, for [111] and [110] faces :

TABLE 7 - WETTABILITY OF MECHANICALLY CLEANED DIAMOND SURFACES

	Advancing Angle Degrees	Receding Angle Degrees	Adhesion Tension mN/m
TP1 [111] Surface	76 ± 5	29 ± 5	40 ± 4
TP3 [110] Surface	71 ± 4	25 ± 5	45 ± 3

fig 23a distribution of adhesion tension on polished [111]

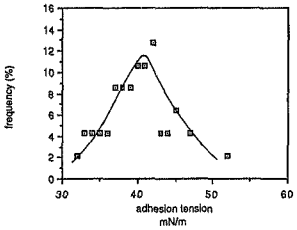
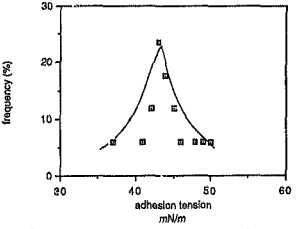


fig 23b distribution of adhesion tension for polished [110]



6.3 Oxidized Diamond Surfaces

Figure 24 shows the effect of treatment of [111] and [110] surfaces in oxygen, at approximately 90 kPa absolute pressure, and progressively higher temperatures. The time of exposure was 0,5 hours at the stated temperature, with progressively longer heating up and cooling times at the higher temperatures.

These figures show that oxidation of the surface, evident as increased wettability or adhesion tension and lower contact angles, begins at approximately 470 K and progresses virtually to completion at 720 K. The adhesion tension approaches 70 mN/m at this point, only slightly less than that for clean glass (72,4). Sappok and Boehm (1968) demonstrate the same effect for diamond powders at 690 K. The [110] surface appears to be more susceptible to oxidation than the [111] surface. The [110] diamond approaches total wettability at a temperature some 50 K lower than does the [111] surface.

The extremely hydrophilic state appeared to be unstable, with a slow but reproducible reversion towards more hydrophobic behaviour. This is shown in Figure 25. This process is more pronounced if the surface is attritioned with alumina. Table 8 shows the results of tests performed on the [111] diamond, immediately after oxidation at 690 K, and then after progressively longer periods of attrition cleaning, using alumina abrasive in a glovebox.

TABLE 8 - EFFECT OF ATTRITION CLEANING ON THE OXIDIZED [111] SURFACE

State	ad. angle degrees	rec angle degrees	adh tension mN/m
Oxidized 690 K	37,3	11,6	64,2
Reclean 3 mins	62,4	23,2	50,0
Reclean 6 mins	70,1	28,0	44,3
Reclean 9 mins	69,0	25,2	45,7
Reclean 12 mins	73,4	28,6	42,1

fig 24a oxidation effects on contact angles

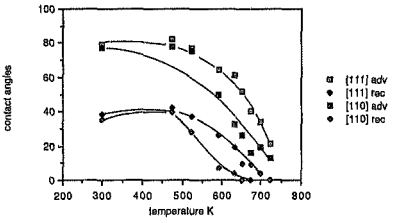


fig 24b oxidation effects on adhesion tension

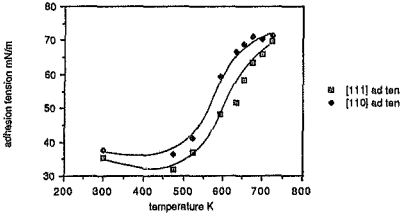


fig 25 recovery from hydrophilic state

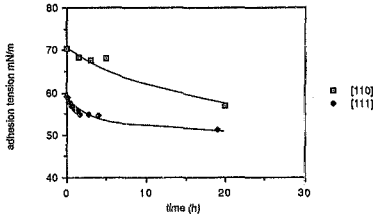
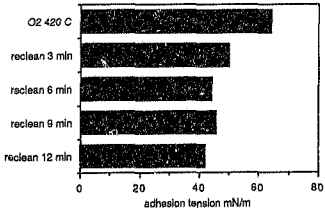


fig 26 effect of attrition on oxidized surface



The trend is shown in Figure 26. Apart from an anomaly at the third cleaning step, which may have been caused by inadvertent contamination, the surface tends towards the value seen for the clean polished surface in Section 6.2. This effect helps to explain the scatter seen in the results for the mechanically cleaned surface. If we conclude that the process of polishing removes microfragments of oxidized surface, and replaces them by new surface which then equilibrates with the aqueous environment at the time of polishing, then there may be areas of the diamond surface which are protected from polishing, because of orientation or rugosity, and therefore persist after a few stages of cleaning. Chemical modification, by for instance, reduction with hydrogen at 1020 K, will not be impeded by surface roughness.

Hydrogenation in Solution

Hydrogenation of surface oxides by an organic hydrogenating agent, lithium aluminium hydride in diethyl ether, was attempted. The technique was first performed on a polished surface, and then on a surface which had been oxidized. An acid rinse is required to decompose aluminium reaction products on the surface.

TABLE 9 - HYDROGENATION BY LITHIUM ALUMINIUM HYDRIDE IN ETHEREAL SOLUTION

State	Adhesion Tension mN/m
Intermediate - polished	46,3
$LiAlH_4$ + acid rinse	45,0
Oxidized	63,9
$LiAlH_4$ + acid rinse	49,4

The acid rinse may have had the effect of decomposing surface oxirane type groups. There is a clear decrease in the wettability, but it is not possible to say whether the hydrophilic species destroyed was a surface carboxylic acid or an epoxide group. Note that there is no significant effect on the wettability of the polished surface, after treatment with lithium aluminium hydride.

Oxidation by Chromic Acid

Oxidation by hot concentrated chromic acid produces a less severe increase in wettability than gaseous oxidation. The [111] surface was exposed to chromic acid (Lelah et al 1979) for ten minutes at 90 °C. This was followed by rinsing with ultrasound and drying in the glovebox.

TABLE 10 - EFFECT OF CHROMIC ACID AND ATTRITION ON THE [111] SURFACE

State	Advancing Angle Degrees	Receding Angle Degrees	Adhesion Tension mN/m
Polished, clean	79	33	37,3
Chromic acid	62	22,5	50,4
Reclean 3 mins	64,7	27,8	47,5
Reclean 6 mins	73,2	27,3	42,6
Reclean 9 mins	73,6	28,9	41,9

This is shown in Figure 27. The chromic acid appears to be less strongly oxidizing than the high temperature oxygen, and the (intermediate) hydrophobic state is achieved with limited attritioning.

6.4 Hydrogenated Diamond Surfaces

Diamonds with [111] and [110] major faces were exposed to hydrogen at progressively higher temperatures. Figure 28 shows that there is no effect until 720 K, at which point the surface becomes significantly more hydrophobic, reaching a maximum at 1020 K. The surfaces were partially oxidized at the start of the series, which accentuates the transition, and the [110] surface started considerably more hydrophilic than the [111] surface. The change is most pronounced at approximately 770 K, which is the range of temperature where the most rapid thermal desorption of CO and CO_2 from diamond powders has been seen (Matsumoto et al 1977). It is possible that the hydrogenation process requires the desorption of a CO group, exposing a reactive surface carbon atom for hydrogenation, rather than splitting of the C-O bond.

fig 27 effect of chromic acid and attrition

fig 28a effect of hydrogen on contact angles

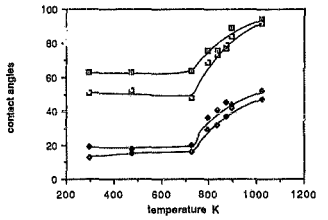


fig 28b effect of hydrogen on adhesion tension

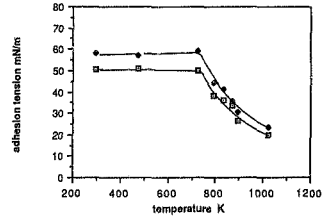


fig 29 effect of attrition on hydrogenated surface

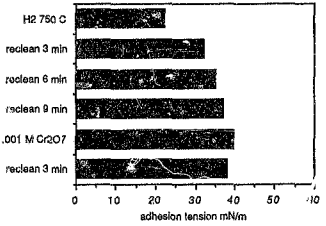
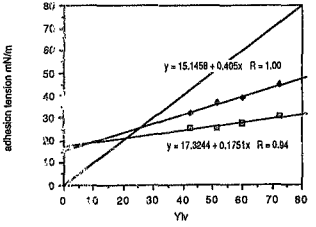


fig 30 Zisman plots for [111]H and [110]Int



The [111] surface appears to be more susceptible to hydrogenation, after partial oxidation, than does the [110] surface. This may be a result of the more favourable sites for oxygen chemisorption on a net [110] face.

The hydrogenated surface was very stable. The diamonds were stored in a desiccator for 10 days and retested, with no significant change in the adhesion tension characteristic of the strongly hydrophobic state.

The hydrogenated surface could be removed by attrition cleaning. Figure 29 shows the result of progressively longer polishing with alumina. After three stages of polishing the adhesion tension approached that of the standard intermediate surface (40 mN/m). At this stage a chemical treatment, with acidified potassium dichromate, was applied. There was a small increase in wettability, indicating that some surface groups were susceptible to mild oxidants. Alternatively this may have been caused by adsorption of a hydrated cation (see Section 9.7) because a subsequent polishing stage produced a slightly more hydrophobic state.

An examination of Figure 26 in conjunction with Figure 29 demonstrates that there is a continuum of states of wettability for the diamond surface, ranging from : very hydrophilic, but relatively unstable, after oxidation at 670 K, with adhesion tension near 70 mN/m,

through a more hydrophobic range, most usually seen on mechanically polished surfaces, with a median adhesion tension at 40 mN/m,

and on to a very hydrophobic state, after hydrogenation at 1000 K, stable against chemical attack at room temperature, with adhesion tension 20 mN/m.

In further discussion the following identification of these states is proposed :

TABLE 11 - CLASSIFICATION OF WETTING BEHAVIOUR

H	The very hydrophobic state
O	The hydrophilic state
Int	The intermediate state

To some extent the intermediate state is a range of states, depending upon the direction of the most recent treatment, oxidation or hydrogenation.

These states can be classed according to adhesion tension :

TABLE 12 - ADHESION TENSION OF THE DIFFERENT CLASSIFICATIONS

State	Adhesion Tension (mN/m)
H	18-25
Low Int	25-40
High Int	40-55
O	55-72

The median of the results for the polished [111] and [110] surfaces (Section 6.2) provides the boundary between low intermediate and high intermediate values. Nassau and Schonhorn (1977) give a contact angle for the polished diamond surface of 47 -55 degrees. If we assume that this is a reasonable average of receding and advancing values, then this corresponds to an adhesion tension of 49-42 mN/m. This is in fair agreement with the present work, particularly since the top face of a brilliant cut diamond (as tested by them) will not be a [111] face, but something closer to [100], likely to have a higher frequency of surface oxides (Verwoerd 1986) and hence potentially more hydrophilic.

6.5 Zisman Plot

The Zisman plot is a recognized tool for characterizing the surface energy of a solid, independent of a particular wetting liquid (Zisman 1964). A method for determination of γc, the critical surface tension of wetting of minerals, using solutions of methanol in water has been given by Kelebek and Smith (1985).

Tests were performed with diamond TP1, with [111] major face in an hydrogenated state and diamond TP3, with [110] major face in an intermediate state.

The results are shown in Table 13 and the Zisman plots appear as Figure 30.

TABLE 13 - DATA FOR ZISMAN PLOTS

[111] Hydrogenated				
Volume % Methanol	γ mN/m	Advancing Angle Degrees	Receding Angle Degrees	Adhesion Tension mN/m
0	72,4	85	41	30,5
5	60,0	82	39	27,5
10	51,4	81	34	25,3
25	42,4	72	26	25,6
100	22,5	0	0	22,5 * excluded
[110] Intermediate				
Volume % Methanol	γ mN/m	Advancing Angle Degrees	Receding Angle Degrees	Adhesion Tension mN/m
0	72,4	72	26	44,6
5	60,0	69	20	38,9
10	51,4	65	0	36,6
25	42,4	59	0	32,1
100	22,5	0	0	22,5 * excluded

* data excluded from plot because total wetting occurred.

Linear regression gives the following equations for the Zisman plots in Figure 30 :

[111] hydrogenated : $\gamma \cos \theta = 0{,}175\ \gamma_{lv} + 17{,}2$
[110] intermediate : $\gamma \cos \theta = 0{,}405\ \gamma_{lv} + 15{,}2$

hence by setting cos θ to 1 and solving we find the critical surface tensions of wetting :

[111] hydrogenated : $\gamma_{crit} = 21$ mN/m
[110] intermediate : $\gamma_{crit} = 26$ mN/m

This can be seen again from the intercept with the diagonal on the plot. Kelebek and Smith (1985) find values of 40 - 45 for coals, 29 for the cleavage plane of molybdenite and 27 for a sulphur crystal face. Zisman quotes 22 for a surface of methyl groups, i.e. a paraffin wax. We conclude that the hydrogenated surface has a character essentially similar to a paraffin wax, and that even the polished surface is mainly composed of hydrophobic, low energy sites.

6.6 Optical Contact Angle Measurement

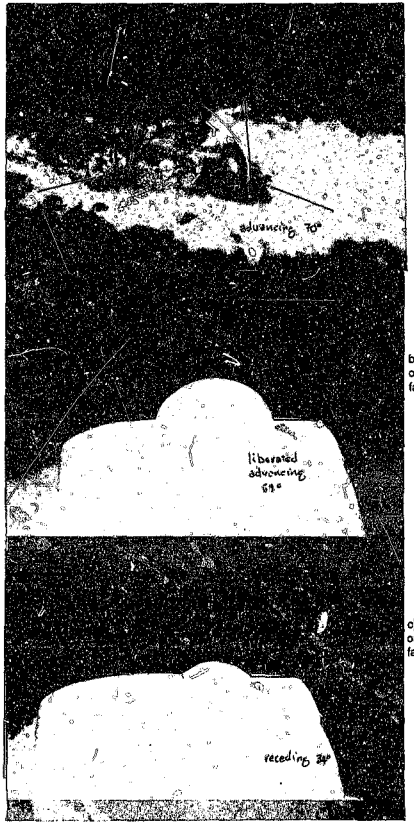
The optical or photographic technique was used to find the advancing and receding contact angles on the surface of good "near octahedral" diamond crystals. Figure 31a shows a diamond still "locked in the kimberlite", Figure 31b shows the advancing angle on the newly liberated surface and 31c shows the receding angle.

Table 14 shows the results found by the author and another independent party of constructions to find the contact angles at the left and right edges of the droplets.

TABLE 14 - OPTICAL CONTACT ANGLE MEASUREMENTS ON NATURAL FACES

	Author's Measurements				Independent Measurements			
	Exposed Surface		Fresh Surface		Exposed Surface		Fresh Surface	
	adv degrees	rec degrees	adv degrees	rec degrees	adv degrees	rec degrees	adv degree	rec degrees
	70	36	76	39	74	37	78	59
	55	34	68	27	52	34	57	24
	78	27	67	25	58	33	57	24
	52	26	77	30	80	32	69	32
	67	35	73	26	78	37	69	30
	78	38	65	30	81	45	80	36
	75		67	32	74	60	69	36
	65		69	34	68		65	
			70	29			81	
			61				62	
							68	
Averages	67,50	32,67	69,30	30,22	70,63	39,71	68,64	34,43

fig 31 photographs from optical contact angle studies

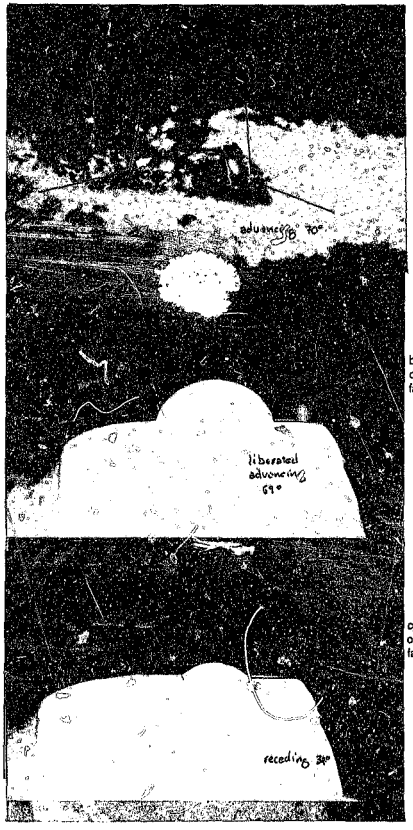


a) advancing angle on a diamond still partially locked in kimberlite rock

b) advancing angle on a freshly liberated face

c) receding angle on a freshly liberated face

fig 31 photographs from optical contact angle studies



a) advancing angle on a diamond still partially locked in kimberlite rock

b) advancing angle on a freshly liberated face

c) receding angle on a freshly liberated face

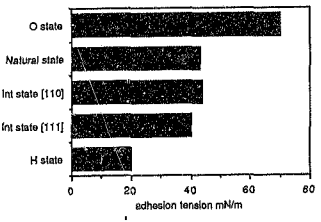
The adhesion tensions calculated from these results are :

exposed surface: 40,0 - 44,3 mN/m
fresh surface : 43,0 - 44,1 mN/m

which are in the range seen for the intermediate state of mechanically polished surfaces.

The advancing angles were generally lower, and the receding angles generally higher, than found by capillarography. This is in part due to relaxation during the time required to make an optical measurement, where capillarographic angles are measured instantaneously, and in part due to evaporation from the droplet. Fortunately the errors tend to cancel in calculating the adhesion tension.

fig 32 relative wettability of natural surface



CHAPTER 7 - RESULTS OF SPECTROSCOPIC METHODS

7.1 Sequence of Experimentation

Historically, the XPS technique was attempted before the RBS or LEED techniques. Because of difficulties with an O(1s) signal derived from the sample holder during XPS, which made quantitative measurement of the oxygen coverage of the surface difficult, the RBS technique was used. There were initial difficulties even here, because of a high background caused by secondary scattering of ions. After solving this problem by the use of a beryllium shield, better quantitative results were obtained from the surface. This indicated an approximately 1/3 monolayer coverage by oxygen, which was then followed up using the XPS technique, using a larger diamond, a goldplated holder for the diamond, and introduction of the diamond by means of a UHV transfer system (see 5.4).

7.2 Rutherford Backscattering Results

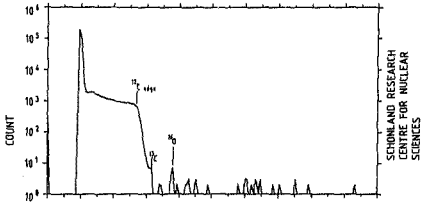
7.2.1 Oxygen Analysis

Experiments with mechanically polished and oxidized surfaces in the early stages were characterized by a high background in the spectra, and no significant difference between polished or oxidized surfaces. Oxygen levels of 0,6 to 0,7 monolayer were calculated. There was often significant level of Fe and Si (up to 0,4 ML). This suggested changes in the cleaning equipment, longer ultrasonic rinsing, and the use of a beryllium shield on the sample holder. The low atomic weight of beryllium causes very little secondary scattering.

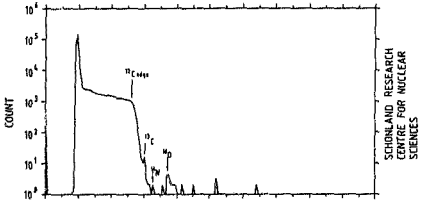
After the inclusion of the beryllium shield, better spectra were obtained. Examples are shown in Figure 33. The use of a logarithmic scale in these spectra, to allow inclusion of the high carbon signal, causes some distortion of the smaller peaks, and zero suppression which obscures the low level background signals. The region of the oxygen peak, channels 70 to 80, was replotted on a linear scale and this is shown in Figure 34. The oxygen peak can be seen, clear of the background.

FIGURE 33 R B SPECTRA

(a) POLISHED 0,32 ML O



(b) HYDROGENATED 0,07 ML O



(c) ADSORBED SPECIES

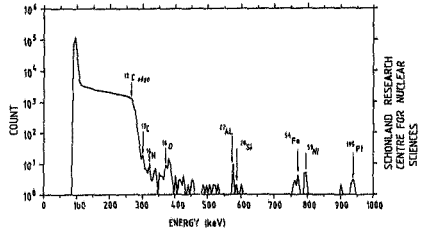


fig 34a composite RB spectrum for [111] int

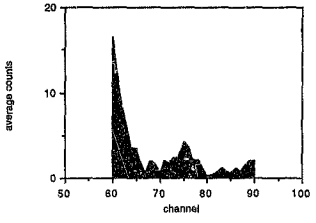
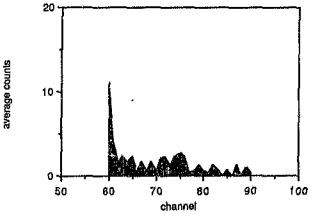


fig 34b composite RB spectrum for [111] H



Quantitative oxygen analyses of diamond surfaces, both polished and chemically modified, were conducted. This was done by a technique (Derry, 1986b) which involved :

1. Summing the counts in the five channels surrounding the oxygen peak (normally at channels 73 to 77).

2. Subtracting off a background count per channel found from the three channels above and below the oxygen peak to give P, the true oxygen peak.

3. Normalizing by a calibrated value of ΔS, the count per channel width for the substrate, which was determined so as to exclude the effects of ion channeling.

4. Multiplying by the system constant :

$$\Delta E_2 \frac{dz}{dE_2} \left(\frac{Zc}{Zi}\right)^2 \rho dia \frac{Nav}{Mc} \cos \theta 1$$

where
- P = counts in surface layer peak
- ΔS = counts per channel in substrate spectrum
- $\Delta E2$ = channel width (energy units)
- dZ/dE_2 = energy to depth conversion factor = 14 A/keV for 1,0 MeV He
- Zc = atomic number of carbon
- Zi = atomic number of oxygen
- ρdia = density of diamond 3,52 g/cm^3
- NAv = Avogadro's number 6,023 10^{23}
- Mc = mass number of substrate = 12 for carbon
- $\theta 1$ = angle between incident beam and detector

This gave the following figures for the oxygen coverage in atoms per cm^2 on the surface of diamond TP2, 5 degrees off [111] :

TABLE 15 - SURFACE COVERAGES CALCULATED FROM RBS SPECTRA

Preparation	Oxygen coverage atoms/m^2	Monolayers
Mechanically polished in water	0,52 10^{19} (±0,1)	0,29
Mech. polished + organic rinse	0,57 10^{19}	0,31
Oxidized at 420 C	0,66 10^{19}	0,37
Hydrogenated at 750 C	0,13 10^{19}	0,07

The fractional monolayer coverage is calculated from the ideal atomic count on a [111] face of diamond, 1,81 X 10^{19} atoms per m^2. Composite spectra in the region of the oxygen peak for the polished (intermediate) case and the hydrogenated surface appear in Figure 34. Although there is an apparent peak at channel 75 in the second case, the overall higher background offsets this in the calculation. It was surprising that the oxidized surface did not give a higher signal. It is possible that the greater oxygen coverage suspected after oxidation is largely in the form of unstable species which desorb under vacuum conditions.

7.2.2 Identification of Adsorbed Species

The RBS technique was used to identify adsorbed species which may be responsible for dramatic changes in the wetting character of the diamond surface (see Section 1.1). A particularly striking case is the effect of water from the kimberlite ore at the Venetia prospect in the Northern Transvaal. This was found in industrial experiments to have a very deleterious effect on the adhesion of diamonds to grease. Exposure of diamonds to this water has been found to increase the adhesion tension (wettability) by 9-10 mN/m after 30 minutes immersion (see Section 9.6). The diamond was exposed to the raw water and to water filtered through a 0,22 micron filter, for 30 minutes. The RB spectra were used to identify adsorbed components. The raw water produced a very "dirty" spectrum, possibly because of suspended dust particles. However, the following could be identified :

TABLE 16 - ADATOMS DETECTED BY RBS

Channel	Mass Number	Species and Comment
61	14	Nitrogen possibly in diamond (Field, 1979b)
76	16	Oxygen surface oxide or adsorbed O
100	23	Sodium-not from filtered water
115	27	*Aluminium major peak*
117	28	Silicon
130	35	Chlorine-not from filtered water
137	40	Calcium-not from filtered water
152-158	54-58	Iron, or cobalt or nickel
185-195		Platinum from cleaning apparatus

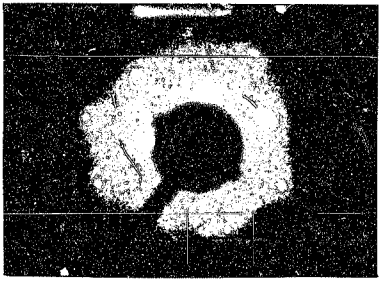
Figure 33c shows the spectrum from one such experiment. The filtered solution gave only two obvious contaminant species at channels 113-116, which could be aluminium or silicon, the major rock constituents, and at 150-158, which could be Cr, Fe or Ni, or a mixture. The latter are more likely to affect the orientation of water molecules at the solid:water interface and further capillarographic experiments with standard solutions were performed to test their effect (see Section 9.7)

7.3 Low Energy Electron Diffraction

LEED analysis was performed on two diamonds, TP0 and TP1, normally just prior to XPS analysis. TP0 is not a well defined crystal face but even so a satisfactory LEED pattern was obtained. On the good [111] face of TP1 an impressive pattern was obtained, without the need for vigorous cleaning. Figure 35 shows the LEED pattern obtained on TP1 at 242 volts without heat treatment. The ratio of spot spacing to the radius of the screen is 0,59. Hence from the relation for spacing of the scattering centres in real space :

$$d = 2310/\sqrt{U} \times 1/0,59 = 253 \text{ pm}$$

fig 35 LEED pattern on [111] 1x1



A similar pattern was obtained for the displaced [111] face at 218 volts. The ratio of spot spacing to screen diameter was 0,61 and hence the spacing of the scattering centres was found to be :

$$d = 2310/\sqrt{U} \times 1/0,61 = 257 \text{ pm}$$

A further pattern was obtained at 387 volts, and the calculation showed the same surface lattice spacing. This indicates a first order pattern in both instances, with spacing as expected for the unreconstructed [111] planar surface. No evidence of reconstruction - half order spots - could be seen in these spectra or those taken after the surface had been heated at 670 K. An hydrogenated surface produced essentially the same pattern, with no evidence of half-order spots.

We conclude that the atoms on the surface of the diamond occupy the same positions as do the carbon atoms in the bulk crystal, and that any heteroatom which is adsorbed on the surface does so in such a way that no regular superlattice, with periodicity at a multiple of the interatomic spacing, is formed.

7.4 X-ray Photoelectron Spectroscopy

An initial program of XPS experiments was prejudiced by a large component of the O(1s) signal derived from the sample holder. In this series the diamond surface appeared to retain between 0,7 and 1,1 monolayers of oxygen in ultrahigh vacuum, which is clearly in conflict with the results from RBS.

To offset this, a larger diamond was used, and a gold plated holder was made for the diamond. Gold has a low sticking probability for oxygen, which we hoped would reduce interference from this source. In addition, the diamond was introduced to the UHV chamber by means of a sample transfer rod, thus eliminating the "bake-out" at 470K. Better spectra were obtained, as shown in Figure 36.

The oxygen (1s) signal appears to be a single peak in the case of polished, annealed and hydrogenated surfaces, with an energy difference C(1s) - O(1s) of 248,0 ± 0,5 eV. In the case of the strongly oxidized surface, the O(1s) peak appears to be broader, with a peak width at half maximum of 4 eV, by comparison with the 2,5 to 3 eV seen in other cases. Also, the energy difference C(1s) - O(1s) is reduced to 246,5 eV, suggesting a chemical shift in the direction of higher kinetic energy, or lower binding energy.

This suggests that oxygen is presented in only one chemical form, but in varying proportion, on the polished, annealed and hydrogenated surface. Because oxygen is divalent, this is thought to be the tertiary hydroxyl group. On the oxidized surface, two forms seem likely, with one type, at the lower binding energy, bonded differently to the carbon atoms. A shift to lower binding energy could be the result of double bonding of surface oxygen atoms and hence greater electrostatic shielding of the core electrons. This could be in the form of the carbonyl or carboxyl groups proposed by Sappok and Boehm (1968) which would be possible strictly only at labile carbons, possessing two or one bonds back into the diamond crystal. Presumably, oxidative etching of the diamond surface produces these as intermediates between tertiary surface oxides and desorbing carbon dioxide. Another possibility is a bridging, or oxirane-type oxygen group, where the electrostatic shielding provided by the adjacent C-O bond is greater than that found on an isolated hydroxyl.

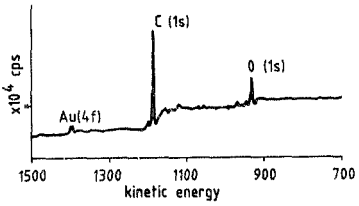
A quantitative estimate of the oxygen coverage on the diamond surface in these experiments is given in Table 17. Use has been made of equation 23 with a correction for analyzer sensitivity.

TABLE 17 - OXYGEN SURFACE ANALYSIS BY XPS

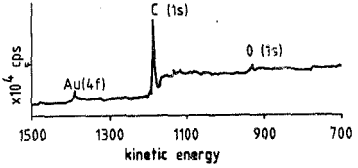
State	Carbon (1s) Peak cps-eV^2 x 10^{-6}	Oxygen (1s) Peak cps-eV^2 x 10^{-6}	Coverage atom/m^2	Mono-layers	Error
Polished	415	54	$7,1 \times 10^{18}$	0,39	0,02
Annealed 500 K	467	34	$4,0 \times 10^{18}$	0,22	0,02
Oxidized 770 K	405	185	$2,5 \times 10^{19}$	1,4	0,05
Hydrogenated 1020 K	325	17	$2,9 \times 10^{18}$	0,16	0,03

fig.36 x-ray photoelectron spectra

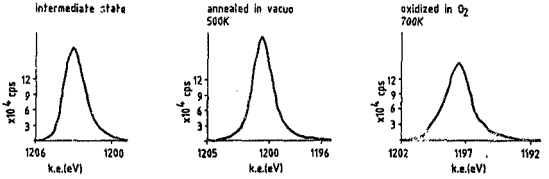
a) intermediate state wide scan



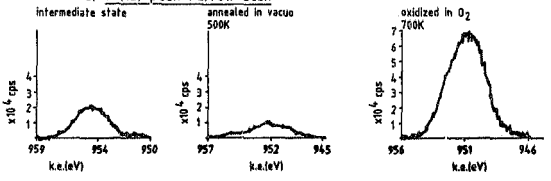
b) hydrogenated state wide scan



c) C (1s) peak narrow scan



d) O (1s) peak narrow scan



Apparently there is significant desorption of the oxygen on heating to as low as 500 K. Evans and Riley (1986) found that temperatures as high as 1220 K were required to reduce the O(1s) peak area down to one percent of the C(1s) peak area. Desorption began from as low as 620 K. The fact that LEED analysis shows no change from the 1 x 1 pattern seen before heating suggests that hydrogen is being adsorbed, or diffusing out of the bulk crystal to satisfy the surface bonds.

The hydrogenation produced a significant reduction in the oxygen signal - from approximately 0,4 to less than 0,2 equivalent monolayers.

The XPS results therefore confirm the RBS analysis, in that less than a half monolayer coverage of chemically bonded oxygen exists on the polished [111] surface, and that this is reduced significantly by hydrogenation or thermal desorption in UHV.

CHAPTER 8 - SURFACE MODEL

8.1 Molecular Model

At this stage we can propose a model for the diamond surface, after reaction with hydrogen or oxygen, which is of use in interpreting these data.

This will tie in some of the results from spectroscopy with the three states observed in wetting experiments.

8.2 Fully Hydrogenated

The fully hydrogenated surface is "bulk-like", i.e. the carbon atoms are very little displaced from the positions they would occupy in the bulk crystal, and each dangling bond exterior to the crystal is terminated by a hydrogen atom. Because of the relatively small size of the hydrogen atom - the Van der Waal's radius is only 120 pm (Mackay et al 1970)- this will occur on all faces without any steric hindrance. This is a conceptually simple way to terminate the diamond surface and evidently preferred by vacuum experimentalists (Pate 1986) and theoreticians (Lopez et al 1981). However, this surface is very hydrophobic, having the properties virtually of a paraffin wax. This state is not observed except in the case of diamond surfaces especially hydrogenated at high temperatures.

Under normal circumstances the surface is expected to take up some, but less than a monolayer coverage of oxygen. Because the remaining bonds will need to be satisfied, and reconstruction can be ruled out on the strength of the LEED results, the balance of the surface atoms may indeed be reacted with hydrogen. Interestingly, the oxygen is very likely bound as hydroxyl groups, (by analogy with silicon [111], Schaefer et al 1984) which means that the total coverage by hydrogen, including the hydrogens of the hydroxyl groups, will approach one monolayer. The deficit will be due to edge sites where oxygen could double bond to the favourably oriented orbitals of two carbon atoms on adjacent layers.

Despite the fact that Pate (1986) considers this to be the natural state for a polished diamond surface, all wettability tests and RBS, XPS vacuum techniques indicate some oxygen on the surface of a mechanically polished diamond surface, but less than half a monolayer. The fully hydrogenated surface seems to be realised only after thermal desorption in vacuum or high temperature hydrogenation in oxygen free hydrogen. Pate (1986) mentions a bake-out in vacuum at 770 K as part of the surface cleaning procedure he adopted prior to analysis. This could conceivably desorb the surface oxygen and replace it with hydrogen diffusing out of the diamond lattice (Mainwood 1982, Tabor 1983).

8.3 Fully Oxidized

The fully oxidized surface presents more difficulties in terms of chemical structure. The simplest model would be monolayer coverage by hydroxyl groups. However, uniform monolayer cr by hydroxyl groups, as in the case of hydrophilic silica (Lasko Kitchener 1969; Stasczuk 1985), is unlikely because of steric hindrance between neighbouring hydroxyl groups. This follows from the spacing of the surface carbon atoms on the [111] surface (see Figure 3) and the Van der Waal's radius of the oxygen atom of 140 pm (Mackay et al 1969). This radius should also be increased in the case of hydroxyl groups to allow for the covalently bonded hydrogen atom in the hydr group. Either way, there will be considerable repulsive interacti when trying to pack these groups onto a hexagonal mesh with spacing of 252 pm. This is not the case on silicon which has a covalent radius of 117 pm, and hence lattice constant 50 % greater than that of diamond (Mackay et al 1969). Wetting tests with silicon [111] wafers are discussed in Appendix 8.

Another structure proposed for the oxidized surface is the bridging (oxirane or "epoxide") group. The shape of bridge is dictated by the sp^3 hybridization of the oxygen atomic orbitals, as in water, and the repulsion of the lone pair electrons in the two non-bonding orbitals. This leads to a vee-shape with an angle between the bonding orbitals of 100 -110 degrees. The formation of surface oxiranes and peroxides in the overhead site above two carbon atoms in the [111] plane requires considerable

deflection of the ordinary bond angles. This kind of site is unlikely except in the case of unusual edge or dislocation sites, where labile carbon atoms are in the correct position. It has been suggested (Verwoerd 1986) that the [100] surface is such an agreeable environment. Unfortunately this is the least frequent surface encountered in practice. (Bansal et al 1972). An indication of the thermodynamic penalty for this deflection can be obtained by consideration of the strain energy involved in some simple organic compounds (Benson 1976).

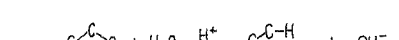
TABLE 18 - ESTIMATION OF STRAIN ENERGIES

Compound	ΔHof (obs) kJ/mol	ΔHof (calc) kJ/mol	Es kJ/mol
Ethylene oxide	-52,5	-168,4	115,9
Benzene	83,2	221,8	-138,6
Furan	-35,3	- 9,2	- 26,1

Furan shows a spacing between the oxygen-bridged carbons of 280 pm, most nearly like the spacing on the diamond [111] surface and so should be a good model. The comparison is clouded slightly by the resonance energy of the pi-bonded ring. Benzene for instance, has a true strain energy of 12,6 kJ/mol, but this is offset by a resonance energy of 151,2 kJ/mol, giving a nett (apparent) strain energy of -138,6 kJ/mole. Even allowing only half of this resonance energy in the five member furan molecule, the true strain energy is approximately :

$$-26,1 - (1/2 * -151,2) = 49,5 \text{ kJ/mol}$$

Ethylene oxide is susceptible to acid solvolysis in water to give ethylene glycol (Roberts and Caserio 1964). This process is possible because the singly bonded carbon atoms in the free glycol molecule allow the two hydroxyls to splay and rotate, preventing steric hindrance. On the rigid diamond surface, this would not be possible. It is possible that a surface ether or epoxide could undergo solvolysis to produce neighbouring hydroxyl and hydride groups and this may help to explain the observed instability of the highly oxidized surface :



The explanation preferred by the author is the irregular etching of the diamond surface, [111] or [110], by high temperature oxygen, so as to produce edges and steps which have the character of [100] faces. This would provide good sites for reaction of oxygen in the bridging form. If this process is allowed to proceed for long, visible etching can be seen, initially as a smoky texture to the surface, and finally as microscopic etch pits. There would still be alternate rows with, for example, true [111] dangling bonds, normal to the surface, which would require alternate adatoms in the form of hydroxyl groups or hydrogen. Consequently, it is unlikely that full monolayer coverage is attained, but potentially as high as 0,8 of a monolayer could be accommodated on a macroscopic [111] face, etched by the alternate removal of three zigzag rows on the [111] plane. The oxirane type oxygens may be susceptible to solvolysis by water, increasing the coverage by hydrogen and hence decreasing the wettability. The etched surface is likely to be more easily polished, even by a soft abrasive, since there will be defined microscopic ridges with cleavage planes parallel to their base. During high temperature oxidation, an etching mechanism could lead to the existence of labile surface C atoms capable of bonding to multiple oxygen atoms, and hence greater than monolayer coverage.

This could explain why the oxidized surface is unstable and reverts towards an intermediate state.

8.4 Intermediate (0,3 monolayer)

Rutherford Backscattering and XPS analyses in this study show near to a third of a monolayer coverage by oxygen. Thomas and Evans (1975) have observed that the diamond surface adsorbs oxygen to the extent of one third of a monolayer, as detected on a polished surface by XPS. In addition, the polished surface has a wettability considerably less than that of a fully oxidized surface. Apparently there is a steric hindrance to the adsorption of more than approximately a third of a monolayer of oxygen.

Uniform One Third Monolayer Coverage

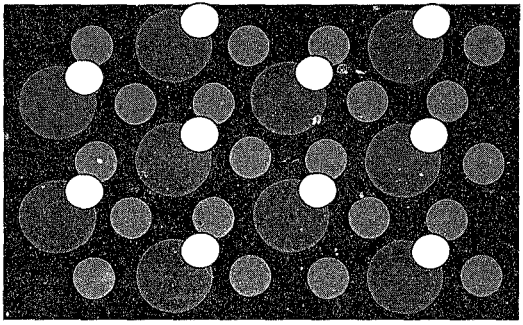
It is possible to propose a configuration of oxygen atoms (in the form of hydroxyl groups) and hydrogen atoms on the [111] surface so that each oxygen is matched by two hydrogens as immediate nearest neighbours in a triangular mesh. This mesh then fits together on the hexagonal [111] surface lattice so that no oxygen has another oxygen as nearest neighbour. This is shown in Figure 37. This would give an ideal one third monolayer coverage by oxygen and a nett hydrophobic character.

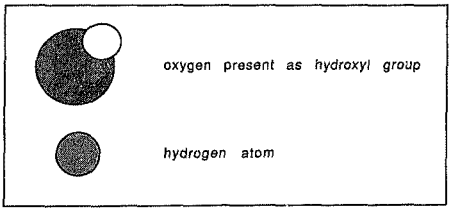
However, there are objections on the grounds of LEED analysis. This arrangement should give rise to a periodicity at twice the real space lattice parameter, and hence half order spots in the LEED pattern. Such spots were never seen which suggests that a true periodic arrangement of oxygen atoms does not occur on the surface. An explanation can be offered, based on the randomized attachment of oxygens, with exclusion of nearest neighbour sites.

Randomized Nearest Neighbour Exclusion

Assume that the surface coverage is generated by a random process after exposure of the fresh diamond surface (by cleaving, abrasion etc). The reactive species is assumed to be water. This follows the methods of Klier and Zettlemoyer (1977) in work on iron [100] crystal face and Schaefer et al (1984) studying the reaction of water with silicon [100] and [111]. An impinging water molecule may have the correct orientation for reaction with the fresh surface, and split into an adsorbed hydroxyl plus hydride (as has been seen on silicon at room temperature). Alternatively, the site on which it impinges may be occupied, or have as its nearest neighbour an adsorbed hydroxyl group which then inhibits reaction of the water by steric effects. A computer program was written to simulate this process of formation of a mixed hydroxyl/hydride surface. Klier and Zettlemoyer (1977) have used this approach to generate a lattice of hydroxyl groups on iron [100]. They then used the simulated lattice as a diffraction grating for a laser and the resulting pattern was compared with a LEED pattern for the true iron [100] surface.

fig 37 ideal 1/3 monolayer coverage by oxygen on the [111] surface





Details of the computer simulation are given in Appendix 6.

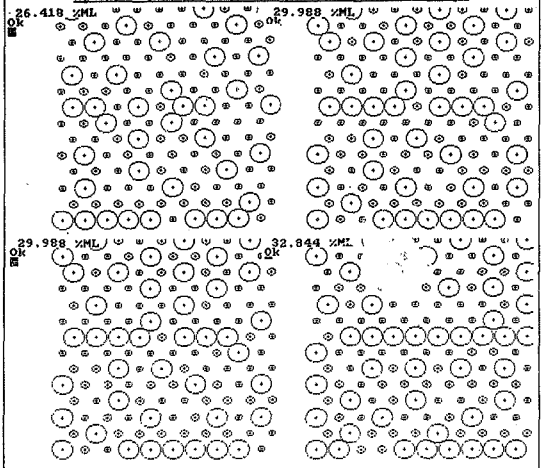
The results of 10 simulations are shown in Table 19 :

TABLE 19 - SIMULATED RANDOM SURFACE COVERAGE

Simulation No.	Surface Coverage (Fraction of a Monolayer)
1	0,307
2	0,300
3	0,328
4	0,300
5	0,264
6	0,300
7	0,293
8	0,286
9	0,307
10	0,314
Average	0,300
Std. Dev.	0,017

Reduced printouts of four of these simulations appear as Figure 38. There is no clear pattern, apart from the higher frequency of oxygens at the edge site, running horizontally across the middle of the figure. This edge defect would in reality be randomized too, so that we could expect no effect on the LEED pattern, which would be dictated principally by the lattice spacing of the substrate carbon atoms. This would explain how a surface with an approximately 30 % coverage by hydroxyl groups, arranged so as to exclude near neighbours, would not produce a change in the LEED pattern from the bulk unreconstructed pattern.

fig 38 simulation of randomized surface coverage



large circle = hydroxyl group
small circle = hydrogen atom

8.5 Interpretation of Diamond Hydrophobicity

Previously there have been two explanations for the native floatability, or inherent hydrophobicity, of minerals. Non-sulphide minerals, such as talc and graphite are layer structured minerals, with weak bonding between the layers. The surfaces formed by shear along these layers are "low energy" surfaces (Gaudin et al 1957) and should therefore be poorly wetted by a liquid of high surface tension such as water. This follows from Young's equation.

In the case of sulphide minerals such as pyrite, chalcopyrite and galena which are not of this layer structure, hydrophobic behaviour has been explained by the formation of one or more monolayers of molecular sulphur the form of chains and rings (Walker et al 1986). Sulphur in this form is hydrophobic because there is no ionic or dipole character, and no site for hydrogen bonding of water molecules.

The inherent hydrophobicity of diamond can be explained, based on the results of this work, by the steric resistance to oxidation of [111] and [110] microfacets on the surface. The carbon atom spacing on these lattice planes, and the orientation of the residual bonding orbitals, prevents oxygen from reacting with more than approximately 33% of the surface. The remaining carbon atoms react with hydrogen to form inert and un-ionizable surface hydrides. These hydrides cause a deficiency in hydrogen- and ionic bonding between water molecules and the diamond surface. As explained by Laskowski et al (1969) and van Oss et al (1986), a surface which is deficient in hydrogen bonding capacity will be poorly wetted by water.

This has positive consequences for the diamond mining industry, because it indicates that the wettability seen in diamonds at certain deposits is not an inherent property of the diamond, nor is it the result of oxidation of the diamond by the atmosphere. Evidence points to the adsorption of some ionic species on the diamond surface. It should be possible to reverse this by suitable pretreatment of the diamondiferous gravel in the diamond recovery plant, using mechanical attritioning coupled with addition of reagents.

CHAPTER 9 - SOLUTION EFFECTS

9.1 Hydration

A major difficulty experienced by Hartley (1978) in his study of diamond surface chemistry was the apparent hydrophilization of diamond after storage under water. He found that diamonds stored under de-ionized water even in a tin container, to prevent silica leaching, became so hydrophilic that no contact angle could be established by the captive bubble technique. Laskowski et al (1968) noted the hydration of silica which had been methylated by treatment with dimethylchlorosilane. The contact angle was reduced from 60 degrees to 10 degrees at pH 6, and the process was more pronounced at higher pH. This was not caused by loss of the surface methyl groups but rather by formation of a stable physically adsorbed layer of water.

Cain et al (1983) reported a similar effect in studies of the receding contact angle of water on siliconized glass. There was a large dependence on the time of exposure to the water - i.e. a hydration effect.

In this work, the nature of the capillarographic test, with repeated cycles over the same area of surface, shows up a similar effect very graphically.

Inspection of Figure 20 shows that successive hysteresis loops are progressively displaced in the direction of higher force, i.e. more wettable surface. The data for the three successive loops in this test are :

TABLE 20 - HYDRATION DURING A STANDARD TEST WITH THREE CYCLES OF WETTING

Cycle Number	Advancing Angle Degrees	Receding Angle Degrees	Adhesion Tension mN/m
1	80,3	29,2	37,7
2	78,4	27,8	39,3
3	77,7	27,6	39,8
Average	78,8	28,2	38,9

The interval between successive cycles is the time to travel twice 35mm at 0,01 mm per second, i.e. 700 seconds, or including turnaround at the limits, 12 minutes per cycle.

By running the test program for longer periods up to 40 cycles, the process can be monitored for up to 8 hours. This is shown in Figure 39, for three states of the surface, a high intermediate (partially oxidized) state, low intermediate or polished state, and a hydrogenated state. The hydration effect is asymptotic, and the hydrated adhesion tension is between 5 and 7 mN/m higher than the intital (dry surface) value. The dry surface value can be restored, as noted by Laskowski et al (1968) for silica, by drying at slightly over 373 K. This is in conflict with Hartley's results (1978) where the hydrated state was found to be irreversible.

Two mechanisms can be proposed to explain this effect.

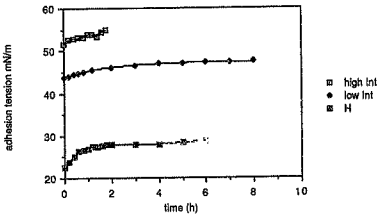
Surface Roughness and Imbibition

Even a well polished surface will have surface irregularities of the order of 0,1 microns, (Neogi and Miller 1982) and possibly even cracks of greater depth. These would be possible sites for the retention of air pockets, giving a net higher contact angle as discussed by Bikerman (1970). The air bubbles would have a high pressure, because of their size and hence curvature, and could be expected to dissolve into the water. Water would then penetrate the cracks. This should be apparent as an increase in wettability, as observed.

Formation of Physically Adsorbed Water Clusters

The fact that the same effect can be seen on hydrophobized vitreous silica plates, which will have very smooth surfaces, (Laskowski and Kitchener 1968) suggests that roughness is not the major cause. The explanation offered by Laskowski involves the existence of a minority of polar (hydrophilic) sites on the silica after methylation. The fact that the maximum contact angle which they observed on the silica was 70 degrees, and not the 108 degress expected of a momolayer of methyl groups, supports this argument.

fig 39 hydration effect in water



The polar sites act as nucleation points for the formation of water clusters which grow to mask the methyl groups and hence give increasingly hydrophilic behaviour. The same explanation can be used in the case of a diamond surface of mixed hydrogen/hydroxyl surface composition.

This effect obviously has a serious impact on tests to determine other solution effects. It is difficult to distinguish the slight effects caused by low level adsorption of ionic species from the concurrent hydration process.

This necessitated some care in the execution of these experiments. The diamond test plates were immersed in the test solution for only the duration of a standard three cycle test, when investigating concentration effects, and the average adhesion tension over the first three cycles was used as a measure.

In tests where the adsorption of an ionic contaminant was strongly suspected, the plot of adhesion tension with time was compared with the hydration curve of Figure 39 to determine the significance of the effect.

9.2 pH

The response of many oxide minerals to flotation is strongly affected by the pH because they are the "potential determining ions" for oxide:water systems, the potential then affecting the adsorption of flotation collector (Finch et al 1979).

In the case of diamond, the ionization of surface groups should lead to sites with greater interaction forces with water molecules, hence a lower solid:liquid interfacial energy and greater wettability.

Capillarographic tests were performed on a mechanically polished (intermediate) surface at a range of pH from 1,0 to 13,0. This is well beyond the range encountered in ordinary mine waters. The results are shown in Figure 40.

fig 40a effect of pH on contact angles

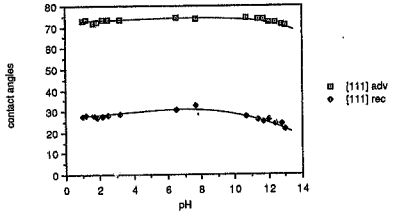


fig 40b effect of pH on adhesion tension

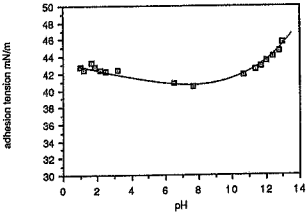


fig 40a effect of pH on contact angles

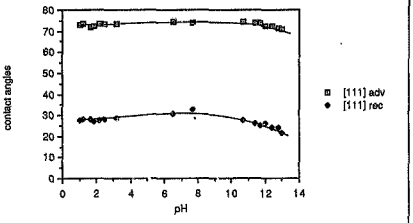
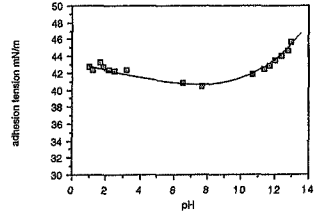


fig 40b effect of pH on adhesion tension



Apparently the diamond surface is most hydrophobic between pH 4 and 11. There may be a slight hydrophilic trend in the range pH < 2. The most obvious effect is a progressive increase in hydrophilicity from approximately pH 12 upwards.

This could be interpreted in the light of the table of acid strengths of some organic acid groups.

TABLE 21 - ACID STRENGTHS OF VARIOUS OH CONTAINING GROUPS

Compound	K_a	Reference and Page
Ethanol	10^{-18}	Roberts & Caserio, 1965 p 384
Cyclohexanol	10^{-18}	Roberts & Caserio, 1965 p 904
Phenol	$1{,}3\ 10^{-10}$	Roberts & Caserio, 1965 p 902
Benzoic acid	$5{,}6\ 10^{-5}$	Roberts & Caserio, 1965 p 510

If the hydroxyl groups on the diamond surface were located on carboxylic acid groups, or in a location where neighbouring carbon atoms are involved in π bonding, we would expect major changes near pH 4 and pH 10 approximately, by analogy with benzoic and phenolic hydroxyl groups. The fact that this does not emerge, but that there is a rapidly increasing effect as pH approaches 14, indicates that the ionizable groups are more like the alcohols:ethanol or cyclohexanol.

This supports the view of the diamond surface consisting of a minority of hydroxyl groups whose nearest neighbours are methyl-like hydrogens.

9.3 Temperature

The effect of temperature on contact angle and wettability was studied by changing the temperature of the thermostat in the range 278 - 308 K. Above 308 K condensation caused experimental difficulties.

fig 41 effect of temperature on Ylv and adhesion tension

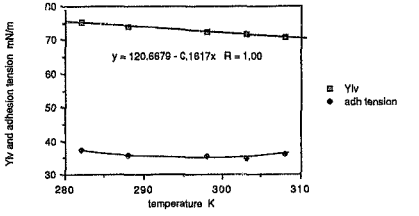
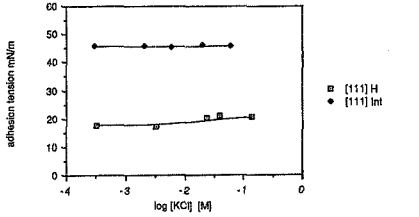


fig 42 effect of ionic strength



The results of a test on a low intermediate [111] surface are shown in Figure 41. The trend towards greater wettability in both directions from 298 K is unexpected.

Above 298 K the advancing angle was reduced, whilst the receding angle dropped only slightly. Below 288 K the receding angle decreased sharply. This could be a reflection of the greater stability of physically adsorbed water films at lower temperature.

At no temperature did the surface become truly hydrophilic. Subtle effects due to the suspected dependence of contact angle and surface entropy on temperature could not be detected from these results (Neumann 1974).

9.4 Ionic Strength

The effect of ionic strength was studied using potassium chloride and sodium chloride, selected because of their pH neutrality and high solubility. Figure 42 shows the effect of potassium chloride at concentrations up to 0,1 M on a hydrogenated surface and a high intermediate surface. There is very little effect in either case, with possibly a slight increase in wettability in the case of the hydrogenated surface.

This is compatible with the view of the diamond surface as a mixture of poorly ionized surface groups such as hydrogens and alcohol-like hydroxyls. Sodium chloride, similarly, had no significant effect. Thus we must interpret the finding of Weavind (1952) on the deleterious effects of "salts" in sea water to include ionic species other than the simple alkali halides.

9.5 Aqueous Oxidants

Hartley (1978) found that aqueous oxidants such as the hypochlorite ion, perchlorate ion and dichromate ion produced a decrease in contact angle and an increase in wettability. Tests were conducted using 0,001 M solutions of these reagents, whereas Hartley observed oxidation effect at

concentrations above 10^{-5} M. The dichromate and perchlorate solutions were acidified to pH3. The hypochlorite solution was at the natural pH of 10. The results are reported in Table 22 showing the net change in adhesion tension, after 30 minutes immersion, and subtracting a correction of 1,5 mN/m, being the shift caused by hydration even in clean water after the same period.

TABLE 22 - OXIDATION BY AQUEOUS OXIDANTS

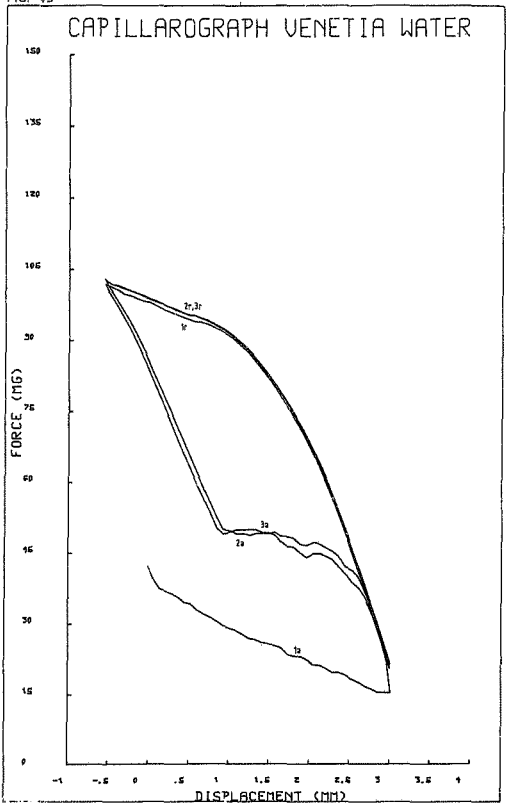
Oxidant	Change in Adhesion Tension
Dichromate ion $-Cr_2O_7$ 0,001 M	+ 0,5
Perchlorate ion $-ClO_4$ 0,001 M	+ 2,3
Hypochlorite ion $-OCl$ 0,001 M	+ 9,9

Apparently only hypochlorite ion is a sufficiently powerful oxidant under these conditions, but even this represents a shift in contact angle of only some 10 degrees. This is nowhere near as strong an effect as oxidation by high temperature oxygen, which produces a change in adhesion tension of 30 mN/m. The difference could be explained if we accept that oxidation of microscopically planar [111] surfaces can occur only by an etching mechanism, realised only at high temperatures, and that aqueous oxidation can affect only easily oxidizable sites, at edges or steps in the surface.

9.6 Plant Water Sampled at the Venetia Deposit

A typical diamond ore which contains many diamonds with hydrophilic character occurs at the Venetia prospect in the Northern Transvaal. Diamonds from the upper reaches of this pipe have a very poor adhesion to grease, and so probably a very hydrophilic surface. A sample of water from a development shaft at Venetia was taken for analysis and used in these experiments.

FIG. 43



J. O. HANSEN, UW CHEM.

An analysis of the water by atomic absorption spectroscopy gave the following major solutes, expressed in kg per megalitre (ppm) :

TABLE 23 - ANALYSIS OF VENETIA SHAFT 5 WATER

(all in mg/dm^3)

pH	Na^+	Ca^{++}	K^+	Mg^{++}	Si^{4+}	Fe^{3+}	Al^{3+}	Cu^{++}	SO_4^{--}	Cl^-
8,1	880	300	107	1140	20	1	1	<1	2080	6180

Total dissolved solids were 17 880 ppm, and total suspended solids were 17 ppm. The difference between the total of the analyzed solutes, and the TDS, approximatley 7200 ppm, is due to carbonate and bicarbonate ion.

The water was filtered at 0,22 microns before use in the capillarographic cell. The surface tension at 25 °C was 72,7 mN/m, a reflection of the high ionic content.

Figure 43 is the capillarograph from the test on a polished [111] surface, showing the large change between the advancing contact angle on the first pass, before the surface had adsorbed any contaminant, and the lower contact angles on the subsequent passes. The first receding pass is over a surface which has been exposed to the contaminant for approximately six minutes, and is therefore depressed, and not very different from the subsequent passes. Clearly some agent in the natural water has a strong hydrophilizing effect on the diamond surface.

Figure 44 shows the effect over a period of five hours immersion. An asymptote is reached within 1 hour. The extent of change of adhesion tension is 14 mN/m, or 300 % higher than the hydration effect seen in milli-Q water after the same period of exposure.

fig 44 Long exposure to Venetia water

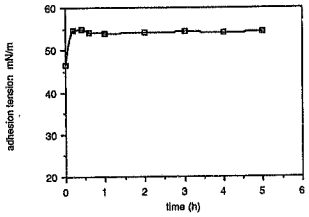
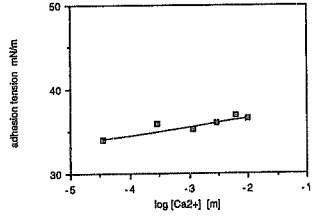


fig 45 effect of calcium ion concentration



The identification of the active species was attempted by two methods :

1. RBS analysis of the contaminated surface - discussed in Section 7.2.

2. Tests with standard solutions of the individual cations - see below.

9.7 Specific Metal Cations

Solutions of AR grade reagents containing calcium, aluminium, ferric and chromic ions were made up. Calibration curves of concentration v conductivity were produced to allow continuous monitoring of the concentration in the cell.

Figures 45, 46, 47 and 48 show the effect of the various ions at concentrations ranging from approximately 10^{-5} M to 0,01 M.

Chromium ions show no effect, calcium and aluminium a slight effect, and the effect of ferric ion is dramatic.

Figure 49 shows the adhesion tension of the intermediate [111] surface after exposure for up to 8 hours to ferric ion.

The mechanism of adsorption of the ferric ion probably involves ligand bonding to one or more hydroxyl group on the surface of the diamond, in the same way that ferric ion can form complexes with polyhydroxy-organic compounds like sugars (Mackay et al 1969 p 175). The hydration sheath of up to six water molecules surrounding the ferric ion would then provide a hydrophilic mask for the surface.

This hydrophilic state could be corrected by light repolishing or washing in dilute hydrochloric acid. This is shown in Figure 50. This mechanism of adsorption on the diamond surface offers an explanation for the wettability of the diamonds at the Venetia prospect. Recent evaluation of the diamond recovery from ore at various depths (Davies et al 1985) showed a correlation between hydrophilic behaviour, depth in the ore body and weathering of the ore. The ore within 40 m of groundlevel had been

fig 46 effect of aluminium ion concentration

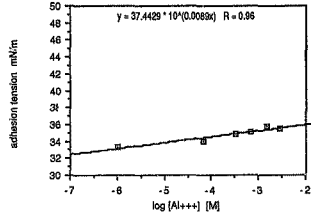


fig 47 effect of chromic ion concentration

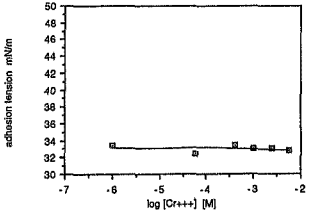


fig 48 effect of ferric ion concentration

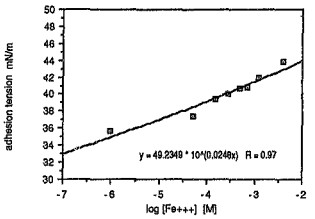


fig 49 effect of ferric ion with time

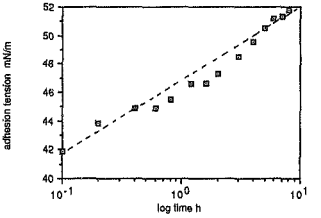
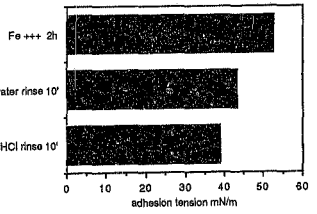


fig 50 removal of ferric ion by water and acid rinse



weathered, with a change of colour, reduced density and presence of reprecipitated minerals such as calcrete and silcrete. In this zone, the diamonds showed more hydrophilic behaviour. It is reasonable to attribute these effects to the percolation of surface water, of higher pH than the natural pH of the kimberlite, and containing ferric and other ions. This explains the phenomenon of hydrophilic or "refractory" diamonds better than the oxidation mechanism advanced by Sappok and Boehm (1968).

9.8 Dynamic Effects

The effect of interface velocity on the contact angles was studied by two techniques :

1. Decreasing the velocity of interface advance to $1,25 \times 10^{-6}$ m/s.

2. Allowing a sixty second relaxation time after each advance or recede before reading the force.

The first approach gave slightly lower advancing angles and slightly higher receding angles at the lower velocity, by approximately 0,6 degrees in each case. The effect is almost cancelled by taking the adhesion tension - a form of mean - but not entirely, because of the nonlinear nature of the cosine function.

The relatively small dependence on velocity is similar to the observation of Johnson et al (1977) for water on silicone coated glass at velocities such that the capillary number is less than 10^{-5}.

The capillary number is the dimensionless group :

$$Ca = \frac{Vn}{\gamma}$$

where V is the velocity m/s
n is the viscosity kg/m s
γ is the surface tension kg/s^2

In these experiments, the capillary number was between 10^{-7} and 10^{-8}. Experiments at higher interface velocities would require a faster weighing system than the electrobalance used here.

The second technique gave considerably higher receding contact angles after relaxation for 60 seconds, by approximately six degrees in most cases, but very similar advancing angles. This is similar to the findings of Bayramli et al (1981) for quartz fibres coated with dimethyl- dichlorosilane, who found a relaxation of the advancing angle of 1,0 degrees, and of the receding angle of 3,0 degrees after stopping from a velocity of 0,004 mm/s.

Hence we might anticipate that advancing angles from these capillarographs are similar to equilibrated contact angles found by optical techniques, but that the receding angles are lower than found by other, non-dynamic measurements.

The dynamic contact angle may differ markedly from the static angle in systems where diffusion of a surfactant is important, or where the de-wetting phase (replacing water) is a viscous fluid (Grader 1986). The latter is likely to be the case in the adhesion process of diamond separation, but investigation of this property, which is principally a function of the adhesive phase, falls outside the scope of this study.

CHAPTER 10 - CONCLUSIONS

The adhesion tension for water on mechanically cleaned diamond [111] and [110] surfaces was found to be 40 and 45 mN/m respectively. This translates to an equivalent average contact angle of 56 and 51 degrees respectively. Under these conditions, the advancing angle is similar or slightly greater than found by static techniques (such as the sessile drop), and the receding angle is considerably smaller, by approximately six degrees, than the receding angle found by static techniques.

The [111] surface was significantly more hydrophobic than the [110] surface, by approximately 5 degrees of contact angle or 5 mN/m of adhesion tension, and this is believed to be caused by the lower frequency of sites suitable for attachment of oxygen groups on the [111] surface.

The adhesion tension of water on silicon [111] was found to be 63 mN/m after polishing and atmospheric oxidation, indicating a contact angle of 30 degrees which is considerably lower than that of diamond. This was thought to be due to a higher coverage by oxygen on the silicon surface.

XPS and RBS studies showed that there are stable oxides on diamond surfaces, formed at room temperature, but that these accounted for only 25 to 40% of the available surface carbon atoms. Enhanced oxidation of the diamond surface begins at approximately 470 K and is accompanied by a large increase in wettability.

An extremely hydrophobic surface, with adhesion tension of 20 mN/m, is achieved after hydrogenation at temperatures higher than 770 K. The wettability of this state was significantly lower (20 mN/m) than either a mechanically cleaned (polished) surface, or the surface of a newly mined diamond.

A diamond surface which was produced by mechanical abrasion has a wettability intermediate between that of an oxidized surface and a hydrogenated surface. The process of polishing is believed to proceed by the breaking out of microfragments with [111] faces so that this process is equivalent to cleaving, but in very small steps. The surface so exposed preserves the bulk arrangement of the surface carbon atoms, as detected by LEED studies which show no evidence of a half order spots, which are characteristic of the 2 x 1 rearrangement.

Consideration of the Van der Waal's radii suggests that there would be a steric hindrance to the formation of a monolayer of oxygen on the [111] surface.

This is supported by the fact that two spectroscopic techniques, RBS and XPS, show oxygen coverages of approximately 0,3 - 0,4 monolayers in this state.

The possibility of oxirane or "bridging" bonding of oxygen between two surface carbon atoms is believed to be unlikely on the [111] and [110] surfaces, because of the high strain energy involved in the cyclic surfaces compound so formed. It is feasible on the [100] surface, and hence at edges and steps in the [111] plane which provide a similar orientation of surface carbon atoms. The existence of such edges and steps on a real, mechanically polished surface allows oxygen coverage of 0,33 monolayer or greater on a macroscopic [111] face, as has been shown by a Monte Carlo simulation of the process of surface reaction with water molecules.

The adhesion tension of diamond is insensitive to pH, except in the extremely alkaline regime. This suggests again that the oxygen is present in the form of tertiary alcohols, and not acid groups.

Equally, there is no dependence on ionic strength in solutions of indifferent electrolytes, potassium chloride and sodium chloride. Oxidation by aqueous oxidants was minimal, except in the case of the hypochlorite ion. Even here, the shift in wetting behaviour was small in comparison with that caused by high temperature oxidation. These results agree with surface structure where the majority of the surface sites are uncharged and inert, such as surface hydrides.

Adsorption of ferric ion, from solutions of concentration greater than 10^{-5}M, produced an increase in the wettability of the surface. This is believed to be a better explanation of the industrial problem of hydrophilic diamonds found in certain ore deposits, than the mechanism of oxidation by the atmosphere as previously proposed.

The inherent hydrophobicity of diamond can be explained, based on the results of this work, by the steric resistance to oxidation of [111] and [110] microfacets on the surface. The majority of surface carbon atoms must be satisfied by formation of surface hydrides.

REFERENCES

Abraham, M.H. et al — "A New Look at Acids and Bases". *Chem. in Br.*, June 1986, pp 551-554.

Adamson, A.W. — "Physical Chemistry of Surfaces", 2nd Ed. Interscience, New York, 1967.

Allain, C. et al — "A New Method for Contact Angle Measurements of Sessile Drops". J. Colloid and Interface Sci. 107, 1985 pp 5-13.

Annegarn, H. — "Low Energy (d, p) Reaction Studies on ^{9}Be, ^{10}Be, ^{11}Be and ^{12}C". Ph.D Thesis, University of the Witwatersrand, 1976.

Arbiter, N. et al — "Surface Properties of Hydrophobic Solids". *Am. Inst. Chem. Eng. Symposium Series*, 71, 1975, no 150, pp 176-182.

Bambakidis, G. McKeown, W.T. — "C_5H_3 Cluster as a Model for the [111] 1 x 1 *Diamond* Surface". Phys. Status Sol., B 126, no 67, 1984. pp 67-70.

Barone, N. Toscano, M. — "A Theoretical Study o. the Relaxation and Reconstuction of the [111] Surface of Diamond". Surf. Sci., 162, 1985, pp 169-174.

Bansal, R.C., Vastola, F.J. Walker, P.L. — "Kinetics of Chemisorption of Oxygen on Diamond". Carbon, vol 10, 1972, pp 443-448.

Barrer, R.M., — "Sorption Processes on Diamond and Graphite: Part I : Hydrogen; Part II: Oxygen, Carbon Dioxide and Carbon Monoxide". J. Chem. Soc. 1936, pp 1256-1269.

Batchelor, G.K. — "An Introduction to Fluid Dynamics". *Cambridge University Press*, Cambridge, 1967, 14.

Bayramli, E. et al — "Tensiometric Studies on Wetting IV". Colloids and Surf. 3, no 3, 1981, pp 279-293.

Bendure, R.L. "Dynamic Adhesion Tension Measurement". J. Colloid and Interface Sci., 42, no 1, 1973, 137-144.

Bharadwaj, P.K. et al "Voltage Optoelectronic Switching in Diamond". Appl. Phys. Lett. 43, 1983, pp 207-209.

Bikerman, J.J. "Physical Chemistry of Surfaces, Academic Press, New York, 1970, 3-5.

Billett, D.F. Ottewill, R.H. "The Dependence of Contact Angle on the Adsorption of Surface Active Agents" in Wetting. Soc. Chem. Ind., Monograph Series 25, 1968, pp 253-271.

Bruton, E. "Diamonds". NAG Press, London, 2nd Ed 1978, pp 210-216.

Cain, J.B. et al "Dynamic Contact Angles on Smooth and Rough Surfaces". J. Colloids and Interface Sci., 94, no 1, 1983, pp 123-130.

Carley, A.F. Roberts, M.W. "An X-ray Photoelectron Study of the Interfaction of Oxygen and Nitric Oxide with Aluminium". Proc. Royal Soc. (London), A, 363, 1978, pp 403.

Crowl, V.T., Wooldridge, W.D.S "A Method for the Measurement of Adhesion Tension of Liquids in Contact with Powders". in Wetting, Soc. Chem. Ind. Monograph Series, 25, pp 200-212, 1968.

Dasher, J. et al "Sticky Surface Concentration of Gravel Size Minerals". Am. Inst. Miner. Met. Trans., 153, 1943, pp 557-562.

Davies, G. "Diamond". A. Hilger, Bristol, 1984, p 13.

Davies, G. Evans, T. "Graphitization of Diamond at Zero Pressure and at High Pressure". Proc. R. Soc. London, A, 328, 1972, pp 413-427.

Davies, R. De Beers Diamond Research Centre Internal Report, 85/1/7, 1985.

Dawson, J.B. "New Aspects of Diamond Geology". in Properties of Diamond, J.E. Field, ed., Academic Press, London, 1979, pp 539-544.

Defoe, M.E. "Diamonds", in Soc. Min. Eng. Mineral Processing Handbook, Am. Inst. Min. Metall. and Pet. Eng. New York, 1985, pp 28-4.

de Gennes, P.G. "Wetting: Statics and Dynamics". Rev. of Mod. Phys., 57, no 3, 1985, pp 827-863.

Derry, T.E. et al "Oxygen and Hydrogen on the Surface of Diamond". Nucl. Instrum. and Methods in Phys. Res. 218, 1983, pp 559-562.

Derry, T.E. et al "Ion Scattering Determination of the Atomic Arrangement of Polished Diamond (111) Surfaces Before and After Reconstruction". Surf. Sci. 167, 1986a, pp 502-518.

Derry, T.E. "Ion Channelling in Diamond". PhD Thesis, University of Witwatersrand, 1978, pp 33-36.

Derry, T.E. Personal communication, 1986b.

Dunstan, D., White, Lee R. "Capillary Pressure Measurement of Contact Angles in Powders and Porous Media". J. Colloids and Interface Sci., 111, no 1, 1986, pp 60-64.

Ertl, G. Küppers, J. "Low Energy Electrons and Surface Chemistry". Verlag Chemie, Weinheim, 1984, 120-149.

Evans, S. Riley, C.E. "Angular Dependence of X-ray Excited Valence-band Photoelectron Spectra of Diamond". J. Chem. Soc. Faraday Trans, 2, 1988, 82, pp 541-550.

Field, J.E. (ed) "Properties of Diamond" : De Beers Industrial Diamond Division Data Sheet, Ascot. 1979a, p3.

Field, J.E. "Physics of Diamonds".
Academic Press, London 1979b.

Fowkes, F.M. "Dispersion Force Contributions to Surface and Interfacial Tensions".
In Contact Angle Wetting and Adhesion". Am. Chem. Soc., *Washington*, 1964, pp 99-111.

Fowkes, F.M. "Predicting Attractive Forces at Interfaces".
Chemistry and Physics of Interfaces II, Sydney Ross (ed), Am. Chem. Soc., Washington, 1971, pp 153-167.

Gaudin, A.M. "Principles of Mineral Dressing".
McGraw Hill, New York, 1939, pp 472-473.

Gaudin, A.M. et al "Native Flotability and Crystal Structure".
Proc. 2nd Int. Congr. Surf. Act. Butterworths Scientific, London, 1957, pp 209-219.

Good, R.J. Elbing, E. "Generalization of Theory for Estimation of Interfacial Energies".
Chemistry and Physics of Interfaces II, Sydney Ross (ed), Am. Chem. Soc., 1971, pp 72-96.

Grader, L. "On the Modelling of the Dynamic Contact Angle".
Colloid and Polym. Sci., 264, no 8, 1986, pp 719-726.

Gutierrez Rodriguez, J.A. et al "Estimating the Hydrophobicity of Coal".
Colloids and Surf., 12, 1984, pp 1-25.

Hartley, C.J. "The Surface Chemistry of Diamond".
PhD thesis, University of London, 1978, pp 77.

Herb, C.A. et al "The Effect of Cross Sectional Geometry on the Accuracy of the Fiber-Wetting Balance".
J. Colloids and Interface Sci., 94, 1983, pp 14-24.

Hiemenz, P.C. "Principles of Colloid and Surface Chemistry".
Marcel Dekker, New York, 1977, pp 209-246.

Himpsel, O.E. et al "Surface States on Reconstructed Diamond [111]".
J. Vac. Sci. Technol., 17, p 1085, 1980.

Himpsel, F.J. et al — "Surface States on Reconstructed Diamond [111]". Phys. Rev. B, 24, no 12, pp 7270-7274, 1981.

Huh, C. Reed, R.L. — "A Method for Estimating Interfacial Tensions and Contact Angles from Sessile and Pendant Drop Shapes". J. Colloids and Interface Sci., 91, no 2, 1983.

Israelachvili, J.N. Ninham, B.W. — "Intermolecular Forces - The long and short of it". J. Colloids and Interface Sci., 58, no 1, 1977, pp 14-25.

Jameson, G.J. Del Cerro, M.C.G. — "Theory for the Equilibrium Contact Angle between a Gas, a Liquid and a Solid". J. Chem. Soc., Faraday Trans., 72, no 1, 1976, pp 883-895

Janczuk, B. et al — "The Influence of n-Alcohols on the Wettability of Hydrophobic Solids". Powder Technol., 45, 1985, pp 1-6.

Jeffreys, H. Jeffreys, B.S — "Methods of Mathematical Physics". Cambridge University Press, Cambridge 1972, pp 155-157.

Johnson, R.E. ..ttre, R.H. — "Contact Angle Hysteresis: Idealized Rough Surface". Am. Chem. Soc. Adv. in Chem. Series, 43, 1964, pp 112-132.

Johnson, R.E. Dettre, R.H. — "Dynamic Contact Angles and Contact Angle Hysteresis". J. Colloids and Interface Sci., 62, no 2, 1977, pp 205-21.

Kelebek, S. Smith. G.W. — "Selective Flotation of Inherently Hydrophobic Minerals". Int. J. Min. Process., 14, 1985, pp 275-289.

Kendig, M.W., Fadner, T.A. — "Influence of Electrochemical Potential on the Displacement of Aqueous Electrolyte from a Copper Surface by Oil". Ind. Eng. Chem. Fundam., 24, 1985, pp 50-55.

Kozlowski, C. Sherwood, P.M.A. — "XPS Studies of Carbon Fibre Surfaces VII". Carbon, 24, no 3, 1986, pp 357-363.

Kuryenkov, I. et al — "Adsorption of Oxygen on Freshly Exposed Diamond Surfaces". Isv. Vyss. Ucheb. Zaved. Tsetn. Met., 6 (1), 1963, pp 32-34.

Lander, J.J.
Morrison, L.
"Low Energy Diffraction Study of the [111] Diamond Surface".
Surf. Sci., 4, 1966, pp 241-246.

Laplace, P.S.
Mechanique Celeste, Couveier, Paris, 1805.

Laskowski, J.
Kitchener, J.A.
"The Hydrophilic-Hydrophobic Transition on Silica".
J. Colloids and Interface Sci., 29, no. 4, 1969, pp 670-678.

Lowther, J.E.
"Hydrogen Adsorption of the [001] Diamond Surface".
Solid State Commun., 56, no 2, 1985, pp 243-245.

Lenard P.,
"Uber Oberflachenspannungsmessung".
Ann. Phys., 4, band 74, 1924, pp 381-404.

Lester, G.R.,
"Contact Angles of Liquids at Deformable Solid Surfaces".
J. Colloid Sci., 16, 1961, pp 315-326.

Lopez, J.P.
Fink, W.H.
"Ab Initio Model Calculations for Adsorption of Atomic Hydrogen on the [100] Face of Diamond".
J. Phys. Chem., 85, 1981, pp 2642-2650.

Lubelkin, S.
University of Bristol Private communication, 1985.

Lurie, P.G.
Ristic, S.
"Contact Angle Measurements between Diamond and Water".
(unpublished) De Beers Report No E.4.7/1.02, Johannesburg, 1972.

Mackay K.M.
Mackay, R.A.
"Modern Inorganic Chemistry".
Intertext, London, 1970, 23.

Mainwood, A.
"Interstitial Hydrogen in Diamond".
Diamond Conference, Oxford, 1982, paper 22.

Mason, S.G.
"Wetting and Spreading - Some Effects of Surface Roughness".
in Wetting, Spreading and Adhesion. J.F. Padday, ed, Soc. Chem. Ind. Washington, 1978, pp 321-326.

Matsumoto, S
Setaka, N.
"Thermal Desorption of Hydrogenated and Water Treated Diamond Powders".
Carbon, 17, 1979, pp 485-489.

Matsumoto,S. et al — "Thermal Desorption Spectra of the Oxidized Surfaces of Diamond Powders". Carbon, 15, 1977, pp 299-301.

McKervey, M.A. — "Synthetic Approach to Large Diamondoid Hydrocarbons". Tetrahedron, 36, 1980, pp 971-992 - writing of the work of W.H. and W.L. Bragg, Proc. Roy. Soc. 89, 1913.

Meyer, O.
Gyulai, J.
Mayer, J.W. — Surf. Sci., 2, 1970, pp 263.

Microscal — Technical Information FMC-3 SV, 10084, London W10 5AL. 1985.

Miyoshi, K.
Buckley, D.H. — "Adhesion and Friction of Single Crystal Diamond in Contact with Transition Metals". Appl. Surf. Sci, 6, no 2, 1980, pp 161-172.

Mitchell, R.H.
Crockett, J.H. — "Diamond Genesis". Miner. Deposits, vol 6, 1971, pp 392-403.

Naidich, Yu.V.
Pereverttailo V.
Loginava, O.B. — "Surface Tension and Adhesion to Graphite and Diamond of Ni-alloy Melts". Russ. J. Phys. Chem., vol 58, no 7, 1984.

Nassau, K.
Schonhorn, H. — "Contact Angle of Water on Gems". Gems and Gemology, 15, Dec. 1977, pp 354-360.

Neumann, A.W. — "Contact Angles and their Temperature Dependence, Thermodynamic Status, Interpretation and Application". Adv. in Colloid and Interface Sci., 4, 1974, pp 105-191.

Neumann, A.W. — "Introductory Lecture on Contact Angles". *in Wetting Spreading and Adhesion.* J.F. Padday (ed), Soc. Chem. Ind., Washington, 1978, pp 3-35.

Noma, T.
Sawaoka, A. — "Fabrication of Diamond-Glass Composites under Microgravity". Jpn. J. Appl. Phys., 24, no 10, 1985, p 1300.

Owens, N. et al "Contact Angles of Pure Liquids and Surfactants on Low Energy Surfaces". in *Wetting, Spreading and Adhesion*, J.F. Padday (ed), SCI, Washington, 1978, pp 128-146.

Oliver, J.F. Hah, C. Mason, S.G. "An Experimental Study of Some Effect of Surface Roughness on Wetting". Colloids and Surf., 1 (1980), pp 79-104.

Padday, J.F. "The Measurement of Surface Tension". in Surf. and Colloid Sci. E. Matijevic, ed, Wiley Interscience, New York, 1969, pp 101-149.

Pandey, K.C. "New Dimerized Chain Model for the Reconstruction of the Diamond [111] (2x1) Surface". *Phys. Rev. B*, 2, no 6, 1982, pp 4338-4341.

Pashley, R.M. "*Surface Forces in Thin Films on Smooth Quartz*". PhD Thesis, University, London, London, 1978 pp 76-77.

Pate, B.B. "The Diamond Surface: Atomic and Electronic Structure". Surf. Sci. 165, 1986, pp 83-142.

Pate, B.B. et al "Photoemission and Stimulated Ion Desorption Studies of Diamond [111] : Hydrogen". J Vac. Sci. Technol. PCSI-9 Proc.s, 1982.

Pate, B.B. et al "Carbon 1s Studies of *Diamond [111]*". Paper SSthA-12 at 1983 Am. Vac. Soc. Meeting, Boston, 1983.

Pate, B.B. et al Waciawski, B.J. "The Diamond [111] Surface : A Dilemma Resolved". *Physica 117B, 1983, pp 783-785.*

Pauling, L. "Nature of the Chemical Bond". 3rd ed, Cornell University Press, Ithaca, New York, 1960

Pendry, J.B. "Low Energy Electron Diffraction". Academic Press, London, 1974, pp 8-17.

Pepper, S.V. "Effect of Electronic Structure of the Diamond Surface on the Strength of the Diamond-Metal Interface". J. Vac. Sci. Technol. 20, no 3, 1982, pp 643-646.

Prins, J. Private Communication, 1986.

Rao, S.R. "Surface Forces in Flotation". Miner. Sci. Eng. 6, no 1, 1974, pp 45-53.

Ralston, R.A.
Wilf, H.S. "Mathematical Methods for Digital Computers". Wiley, New York, 1960, p 334.

Rebinder, P.A. "Enrichment of Non-metallic Minerals by Flotation". IGD AN SSSR, 1952.

Schlossin, H.H. Proc 1st Congr. Int. Soc. Rock Mechanics, Lisbon, 1966.

Schoeffer, J.A. et al "Adsorption of H, O and H_2O at Si [100] and Si [111] Surfaces in the Monolayer Range". J. Vac. Sci. Technol. 82, no 3, 1984, pp 359-365.

Scofield, J.H. "Hartree-Slater Subshell Photo-ionization Cross-sections at 1254 and 1487 eV". J Electron Spectrosc. and Relat. Phenom., 8, 1976, pp 127-139.

Sappok, R.
Boehm, H.P. "Chemie der Oberflache des Diamanten - I and II", Carbon, 6, 1968, pp 283-295, pp 573-588.

Shergold, H.L.
Hartley, C.J. "The Surface Chemistry of Diamond". Int. J. Miner. Process, 9, 1982, pp 219-233.

Staszcuk, P. "Determination of Water Film Pressure and Surface Free Energy on Graphite". Mater. Chem. and Phys., 14, 1986, pp 279-287.

Tabor, D. "Some Physical Aspects of the Diamond Surface". Diamond Res., 1975, pp 9-12.

Tabor, D. "Hydrogen in and on Diamond".
Diamond Conference, Cambridge, 1983, paper 37.

Tanaka, T.
Kanemoto, K. "Wetting of Diamond by Liquid Metals with Low Melting Points".
Takamatsu Technical College, 13, 1977.

Thomas, J.M. "Adsorbability of Diamond Surfaces".
in Properties of Diamond, J.E. Field ed, Academic Press, London, 1979, pp 211-243.

van Oss, C.J. et al "Role of van der Waals Forces and Hydrogen Bonds in Hydrophobic Interactions between Biopolymers and Low Energy Surfaces".
J. Colloid and Interface Sci., 111, no 2, June 1986, pp 378-390.

Verwoerd, W. Private communication 1986.

Vidali, J. et al "Helium as a Probe of the [111] Surface of Diamond".
Phys. Rev. Lett., 51, no 2, 1983, p, 118-121.

Waclowski, B.J. et al "Direct Verification of Hydrogen Termination of the Semi-conducting Diamond [111] Surface".
J. Vac. Sci. Technol., 21, 1982, p 368.

Walker, G.W. et al "Hydrophobic Effect of Sulphur and Xanthate on Metal and Mineral Surfaces".
Int. J. Miner. Process, 18, 1980, pp 119-137.

Watermeyer, B. "Diamond Cutting".
Purnell Cape Town, 1980, pp 155-158.

Weavind, R.G. "Treatment and Recovery of Refractory Diamonds".
J. Chem. Met. Miner. Soc. S. Afr., 1952, pp 243-264.

Wilks, J. "Experiments on Polishing of Diamond". Nature, 243, 1973, pp 15-18.

Young, T. "An Essay on the Cohesion of Fluids". Phil. Trans. Royal Soc. (London), 95, *1805, pp 65-87.*

Zettlemoyer, A.C. "*Hydrophobic Surfaces*". in F.M. Fowkes' book of the same name, Academic Press, New York, 1969, 7.

Zisman, W.A. "Relation of Equilibrium Contact Angle to Liquid and Solid Constitution". in Contact Angle Wettability and Adhesion. Am. Chem. Soc., Washington, 1964, pp 1-51.

APPENDIX 1 - DERIVATION OF THE THERMODYNAMIC CONTACT ANGLE

The following derivation is for the case of a liquid at the face of a plane vertical plate or wall, which is a useful geometry for the system of capillarography (Mason 1978). An additional proof for a more general case of a vertical surface is given by Neumann (1974).

A liquid of surface tension γ_{lv} and density ρ is brought into contact with a semi-infinite vertical wall or plate and rises or is depressed to form a meniscus of height h see Figure A1.1. The profile of this meniscus was solved analytically by Laplace, and shown to have the form :

$$\frac{z^2}{a^2} = 1 - \cos\phi \qquad \ldots\ldots (A1.1)$$

where z is the height above the plane surface of the free liquid
a is the Laplace capillary constant = $2\gamma/\rho g$, characteristic of the liquid
ϕ is the angle made by the gradient of the liquid surface at height h, measured to the horizontal

i.e. $\tan\phi = \frac{dz}{dx}$

Note that this form is independent of x, the horizontal co-ordinate, and the parameter, a, is fixed for a single fluid at constant temperature.

Assume that the height h, at which the meniscus meets the solid wall, is variable. It would be in practice, since the meniscus can move up or down the wall. The wetting equilibrium occurs at the height where the sums of the interfacial and other relevant energy terms are minimized. The contact angle is the complement of the slope, $90-\phi$, at the height h.

Now consider a small increase in h, dh, caused by a microscopic advance of the wetting line. The height of the meniscus at the wall is now h+dh. The energy terms associate with this move are (per unit width of the meniscus):

solid:vapour interface decrease : $-\gamma_{sv}\, dh$

solid:liquid interface energy increase : $\gamma_{sl}\, dh$

to obtain the increase in the liquid:vapour interface, refer to the construction in Figure A1. The increase in length of the curved meniscus can be found by translating the origin along the x axis by a distance dx, so that the height of the meniscus at this point is again h, *i.e. as before* the meniscus rise. To first order approximation

$dx = dh \cot \phi$ Where ϕ is the slope at the wall

This move has excluded a section of the meniscus of length dl where :

$dl = dh \operatorname{cosec} \phi$

and far from the wall, where the slope of the meniscus tends to zero, this translation will include an increment of length dx. Otherwise, between the new translated origin and the far liquid surface (where $z \to 0$), the meniscus has the same shape and extent, since this is defined only by the capillary constant which does not change.

Therefore, the net change in meniscus length is :

$dl' = dl - dx = dh\ (\operatorname{cosec} \phi - \cot \phi)$

The net increase in interfacial energy of *the water:air interface* is therefore :

$$\gamma_{lv}\, dh\ (\operatorname{cosec} \phi - \cot \phi)$$

In addition, the translation of the axes has excluded a volume of liquid, *which has* been lifted from the plane surface (taken to be zero potential energy). Everywhere else, the matching of the meniscus after the translation with that before the translation reveals no net energy change.

Hence the volume of the increment can be found :

$$(h + \frac{dh}{2})\, dx = h\, dh \cot \phi$$

neglecting 2nd order terms.

The gravitational potential energy of the volume follows by integration :

$$d(Pe) = \frac{1}{2} \rho g\, h^2\, dh \cot \phi$$

The total energy change is therefore :

$$-\gamma_{sv}\, dh + \gamma_{sl}\, dh + \gamma_{lv}\, dh\, (\text{cosec } \phi - \cot \phi) + 1/2\ \rho g h^2\, dh \cot \phi = dG$$

At the minimum : $dG/dh = 0$ hence :

$$-\gamma_{sv} + \gamma_{sl} + \gamma_{lv}\, (\text{cosec } \phi - \cot \phi) + 1/2\ \rho g h^2 \cot \phi = 0$$

since $\frac{2\, \gamma_{lv}}{\rho g} = a^2$ the Laplace capillary constant, this becomes

$$\gamma_{sv} - \gamma_{sl} - \gamma_{lv}\, (\text{cosec } \phi - \cot \phi) = \frac{h^2}{a^2}\, \gamma_{lv} \cot \phi$$

at the wall, and as $dh \to 0$.

$$\gamma_{sv} - \gamma_{sl} - \gamma_{lv}\, (\text{cosec } \phi - \cot \phi) = \frac{h^2}{a^2}\ \gamma_{lv} \cot \phi$$

Also, $\frac{h^2}{a^2} = 1 - \cos \phi$

so by substitution and rearrangement :

$$(\gamma_{SV} - \gamma_{Sl})/\gamma_{lV} = \text{cosec}\ \phi - \cot\ \phi\ \cos\ \phi = (1-\cos^2\ \phi)/\sin\ \phi = \sin\ \phi$$

Since the slope, ϕ, is the complement of the contact angle at the wall

$$(\gamma_{SV}-\gamma_{Sl})/\gamma_{lV} = \cos\ \theta \qquad \ldots\ (1)$$

It is important that this angle is defined by a macroscopic energy balance, independent of core region effects. Optical observation of this angle is often difficult, even more so than for a sessile drop. The angle can be found indirectly by two means, both capable of high precision.

Capillary Height

By rearranging the equation for the meniscus at the wall :

$$h = a\ \sqrt{1-\sin\ \theta}$$

so the capillary rise is a good measure. The technique has been used by Cain et al (1983) who recommend a platelet size of 2 cm or more to obviate effects caused by the meniscus curvature near the ends.

Meniscus Weight

In the capillarographic technique, the weight of the meniscus is found by precision weighing. Bikerman (1970) has integrated the equation for the meniscus volume of the meniscus of Figure A.1 by trigonometric substitution and shown :

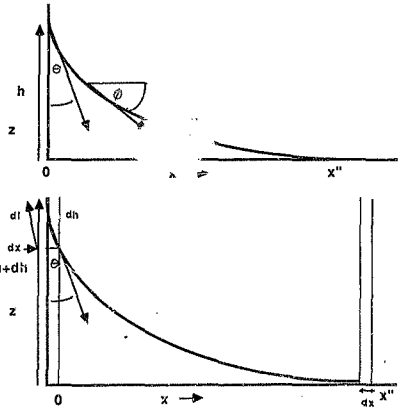
$$W = \gamma_{lV}\ \cos\ \theta$$

so that, if γ_{lV} is known from an independent measurement, θ can be calculated directly. Note that no assumptions about resolution of surface tension components at the three phase line are required in this derivation. Nevertheless, it is consistent with the tension/energy duality

of surface tension that the weight of the meniscus lifted per unit length is numerically equal to the vertical component of the surface tension. In the case of a real platelet of finite dimensions, there will be edge effects. The curvature caused by a corner will depress the meniscus, for uniform contact angle, but the weight of the meniscus, per unit length of wetted surface, will remain as above because of the fanlike shape of the meniscus at a corner.

Similarly the weight of a meniscus surrounding a curved body, but with vertical sides, e.g. a rod, is still the vertical component of the surface tension, integrated around its perimeter (Herb et al 1983). The only exception is a body with internal channels causing "wicking", a situation unlikely with diamond test plates.

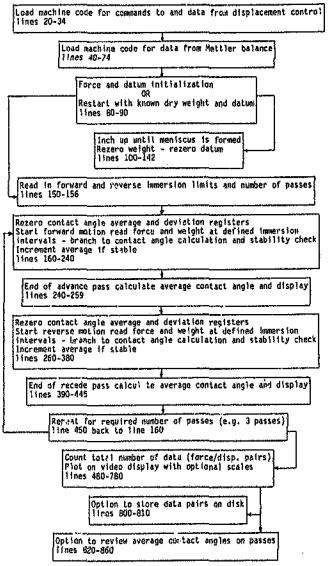
fig A1 derivation of Young's equation by energy method vertical plate with gravitational potential



co-ordinate x axis shifted by dx to right

APPENDIX 2 - FLOWSHEET FOR COMPUTER CONTROLLED EXPERIMENT

The flowsheet for the supervisory program is as indicated in the following diagram: (line numbers refer to program CAPGAL, Appendix 3).



End of main program line 930

Subroutine to plot on VDU	Lines 1000-1170
Subroutine for inching advance	Lines 1600-1620
Subroutines for advancing and receding motion	Lines 1800-2040
Subroutine for displacement in mm	Lines 2200-2215
Subroutine for emergency stop	Lines 2300-2320
Subroutine to calculate contact angle	Lines 2400-2560
Subroutine to check angle stability - buoyancy slope	Lines 2580-2600
Subroutine to unwind controller near end points	Lines 3000-3060
Subroutine to store data on disk	Lines 5000-5100

APPENDIX 3 CONTROL COMPUTER PROGRAM

This program was written in AppleSoft Basic for an Apple IIe Computer. A listing follows. Note that the command of the form "&--" is a macro command, not normally found in Apple Basic, which accesses the Galil motion control system. This allows commands for relative motion (PR), telling of position (TP) and waiting for specified period (WT in milliseconds).

```
]LIST 0-100

10  REM    CAPILLAROGRAPH
12  REM      TESTPLATE 1
14  REM
16  DIM A(800),ST(800),TA(10),IR(10)
18  REM  LOAD MACHINE CODE FOR DISP
20  PRINT  CHR$ (4);"BLOAD SIVY.S": PRINT  CHR$ (4);"RELOAD SIVY.S3"
22  POKE 115,204: POKE 116,146: REM  MEMEM AT 37580
24  CALL 773: REM.  INIT SERIAL CARD
26  REM   SET CONTROLLER CAIN
28  A "CR800";: A "D80;"
30  POKE 772,0: REM  SCREEN ECHO OFF
32  REM  SET MOTION COMPLETE FLAG
34  REM   A"41;"
40  REM  COMMS TO METTLER
50  POKE 1160,0: REM  2400 BAUD
52  POKE 1402,4: REM.  EVEN PARITY
54  POKE 1914,0: REM  7 DATA BITS
58  RECLIVE = PEEK (110) * 256 + PEEK (109) - 31
60  REMEM RECLIVE
90  FOR I = RECLIVE TO RECLIVE + 40
62  READ D: POKE I,D: NEXT I
64  DATA  32,74,255,120,162,21,142,14,  0,173
66  DATA  12,  4,10,  5,130,240,253,233,  1,240
68  DATA  247,173,100,192,  10,208,240,240,230,  32
70  DATA   5,194,173,122,  0,157,  0,  4,232,224
72  DATA  130,240,242,14c,255,  4,  76,  83,255
74  PRINT
76  REM  INSTRUCTION FOR EAPT
78  PRINT "  CAPILLAROGRAPH OF TESTPLATE 1"
82  INPUT "START ? Y/N";G$
84  IF G$ = "N" THEN 136
86  INPUT "DRY WEIGHT ?";WO
88  INPUT " HAS A YOU HAVE RETURNED TO WEIGHT ZERO AND DEFINED HOME?";G$

90  IF G$ = "Y" THEN  GOTO 130
92  STOP
100  REM  SEND DATA
104  REM  DRY WEIGHT
106  GOSUB 700
108  WO$ =  MID$ (A$,5,8):WO =  VAL (WO$)
110  PRINT "WEIGHT : DRY WT = ";WO
112  GOSUB 1000
114  GOSUB 700
116  WW$ =  MID$ (A$,5,8):WW =  VAL (WW$):ST = WW - WO
118  IF  ABS (ST) > 0.0002 THEN 130
119  IF  PEEK ( - 16384) = 211 GOTO 2300
120  WO = WW: GOTO 114
130  A "DH;": PRINT " WEIGHT ZERO FOUND"
132  PRINT "DRY WEIGHT = ";WO
135  XK = WO: REM   WEIGHT ZERO
136  ZO = 0: REM  ZSHELF
140  J = 1: REM  DATA COUNTER
142  X(0) = XK: REM  XSHELF
150  REM     FORWARD PASS LENGTH &                  REPTS
152  READ ZF,ZR,NR: DATA  3,-.5,3
154  PRINT "BEGIN": GET B$
156  FOR R = 1 TO NR: REM  NO OF PASSES
160  REM  FORWARD MOTION
```

```
]LIST 160-500

100  REM  FORWARD MOTION
162 TA(K) = SU:DS = "ADV":SU = U:SD = U:L = U:CS = U
165  GOSUB 1840
170  ZT(J) = ZS: GOSUB 790
174  WW$ =  USING "###.##";A(J) =  VAL (WW$)
176  REM  CALCULATE CONTARC
182  GOSUB 2600
190  REM  CHECK FOR STABILITY
194  IF IS = 1 THEN 260
198 SU = SU + CI:SD = SD + CI * CI:L = L + 1
196  PRINT : PRINT "ANGLE STABLE": PRINT
200 CS = CI
210  PRINT "DATUM : ";ZT(J)
214  PRINT "FORCE : ";A(J)
216  PRINT "CONTACT ANGLE : ";CI
220  IF PEEK ( - 16384) = 211 GOTO 2300: REM   ABORT = TYPE "S"
225 J = J + 1
240  REM  CHECK ENDPASS
244  IF ZS < = ZR THEN 165
245  IF L > 1 THEN 250
248 TA(K) = SU:DA(K) = J: GOTO 254
250 TA(K) = SU / L:DA(K) =  SQR ((SD - L * TA(K) ^ 2) / (L - 1))
252  PRINT " AVE ";ZS" ANGLE ON PASS ";K" IS ";.01 *  INT (100 * TA(K)
     )
254  PRINT " STD DEV IS ";.01 *  INT (100 * DA(K))
256  REM  PREVENT RESTART JITTER
258  GOSUB 3040
259  FOR  = 1 TO 500: NEXT L
260  K =  + 1: REVERSE PASS
275 TR(K) =  USING "###.##":SU = U:SD = U:L = U:CS = U
281  GOSUB 2600
282 ZT(J) = ZS: GOSUB 790
284 WW$ =  USING "###.##";A(J) =  VAL (WW$)
286  REM  CALCULATE CONTARC
290  GOSUB 2400
300  REM  CHECK FOR STABILITY
310  IF IS = 1 THEN 340
320 SU = SU + CI:SD = SD + CI * CI:L = L + 1
330  PRINT "ANGLE STABLE "
340 CS = CI
350  PRINT "DATUM : ";ZT(J)
360  PRINT "FORCE : ";A(J)
370  PRINT "CONTACT ANGLE : ";CI;" ";DS
372 J = J + 1
375  IF  PEEK ( - 16384) = 211 GOTO 2300
380  REM  CHECK ENDPASS
390  IF ZS > ZR THEN 280
395  IF L > 1 THEN 405
396 TA(K) = SU:DA(K) = 0: GOTO 410
405 TR(K) = SU / L:DR(K) =  SQR ((SD - L * TR(K) ^ 2) / (L - 1))
410  PRINT " AVE ";ZS" ANGLE ON PASS ";K" IS ";.01 *  INT (100 * TR(K)
     )
415  PRINT " STD DEV IS ";.01 *  INT (100 * DR(K))
440  IF J > 599 GOTO 480
442  REM  PREVENT RESTART JITTER
444  GOSUB 3040
445  FOR L = 1 TO 500: NEXT L
450  NEXT K
456 CO = J: GOTO 500
500  REM  OPTION TO PLOT
```

```
]LIST 500-1130

500  REM  OPTION TO PLOT
510  X0 =  - 1:X1 = 4: REM  DISP RANGE
540  INPUT "CHANGE X RANGE OF PLOT ?";C$
550  IF C$ < > "Y" THEN 580
560  INPUT "X0,X1 ?";X0,X1
580  PRINT : PRINT
590  REM  FIND YMIN AND YMAX
600  Y1 = X(1):Y2 = X(1)
610  FOR I = 2 TO CO - 1
620  IF X(I) < Y1 THEN Y1 = X(I)
630  IF X(I) >  = Y2 THEN Y2 = X(I)
640  NEXT I: PRINT "YMIN,YMAX";" ";Y1;" ";Y2
650  INPUT "Y0,Y1 : ";Y0,Y1:YY = .01
660  PN$ = ";": GOSUB 1030
670  FOR I = 1 TO CO - 1:XP = ZT(I):YP = X(I): GOSUB 1000:PN$ = "I": NEXT
     I
680  GOSUB 1050
690  GET A$
695  TEXT : HOME : VTAB 1: GOTO 800
700  REM  FLIGHT INPUT
720  CALL RECEIVE
730  A$ = ""
740  FOR I = 0 TO  PEEK (767) - 3
750  D = PEEK (512 + I) - 128
760  IF D > 96 THEN D = D - 32
770  A$ = A$ + CHR$ (D): NEXT I
780  RETURN
800  REM  OPTION TO STORE DATA FOR PLOTTING
805  INPUT " SAVE TO DISK";A$
810  IF A$ = "Y" THEN  GOSUB 840
820  INPUT "RECALL RECORD ? ";C$
830  IF C$ = "Y" GOTO 850
840  GOTO 860
850  PRINT "PASS";"  ADV";"  REC"
860  FOR K = 1 TO 4: PRINT "  ";A(K);"  ";TA(K);"  ";TB(K): NEXT K
930  RETURN: RECEIVE + 51: END
950  REM
960  REM  SCALEOUTLES
1000  REM ==>> CRT ROUTINES <<==
1010  GOSUB 1070: IF PN$ = "I" THEN XOLD = XV:YOLD = YV
1020  HPLOT XOLD,YOLD TO XV,YV:XOLD = XV:YOLD = YV: RETURN
1030  REM ==>> PLOT ON <<==
1040  HCOLOR= 7: HGR : RETURN
1050  REM ==>> PLOT OFF <<==
1060  RETURN
1070  REM ==>> CONVERT <<==
1080 XV =  INT (279 * (XP - X0) / (X1 - X0)): IF XV < 1 THEN XV = 1
1090  IF XV > 270 THEN XV = 278
1100 YV =  INT (159 * (1 - (YP - Y0) / (Y1 - Y0))): IF YV < 1 THEN YV = 1

1110  IF YV > 158 THEN YV = 158
1120  RETURN
1130  REM ==>> AXES <<==
```

```
LIST 1130-3000

1130  REM ==>> AXES <<==
1140  XP = XTYP + W: GOSUB 1670: HPLOT W,YV TO 279,YV: HPLOT XV,W TO XV,15
      9
1150  IF TX > 0 THEN WX = 1 + (X1 - X0) / TX:XP = X0: FOR IX = 1 TO NX:YP
      = Y: GOSUB 1670: HPLOT XV,YV TO XV,(YV - 5):XP = XP + TX: NEXT IX
1160  IF TY > 0 THEN WY = 1 + (Y1 - Y0) / TY:YP = Y0:XP = X: FOR IY = 1 TO
      NY: GOSUB 1670: HPLOT XV,YV TO (XV + 5),YV:YP = YP + TY: NEXT IY
1170  RETURN
1180  REM  INCR UP TO START
1610  & "PR1;": & "BG;": REM  0.01 MM UP
1620  & "TP;": REM  TELL POSITION
1630  GOSUB 2200: REM  CONVERT Z
1640  RETURN
1800  REM  DEFINE ADVANCING MOTION
1810  & "PR4;": & "0,Z4,0;": & "PR5;": & "EG;"
1815  FOR K = 1 TO 1000: NEXT K
1820  & "TP"
1830  GOSUB 2200: REM  CONVERT Z
1840  RETURN
2000  REM  DEFINE RECEDING MOTION
2010  & "PR-4;": & "0,-Z4,0;": & "1,P5;": & "EG;"
2015  FOR K = 1 TO 1000: NEXT K
2020  & "TP"
2030  GOSUB 2200: REM  CONVERT Z
2040  RETURN
2200  Z = 3.81 * Z
2210  IF Z > 15L THEN Z = Z - 167772.16
2215  ZS = Z
2220  RETURN
2300  REM  EMERGENCY STOP
2310  & "MO;": REM  MOTOR OFF
2320  STOP
2400  REM
2410  REM  CALCULATE CONTACT ANGLE
2420  CM = 73.8:RO = 996
2430  LL = 25
2450  V = 0.0007* EO - 0.735 - 06 * LL ^ 2:H = RO * V
2500  GL = (1.596 - 0.0007 * LL) * GN
2510  FT = F + 1000 * (X(J) - AR):TH = FT / CL
2520  IF TH > 1 THEN 2550
2530  CT = - ATN (TH / SQR ( - TH * TH + 1)) + 1.57:C1 = 57.29 * CT:C
      T = 0.01 * INT (100 * CT)
2540  GOTO 2560
2550  PRINT "TOO FEEDING F/CL= ";TH
2560  CT = 0
2580  REM  STABILITY CRITERION
2582  IF  ABS (Z - Z0) > 0.03 THEN 2586
2584  IS = 0: GOTO 2590
2585  REM  CHECK BUOYANCY SLOPE
2586  D1 = 1000 * (X(J - 1) - A(J)) - F + FO: IF  ABS (D1) >  = 0.3 THEN Z
      590
2588  IS = 1: GOTO 2590
2590  IS = 0
2595  FO = F:Z0 = Z
2600  RETURN
3000  REM  PREVENT RESTART JITTER
```

```
LIST 3000-3100

3000  REM  PREVENT RESTART JITTER
3010  A "PR-1;": A "WT600;": A "RP8;": A "SC;"
3020  RETURN
3030  REM  PREVENT RESTART JITTER
3050  A "PR 1;": A "WT600;": A "RP8;": A "SC;"
3060  RETURN
5000  REM  STORE ON DISK
5010  INPUT "STEPSIZE ?: ";JS
5020  K = INT (CC / JS)
5030  INPUT "FILENAME:";FD$: PRINT  CHR$ (4);"OPEN";FD$: PRINT  CHR$ (4);
      "DELETE";FD$: PRINT  CHR$ (4);"OPEN";FD$: PRINT  CHR$ (4);"WRITE";FD
      $
5040  PRINT K
5050  KK = CC
5060  FOR I = 1 TO KK STEP JS
5070  PRINT I: PRINT X(I): PRINT Z1(I)
5080  NEXT I
5090  PRINT  CHR$ (4);"CLOSE";FD$
5100  RETURN
```

APPENDIX 4 - DERIVATION OF THE LEED EQUATION FOR SPOT SPACING

The de Broglie equation gives the equivalent wavelength of an electron

$$\lambda = \frac{h}{mv} \quad \ldots. (A4.1)$$

h = Planks constant $6{,}63 \times 10^{-34}$ J-S
m = Mass of electron $9{,}11 \times 10^{-31}$ kg
v = Velocity of electron.

At the energies used in practice, relativistic effects are not important and the velocity can be substituted by the classical equation for kinetic energy

$$v = \sqrt{\frac{2E}{m}} \quad \ldots. (A4.2)$$

or $$v = \sqrt{\frac{2eU}{m}} \quad \ldots. (A4.3)$$

Where :
e = electronic charge $1{,}602 \times 10^{-19}$ Coulomb
U = Accelerating voltage.

We have by substituting (A4.3) in (A4.1)

$$\lambda = \sqrt{2meU/h^2} \;\ldots. (A4.4). \; (\lambda \text{ in m})$$

From consideration of reciprocal lattice theory of diffraction (Pendry 1974), the beams reflected back from a diffracting surface lattice, or mesh, will interfere constructively at a set of angles θ to the normal where

$$\sin \theta_{hk} = \frac{|g_{hk}|}{2\pi\lambda} \quad \ldots. (A4.5) \quad \text{(Jeffreys et al 1972)}$$

and $\tilde{g}_{hk}$ is the lattice vector in reciprocal space.

$$\tilde{g}_{hk} = 2\pi (h \tilde{b}_1 + k \tilde{b}_2) \ldots. (A4.6)$$

where h, k are integers
$\tilde{b}_1$ $\tilde{b}_2$ are the reciprocal lattice basis vectors

$\tilde{b}_1$ and $\tilde{b}_2$ are found by matrix algebra.

Let $\bar{\bar{A}}$ be the (2x2) matrix defining the real space mesh of the diamond

$$\bar{\bar{A}} = \begin{pmatrix} a_{11} & a_{12} \\ a_{21} & a_{22} \end{pmatrix} \quad \ldots. (A4.7)$$

APPENDIX 4 - DERIVATION OF THE LEED EQUATION FOR SPOT SPACING

The de Broglie equation gives the equivalent wavelength of an electron

$$\lambda = \frac{h}{mv} \quad .... (A4.1)$$

h = Planks constant $6{,}63 \times 10^{-24}$ J-S
m = Mass of electron $9{,}11 \times 10^{-31}$ kg
v = Velocity of electron.

At the energies used in practice, relativistic effects are not important and the velocity can be substituted by the classical equation for kinetic energy

$$v = \sqrt{\frac{2E}{m}} \quad .... (A4.2)$$

or $$v = \sqrt{\frac{2eU}{m}} \quad .... (A4.3)$$

Where :
e = electronic charge $1{,}602 \times 10^{-19}$ Coulomb
U = Accelerating voltage.

We have by substituting (A4.3) in (A4.1)

$$\lambda = \sqrt{2meU/h^2} \;.. (A4.4). \; (\lambda \text{ in m})$$

From consideration of reciprocal lattice theory of diffraction (Pendry 1974), the beams reflected back from a diffracting surface lattice, or mesh, will interfere constructively at a set of angles θ, to the normal where

$$\sin \theta_{hk} = \frac{|g_{hk}|}{2\pi\lambda} \quad .... (A4.5) \quad \text{(Jeffreys et al 1972)}$$

and $\tilde{g}_{hk}$ is the lattice vector in reciprocal space.

$$\tilde{g}_{hk} = 2\pi (h \tilde{b}_1 + k \tilde{b}_2) \quad .... (A4.6)$$

where h, k are integers
$\tilde{b}_1$ $\tilde{b}_2$ are the reciprocal lattice basis vectors

$\tilde{b}_1$ and $\tilde{b}_2$ are found by matrix algebra.

Let $\tilde{\tilde{A}}$ be the (2x2) matrix defining the real space mesh of the diamond

$$\tilde{\tilde{A}} = \begin{Bmatrix} a_{11} & a_{12} \\ a_{21} & a_{22} \end{Bmatrix} \quad .... (A4.7)$$

and $\begin{pmatrix} \tilde{a}_1 \\ \tilde{a}_2 \end{pmatrix} = \tilde{\tilde{A}} \cdot \begin{pmatrix} \hat{x} \\ \hat{y} \end{pmatrix}$ $\hat{x}$ $\hat{y}$ are unit vectors in real space.

$\tilde{a}_1$, $\tilde{a}_2$ are the basis vectors of the real space mesh.

For diamond, let d be the spacing between adjacent top layer carbon atoms in the diamond surface. (252 pm in the ideal [111] surface).

$$\text{Then } \tilde{a}_1 = \begin{pmatrix} \sqrt{3} & \frac{1}{2} \\ \frac{2}{2} d & d \end{pmatrix} \quad \text{.... (A4.8)}$$
$$\tilde{a}_2 = \begin{pmatrix} 0 & d \end{pmatrix}$$

are the real space basis vectors.

$$\tilde{\tilde{A}} = d \begin{bmatrix} \frac{3}{2} & -\frac{1}{2} \\ 0 & 1 \end{bmatrix}$$

$$\begin{pmatrix} \tilde{b}_1 \\ \tilde{b}_2 \end{pmatrix} = \tilde{\tilde{A}}^{-1} \begin{pmatrix} \hat{x} \\ \hat{y} \end{pmatrix} = \frac{1}{d} \begin{bmatrix} \frac{2}{\sqrt{3}} & 0 \\ \frac{1}{\sqrt{3}} & 1 \end{bmatrix} \begin{pmatrix} \hat{x} \\ \hat{y} \end{pmatrix}$$

where $\tilde{\tilde{A}}^{-1}$ is the inverse of matrix $\tilde{\tilde{A}}$.

$$\text{hence } \tilde{b}_1 = \begin{pmatrix} \frac{2}{\sqrt{3}d} & 0 \end{pmatrix} \quad \text{.... (A4.9)}$$

$$\tilde{b}_2 = \begin{pmatrix} \frac{1}{\sqrt{3}d} & \frac{1}{d} \end{pmatrix}$$

and $|b_1| = |b_2| = \frac{1}{d}\sqrt{\frac{4}{3}}$ .... symmetry is preserved

and $|\Delta g| = |b_1| = |b_2|$

hence the angular spacing between two adjacent beam spots in any direction is :

$$\Delta (\sin \phi) = \frac{|\Delta g|}{2\pi\lambda} = \frac{2\pi}{d} \cdot \sqrt{\frac{4}{3}} \cdot \frac{1}{2\pi} \cdot \sqrt{\frac{h^2}{2meU}} = \frac{h}{d} \cdot \sqrt{\frac{2}{meU}} \quad \text{.... (4.10)}$$

Substituting MKS values for h, m, e we have

$$\Delta (\sin \phi) = 1{,}417 \times 10^{-9} \frac{1}{d} \cdot \frac{1}{\sqrt{U}} \qquad d \text{ in metres}$$

$$\text{or } \Delta (\sin \phi) = 1417 \frac{1}{d} \cdot \frac{1}{\sqrt{U}} \quad \ldots\ldots \text{(A4.11)} \quad d \text{ in pm.}$$

The emergent beams form spots with spacing Δs on a hemispherical screen, with radius r. In the VG system, the screen is not a full hemisphere, but subtends 104° (out of maximum 180°).

Hence, the projected radius, as seen on a photograph is $\rho = r \cos (104/2)$

$$= 0{,}616\ r$$

$$\textit{Then } \Delta (\sin \phi) = \frac{\Delta s}{1{,}624\rho} = 1417 \frac{1}{d} \frac{1}{\sqrt{U}}$$

$$\text{or} \qquad d = 2301 \frac{\rho}{\Delta s} \frac{1}{\sqrt{U}} \qquad \ldots\ldots \text{(A4.12)}$$

This allows calculation of the diamond lattice spacing, d in pm, from the ratio of the spot spacing to screen diameter, and the electron beam voltage.

APPENDIX 5 - WETTING RESULTS ON CLEAN POLISHED SURFACES

Face	[111]	[111]	[111]	[110]	[110]	[110]
	Advancing Angle	Receding Angle	Adhesion Tension	Advancing Angle	Receding Angle	Adhesion Tension
	75,0	27,0	41,7	72,9	25,7	43,3
	74,2	28,5	41,7	65,0	20,7	49,2
	77,0	28,0	40,2	72,0	32,1	41,9
	72,5	26,7	43,3	69,9	26,5	44,9
	71,5	29,8	43,0	68,0	28,4	45,5
	75,0	30,0	40,8	69,2	28,5	44,7
	81,9	37,4	33,9	72,7	26,3	43,3
	69,0	25,2	45,8	75,4	20,3	43,1
	80,2	31,5	36,3	75,6	22,6	42,5
	77,8	35,9	37,0	69,0	15,0	48,0
	79,8	36,5	35,6	73,7	25,1	42,7
	77,6	34,5	37,7	69,0	22,9	46,4
	77,2	34,9	37,8	77,5	34,1	37,9
	73,4	28,6	42,2	73,6	23,9	43,3
	80,3	28,2	38,1	63,6	16,8	50,8
	78,6	33,8	37,3	70,6	21,4	45,8
	69,5	24,8	45,6	70,0	29,0	44,1
	73,8	33,4	40,4			
	73,6	28,9	42,0			
	78,7	26,4	39,6			
	76,0	25,0	41,6			
	77,0	31,0	39,2			
	77,0	30,0	39,5			
	84,0	32,0	34,5			
	79,0	27,0	39,2			
	80,0	29,0	38,0			
	76,4	22,5	42,0			
	74,0	29,3	41,6			
	74,1	30,9	41,0			
	75,5	29,6	40,6			
	69,0	15,9	47,9			
	84,5	35,1	33,1			
	78,5	30,0	38,6			
	72,2	28,5	42,9			
	78,0	31,0	38,6			
	83,0	36,2	34,3			
	80,0	37,5	35,1			
	70,0	27,0	44,7			
	74,5	24,3	42,7			
	62,0	13,0	52,3			
	75,0	24,5	42,3			
	69,2	19,5	47,0			
	86,0	35,0	32,2			
	77,7	23,8	40,9			
	80,6	34,0	36,0			
	69,7	23,5	45,8			
	71,5	?	,4			
Ave,	75,9		,3	71,0	24,7	44,5
StdDev	4,6		4,0	3,5	4,9	2,9

APPENDIX 6 - COMPUTER SIMULATION OF RANDOM COVERAGE

This appendix describes the Monte Carlo simulation of hydroxyl group attachment at the exposed diamond [111] surface.

Assumptions

We assume that water molecules approach the newly exposed [111] surface - free orbitals act as nucleophiles to stick down the oxygen atom as a hydroxyl group, setting free a hydrogen atom to react with a neighbouring free orbital.

The oxygen (water molecule) will stick if and only if :

a) The site on which it impinges is free of OH and H groups

b) Its nearest neighbours are free of OH (but may have H's)

c) Once the $-OH_2$ is in position, its displaced hydrogen must react with a neighbouring site - five tries at random directions are allowed - simulating the thermal rotation of the $-OH_2$ about the new CO bond axis if no free H site is found, the H_2O will desorb.

d) At edge dislocations, the nearest neighbour restriction on OH is lifted, because of the possibility of bridging bonds (2nd layer bonds) and the greater interatomic spacing possible by bond deformation towards the step.

An edge is allowed every 7 atomic rows, simulating a macroscopic face which is 7 degrees off a true [111] axis. Water molecules impinge randomly on the surface, simulated by a random generator computer routine. After sufficient hits have occurred so that no further reactible sites are available (approximately 250 for the grid size used here) the whole surface array is displayed, and where hydrogens from the water reaction are lacking, they are made up by adventitious hydrogen from another source, for instance diffusion from the bulk. The fraction of monolayer (per C atom) is displayed as a percentage.

Programs

Program CSRAND.BAS was used for the simulation.

The [111] spacing of 7 rows was simulated on a grid of 14X10 = 140 sites. The sites are laid out in the hexagonal mesh of the [111] surface. Matrices dedicated to O and H keep track of the existence of OH and H at each site, and the build up can be viewed at a preselected interval. In order to store the hexagonal mesh, there are 14 rows of 10 atoms, reading down the page, but they are stored by the program as seven double rows, odd cross indices being higher on the page than even (and 0).

Results

The results of 10 simulations are :

mulation No.	1	30.7
	2	30.0
	3	32.8
	4	30.0
	5	26.4
	6	30.0
	7	29.3
	8	28.6
	9	30.7
	10	31.4
Average		30.0
Std. Dev.		1.7

Reduced printouts of four of these simulations appear as Fig 38.

There is no clear pattern, apart from the higher frequency of oxygens at the edge site , running horizontally across the middle of the figure. This edge defect would in reality be randomized too, so that we could expect no effect on the LEED pattern which would be dictated principally by the lattice spacing of the substrate carbon atoms.

This would explain how a surface with an approximately 30 % coverage by hydroxyl groups, arranged so as to exclude near neighbours, would not produce a change in the LEED pattern from the bulk unreconstructed pattern.

APPENDIX 7 - ELLIPSOMETRIC MEASUREMENTS

Ellipsometric Detection of Surface Graphitization

It has been suggested (Prins 1986) that the hydrophobicity of the hydrogenated surface may have been caused by graphitization of the diamond surface at the temperature of 1020 K used. Graphite has been reported to have a contact angle of approximately 80 degrees, measured by the sessile drop method (Arbiter et al 1975).

There was also a slight surface conductivity measurable using a digital multimeter after the hydrogen treatment, which might be caused by a graphitic layer, although Pepper (1982) has seen surface conductivity in diamond surfaces after vacuum annealing at 1200 K and graphitization does not begin in vacuum until over 1800 K. Also, hydrogen is reported as an inhibitor for graphitization (Davies et al 1972).

Ellipsometric measurements were made on the [111] and [110] surfaces in two states :

Polished with alumina in water - the intermediate hydrophobic state

Hydrogenated at 1020 K for 1 hour in 1 bar hydrogen

The measurements were performed using a Rudolph Research auto EL ellipsometer at the Randse Afrikaanse University, Department of Electrical Engineering. The obverse side of the diamond platelets and the sides were painted with Rotring black drawing ink to reduce secondary reflections - a big problem with diamond.

A sample of Acheson pyrolitic graphite, polished on wet water paper was also studied, to extract appropriate values for the real and imaginary parts of the refractive index of graphite.

At least six readings were taken on each surface, and the results are presented in the table.

The resistance of the surface, was measured by a Fluke digital multimeter with probe spacing of 3 mm on the surface. This is a relatively crude method, but the large difference in the readings makes it significant.

Sample	Surface Resistance (ohm)	Delta Degrees	Psi Degrees	n Refractive Index
[111] polished	> 30 Mohm	13,6 ± 2,5	4,40 ± ,16	2,40
[111] hydrogenated	100 ± 50 kohm	22,2 ± 3,0	4,78 ± ,14	"
[110] polished	> 30 Mohm	6,89 ± 1,5	4,32 ± ,02	2,41
[110] hydrogenated	50 ± 20 kohm	9,69 ± 3,3	4,27 ± ,09	"
graphite	< 1 ohm	52,4 ± 2,6	12,5 ± ,5	2,09

The ellipsometric technique detects a small change after hydrogenation. A multifilm model using the optical constants determined for graphite indicate that the a film of graphite of thickness 400 pm would be required to explain the increase in Psi from 4,40 to 4,78. However, a layer of this thickness should be detected by XPS (see Section 7.4). The most likely explanation is a change in the number of adsorbed water layers, caused by the reduced hydrophilicity. This effect has been studied by Pashley (1978) for quartz using ellipsometry.

The minute conductivity of the surface may be due to some changes in the band structure of the diamond when the surface desorbs the oxygen and takes up surface hydrogen.

APPENDIX 8 - WETTABILITY OF SILICON

A fragment of a silicon wafer of a defined [111] crystal orientation was obtained from the Schonland Centre for Nuclear Sciences. The fragment was formed into a platelet by breaking and grinding. A Laue photograph revealed that the flat faces were true [111] crystal planes.

The wafer was cleaned by ultrasonic agitation for 30 minutes in 10% Contrad cleaning solution followed by three changes of miilli-Q water and dried by indirect heating in a glove box.

The platelet was then tested using the capillarographic technique as applied to diamonds. The perimeter was 17,6mm.

Figure A8.1 shows the capillarograph in this "as received" state. The advancing contact angle reduced rapidly from 48 degrees on the first pass to 36 degrees on the third pass, and the receding contact angle from 18 degrees on the first pass to 14 degrees on the third pass. The mean adhesion tension was 62 mN/m by comparison with diamond [111] which shows approximately 40 mN/m after the same preparation. The hydration effect was also much more pronounced, the adhesion tension rising from 59 to 64 mN/m in 0,6 hour.

This suggests that the silicon [111] surface has a higher frequency of hydrophilic hydroxyl groups (silanol groups) than the diamond [111].

The silicon plate was then heated in oxygen to 670 K in the tube furnace of Figure 15 and retested. The capillarograph is shown in Figure A8.2. This shows almost perfect wetting. The first advancing contact angle was 6 degrees and all subsequent passes were at zero degrees.

This should be compared with the topmost capillarograph of Figure 21, for diamond [111] oxidized at the same temperature. This figure showed a small receding angle, of approximately 8 degrees, and a complicated advancing behaviour, with the three phase line alternately sticking and slipping, but

with an average advancing angle of 40 degrees. This leads to an adhesion tension of 64 mN/m, considerably less hydrophilic than the silicon [111].

The conclusion is that the silicon [111] surface retains a higher coverage of hydroxyl groups than diamond at room temperature, and that heating in oxygen produces a uniform very wettable surface on the silicon surface, possibly monolayer coverage by hydroxyl groups. This is compatible with the theory of steric hindrance to oxygen uptake on the diamond surface, where the interatomic spacing on the [111] surface is only 252 pm. The spacing of surface atoms on the silicon surface is 383 pm (from geometrical calculation, and the silicon covalent radius of 117 pm). Hence oxygen atoms, in the form of hydroxyl groups can be accommodated on every surface atom.

The moderate hydrophobicity of the atmospherically oxidized surface may be the result of surface hydrides formed by the reaction of water vapour with the silicon surface, which occurs even at room temperature, as discussed by Schaeffer et al (1984).

FIG. A8.1

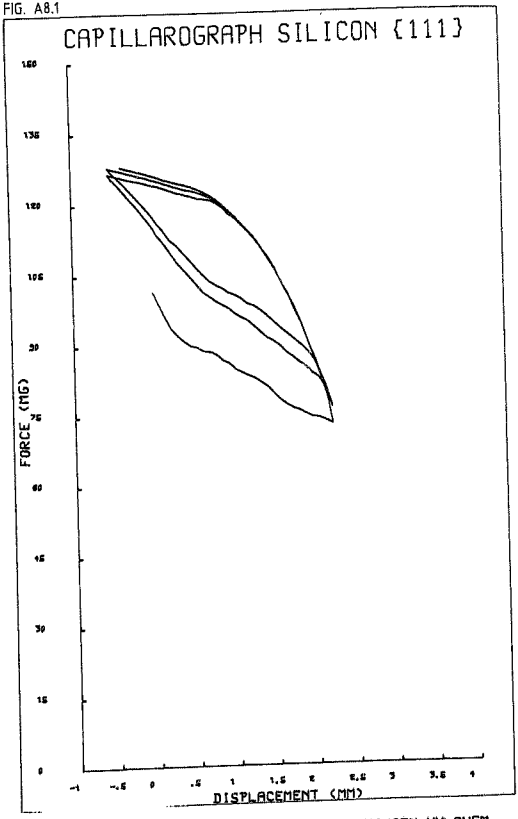

CAPILLAROGRAPH SILICON {111}
FORCE (MG)
DISPLACEMENT (MM)
J.O.HANSEN, ULF CHEN

FIG. A8.2

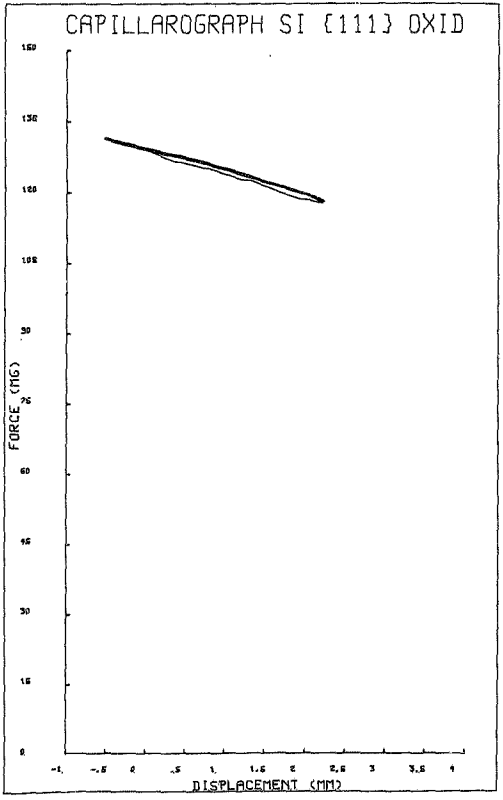
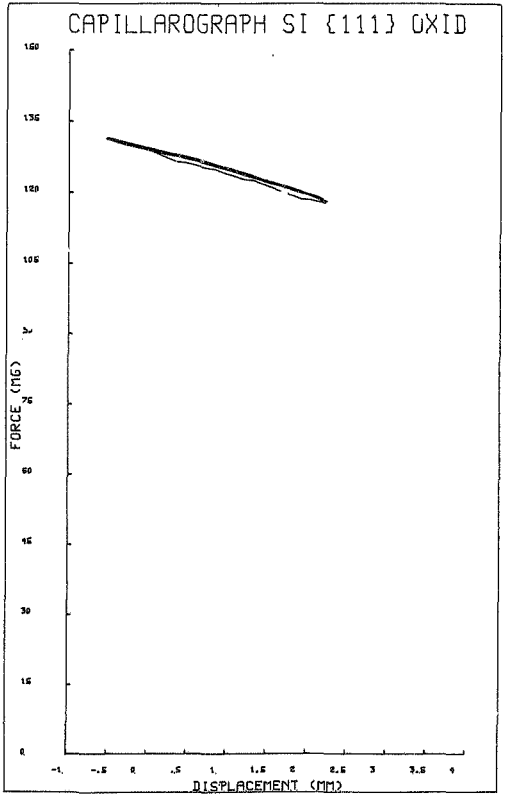
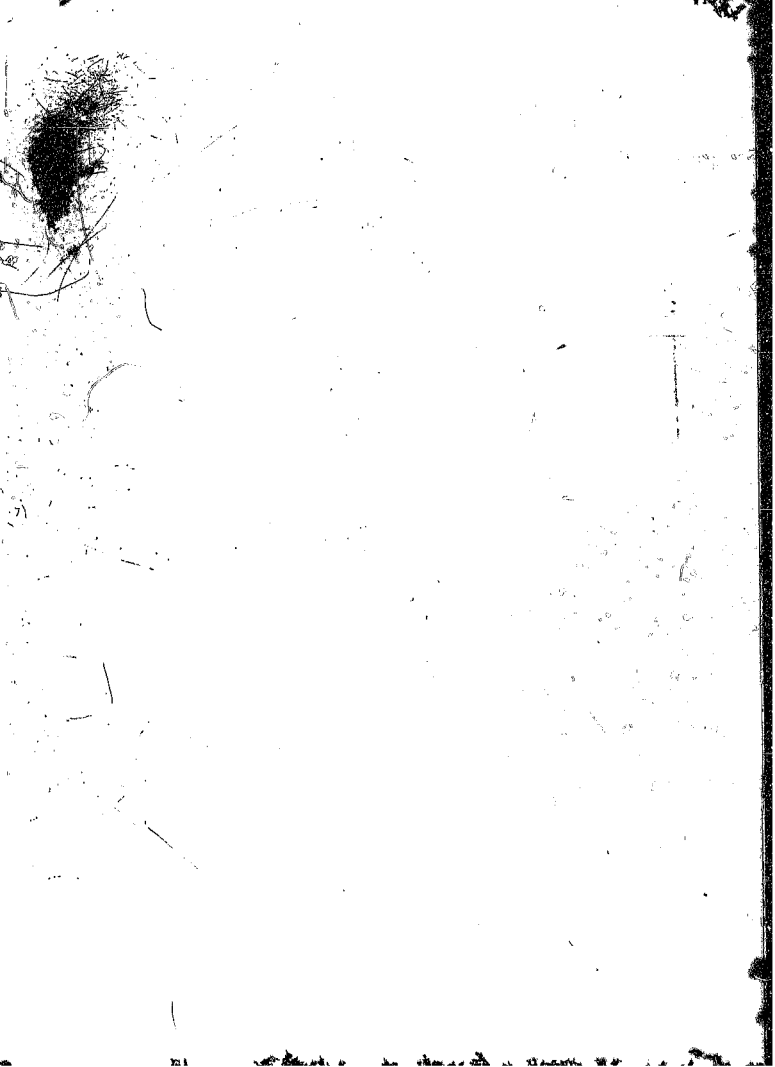

CAPILLAROGRAPH SI {111} OXID
FORCE (MG)
DISPLACEMENT (MM)
J. D. HANSEN, UU CHEM.

FIG. A8.2


CAPILLAROGRAPH SI {111} OXID
FORCE (MG)
DISPLACEMENT (MM)
J. D. HANSEN, UW CHEM



Author Hansen John Olaf
Name of thesis Wetting Of The Diamond Surface. 1987

PUBLISHER:
University of the Witwatersrand, Johannesburg
©2013

LEGAL NOTICES:

Copyright Notice: All materials on the University of the Witwatersrand, Johannesburg Library website are protected by South African copyright law and may not be distributed, transmitted, displayed, or otherwise published in any format, without the prior written permission of the copyright owner.

Disclaimer and Terms of Use: Provided that you maintain all copyright and other notices contained therein, you may download material (one machine readable copy and one print copy per page) for your personal and/or educational non-commercial use only.

The University of the Witwatersrand, Johannesburg, is not responsible for any errors or omissions and excludes any and all liability for any errors in or omissions from the information on the Library website.